THE ROLE OF POLYCOMB REPRESSIVE COMPLEX PROTEINS IN MAREK'S DISEASE VIRUS (MDV) LATENCY AND LYMPHOMAGENESIS

by

Nicholas Egan

A thesis submitted to the Faculty of the University of Delaware in partial fulfillment of the requirements for the degree of Master of Science Biological Sciences

Summer 2018

THE ROLE OF POLYCOMB REPRESSIVE COMPLEX PROTEINS IN MAREK'S DISEASE VIRUS (MDV) LATENCY AND LYMPHOMAGENESIS

by

Nicholas Egan

Approved: _____
Mark S. Parcells, Ph.D.
Professor in charge of thesis on behalf of the Advisory Committee

Approved: _____
E. Fidelma Boyd, Ph.D.
Chair of the Department of Biological Sciences

Approved: _____
George H. Watson, Ph.D.
Dean of the College of Arts and Science

Approved: _____
Douglas J. Doren, Ph.D.
Interim Vice Provost for Graduate and Professional Education

ACKNOWLEDGMENTS

I would like to take this time to acknowledge the following people for their contributions to this work and their general support. First, I would like to thank my research advisor, Dr. Mark S. Parcells, for his mentorship, support, and belief in my abilities. His passion and dedication to his work has greatly impacted me as a scientist. I wish to thank both Dr. Deni Galileo and Dr. Robert Sikes for their patience and guidance throughout my career at the University of Delaware. Both have provided invaluable criticism, helping fine-tune the way I think as a scientist.

I want to thank Dr. Carlton R. Cooper for his friendship and counsel in how to become a better educator. His philosophies on education will be forever instilled upon me throughout the entirety of my career. I wish to thank Dr. Erica M. Selva for her understanding and compassion. Her hard work and dedication to all the graduate students in the Biological Sciences program has not gone unnoticed. I would also like to thank Dr. Jeffery Caplan for lending his technical expertise in acquiring all our images and localization data. I also wish to thank Betty Cowgill for her organization, compassion, and aid throughout this entire process.

I wish to acknowledge current and past members of the Parcells lab; Phaedra Tavlarides-Hontz, Sabarinath Neerukonda, Joseph Patria, Imane Assakhi, Nirajan Bhandari, Matt Bott, Kenneth Elliot, Lakshmi Sastry, and Nola and Veronica Parcells.

I would like to thank the 329 Paper Mill Bow Bros (Anders Kiledal, Chris Materna, and Michael Pavia), Karen Christie, and Collen Pike for their camaraderie,

support and overall friendship. They made the time I spent in Newark truly memorable.

Additionally, I would like to acknowledge Squad. Their dedication and determination to achieve their goals have inspired me to do the same. They help me push myself to get something that I deserve. I would also like to thank Porpy for the lifetime of friendship we have shared.

Of course, I would not be here without the love and support of my loving parents, Carol and Robert LasCasas. I would like to thank my sister, Puff, for her love and admiration. I also wish to thank my brother, Twan, for challenging me to become the best version of myself I can be. Additionally, I would like to thank Cayla, for her support and friendship. Finally, my Aunt Jan, Uncle Chuck, Lauren, and Jeremy for their endless love and support.

TABLE OF CONTENTS

LIST OF FIGURES

ABSTRACT

Marek's Disease Virus (MDV) is the causative agent of Marek's disease (MD), a pathology associated with a rapid formation of T-cell lymphomas in chickens. MDV-induced T-cell lymphomagenesis is associated with the latent infection of CD4+ T-cells causing tumor formation within a few weeks of infection. A specific viral oncoprotein (Meq) and splice variants of this protein (Meq/vIL8 and MeqvIL8Δexon3) are expressed as MDV establishes latency, in primary lymphomas and in lymphoma-derived cell lines. Furthermore, we have discovered that these latently-associated splice-variant proteins interact with a host polycomb repressive complex (PRC-1) protein, Bmi-1 (B-cell Moloney leukemia virus integration site 1). PRCs regulate cell differentiation and development through targeted modification of chromatin, resulting in the silencing of gene expression. Specifically, Bmi-1 is associated with gene silencing through chromatin remodeling via ubiquitin ligase activity of lysine 119 on histone 2A (H2AK119). Yet, this complex does not act alone. PRC-2 protein, EZH2 (Enhancer of *zeste* homolog 2), will initially tri-methylate lysine 27 of histone 3 ($H3K27me_3$), forming a docking site for PRC-1.

The focus of this project was to characterize the interactions between the viral oncoproteins of MDV (Meq and two of its splice-variants, Meq/vIL8 and Meq/vIL8Δexon3) and host PRC proteins, as they related to cellular transformation

and the maintenance of viral latency. This was done through inhibition of Bmi-1 and EZH2 through chemical inhibitors (PTC-209 and GSK-126, respectively) and with siRNA knock-downs examining viral reactivation in MDV-transformed T-lymphoma cell lines (UA22 and UD35 cells). UA22 cells have been transformed by RB1B-pp38-smGFP (with a GFP tag downstream of pp38, a major early lytic phase antigen). To this end, viral reactivation has been examined through flow cytometry analysis of GFP expression. Viral reactivation has also been examined through RT-qPCR, and viral genome copy numbers via qPCR. Further interaction between Bmi-1 and Meq proteins was also characterized through bioimaging methods (co-localization, FRET, and FRAP analysis). Our data suggest that EZH2-mediated histone trimethylation is involved in MDV genome silencing during latency, and that Bmi-1-mediated repression is longer term and is primarily involved in cellular transformation. Moreover, we found that Meq-splice-variant proteins have increased affinity for Bmi-1, causing its translocation from the nucleoplasm into the nucleolus, and decreasing its mobility. Our findings extend our previous research and further associate MDV latency with cellular transformation pathways involving PRCs, pathways identified in numerous human malignancies, including Hodgkin's lymphoma.

Chapter 1

INTRODUCTION

Marek's disease (MD) is a pathology affecting chickens, causing immunosuppressive, inflammatory, and lymphoproliferative lesions to occur throughout the host (Osterrieder, Kamil, Schumacher, Tischer, & Trapp, 2006). Lesions develop in the liver, heart, spleen, kidneys, nerves (causing demyelination), and skin. Common signs of this disease include skin leukosis, dermatitis, paralysis, stunting, and neurological signs, including ataxia and torticollis. Ultimately this disease leads to the permanent immunosuppression of the host, followed by death (M.S Parcells, Burnside, & Morgan, 2012). This disease occurs worldwide, infecting essentially all chickens that come in contact with the infectious agent, making it one of the most serious poultry conditions (Calnek, 1986).

The infectious agent that causes this disease is Marek's disease virus (MDV), an avian *alphaherpesvirus* (Cebrian, Kaschka-Dierich, Berthelot, & Sheldrick, 1982) that causes lymphoma development in chickens as early as 2-3 weeks of infection (Ross, 1999), around the time that the virus enters latency. Indeed, there have been multiple reports of increased virulence of MDV, leading towards decreased vaccination efficiency (Witter, 1983) and (Witter, 1997).

Of the putative 103 proteins encoded by the MDV genome (Tulman et al., 2000) one oncoprotein is of particular interest to this work. This is Meq (Marek's disease virus EcoRI Q-fragment-encoded protein), a basic leucine zipper (b-ZIP)

protein, which shares many characteristics of other known oncoproteins (Levy et al., 2005).

Preliminary analysis has linked a latently-expressed splice-variant form of Meq (Meq/vIL8) to cellular Bmi-1 (B-cell Moloney leukemia virus integration site 1), a host protein part of polycomb repressive complex (PRC)-1. PRCs are transcriptional repressors that act via chromatin remodeling to silence specific genes, and are highly conserved across classes of organisms (Sparmann & van Lohuizen, 2006). The deregulation of these protein complexes often leads to increased proliferation, migration, and apoptosis resistance, contributing to cellular transformation and tumorigenesis (Sparmann & van Lohuizen, 2006).

The interaction between these Bmi-1 and Meq/vIL8 provides critical insight into the relationship between the establishment and maintenance of MDV viral latency within the host, and the mechanisms leading to MDV-mediated T-cell lymphoma formation. The remarkably short latency period that leads to MDV-induced T-cell lymphomas provides a unique model to examine virally induced oncogenesis (Lee, Liu, Cui, & Kung, 2003). The work described here builds on the Parcells lab discovery that a splice variant of the MDV-encoded viral oncoprotein Meq (Meq/vIL8) interacts with Bmi-1.

1.1 History of MDV

Jozsef Marek originally described what was later termed Marek's disease (MD) in 1907, identifying inflammation of major nerves associated with the paralysis of egg-laying chickens. Marek termed this phenomenon "range paralysis" (Marek, 1907). Alwin Pappenheimer, in further research describing the lesions found in range paralysis, began to examine the transmission pathway from host to host, as well as the

association of the agent with lymphomas, and coined the term, *neurolymphomatosis gallinarum* (Pappenheimer, Dunn, & Seidlin, 1929).

MD was described incompletely for the next thirty years, until the evolution of MDVs that caused tumors in ~12 weeks aided in the (Churchill & Biggs, 1968) isolation of the causative agent in cell culture. (Churchill & Biggs, 1968) identified what is now known as Marek's disease virus (MDV), and distinguished this from avian leucosis viruses (ALVs). Since this discovery, three antigenically-related serotypes have been described (Bulow & Biggs, 1975). Serotype 1 and 2 include naturally oncogenic strains of MDV, and smaller non-pathogenic strains, respectively. Serotype 3 consists of a nonpathogenic and likewise non-oncogenic herpesvirus of turkeys (HVT) (Davidson, Malkinson, & Weisman, 2002). Since their initial description in the late 1960s, MDV serotype-1 (MDV-1) strains have increased in virulence, apparently due to husbandry and vaccination practices (Atkins et al., 2013; Read et al., 2015; Witter, 1983, 1997).

Since the early 1970s, a naturally nonpathogenic strain of HVT had been used as the predominant vaccine against MDV on poultry farms (Okazaki, Purchase, & Burmester, 1970). Reports of increased mortality in HVT-vaccinated birds (vaccine breaks) led Witter to develop a nomenclature system, based on pathogenicity in HVT-vaccinated birds, of MDV strains (Witter, 1983).

In the US, HVT-vaccination provides protection (greater than 66%) against virulent (vMDV) strains, while very virulent (vvMDV) cause MD in greater than 33% of HVT-vaccinated chickens (Witter, 1983). This observation lead to the combining of an MDV-2 virus (SB-1) with HVT to for a bivalent vaccine that was implemented in the US by the mid-1980s (Calnek, Schat, Peckham, & Fabricant, 1983). Within a

decade of moving to bivalent vaccination, there was an emergence of a more virulent pathotype (very virulent plus) MDVs (vv+MDV) field strains. These strains cause early mortality, greater severity in lesions, occur in a shorter timeframe, and could cause MD in bivalently vaccinated chickens (greater than 33% MD incidence) (Witter, 1997).

The entire genome of a vvMDV-1 isolate, Md5, was sequenced in its entirety (Tulman et al., 2000), along with whole or partial representatives of the other two serotypes (Afonso et al., 2001; Izumiya, Jang, Ono, & Mikami, 2001; Kingham et al., 2001; Lee et al., 2003).

Additionally, MDV has since been reclassified into the subfamily *Alphaherpesvirinae* with the genus *Mardivirus* (Marek's disease-like virus) (Osterrieder, 2004). Further, the serotype classification system was replaced by recategorizing MDV-1, MDV-2 and MDV-3 serotypes as different viral species, based on DNA homology (Osterrieder, 2004).

Since the sequencing of the MDV genomes, cosmid and bacterial artificial chromosome-based infectious clones have been developed for the more systematic study of MDV gene function (Reddy, Sui, Wu, & Lee, 1999).

1.2 Pathogenesis of MDV

The pathogenesis of MDV was painstakingly dissected in the 1980s by a group at Cornell University and their model of infection remains relevant to our current understanding (Calnek, 1986). MDV infects its host solely via horizontal spread, with exposure occurring via inhalation of dander containing MDV virion particles (Calnek, 2001). Upon early phagocytosis by lung epithelium, MDV infects recruited bursa-derived lymphocytes (B-cells), macrophages, and thymus-derived lymphocytes (T-

cells) during replication but establishes latency primarily in CD4+ T-cells, which are also the target of malignant transformation within the host (Baaten et al., 2009; Shek, Calnek, Schat, & Chen, 1983).

MDV pathogenesis occurs through an intricate pathway involving four discernable phases: early cytolytic infection, latency, secondary cytolytic infection, and transformation (Calnek, 1986).

1.2.1 Early Cytolytic Infection

Early replication occurs after the virus is inhaled via infectious dander, occurring within a few days of exposure to the virus. Upon entry, the virus begins infecting B-cells, macrophages, and dendritic cells recruited to the lung epithelium (Baaten et al., 2009) At three days post infection (pi), the virus can be detected in lymphocytes located in the thymus and bursa of Fabricius, followed by cells in the spleen, where the virus will continue lytic replication and infect B-cells, T-cells, and macrophages in these organs (Baigent S. J., 2004).

At five days pi, interferon-gamma (IFNγ), and interleukin (IL-18) mRNA levels are increased in the spleen, correlating with an increased presence of MDV DNA in the spleen, as well (Baaten et al., 2009). Interestingly, Baaten *et al*. depleted B-cells from the host by performing bursectomies on chicks, leading to a significant decrease in viremia and increasing survival, providing evidence that B-cells are a necessary part of the MDV initial entry. Another hallmark of lytic infection is the downregulation of major histocompatibility complex (MHC) class I on the infected cell surface, causing the virus-infected cells to be less susceptible to lysis by CD8+ T-cells (Hunt et al., 2001). Recently, it was found that MDV specifically decreases the expression of MHC-I (BF-2) alleles essential for CTL activation, but not MHC-I (BF-

1) alleles essential for NK cell activation (Kim, Hunt, Parcells, van Santen, & Ewald, 2018).

Eventually, these organs will undergo lymphoid depletion and atrophy due to apoptosis of infected cells (Morimura, Hattori, Ohashi, Sugimoto, & Onuma, 1995). This destruction of tissue induces an innate response, leading to the expression and release of pro-inflammatory cytokines (IL-1β, IL-8, IL-18, etc.) and type I interferons, causing viral replication impairment (Kaiser, Underwood, & Davison, 2003).

1.2.2 Latency

The virus will continue lytic replication in the host for the next seven to ten days post infection (Baigent, Ross, & Davison, 1998). It is at this point that the virus enters latency in CD4+ T cells (Shek et al., 1983), but can establish latency in CD8+ T-cells as well (Baigent et al., 1998). This shift from lytic to latent infection takes place around 7-10 days post infection (dpi) in chickens challenged after two weeks of age. This shift takes longer (21dpi) in chickens infected at hatch (M.S Parcells et al., 2012). Latently infected T-cells express MHC class-II antigen (immune antigen, Ia), CD3, and alpha/beta T-cell receptor (TCR-2) (Schat, Chen, Calnek, & Char, 1991). Different subsets of T lymphocytes are transformed by MDV, but the presence of Ia is indicative of the fact that the T-cell must be in an active form for MDV to successfully infect them (Schat et al., 1991).

Upon entry into latency, the MDV genome will integrate into the telomeres of the host (Delecluse, Schuller, & Hammerschmidt, 1993). During latency, genes associated with lytic replication are no longer active, while MDV oncoprotein Meq is still expressed, both transcriptionally and translationally (Arumugaswami et al., 2009). A decrease in viral antigens, and a decrease in viral genomes also define the latent

phase of MDV. Only a handful of transcripts are expressed while the virus is in this latent state, and these transcripts originate from the border between the TR_L/IR_L regions of the MDV genome (Osterrieder, 2004). Other genes expressed during latency include UL36 (a major tegument protein), RLORF4, vTR and the LATs (Parcells M.S, 2012).

More recently, MDV-latency has been associated with histone modifications of the viral and host genome (Brown, Nair, & Allday, 2012; Mitra et al., 2015). Specifically, tri-methylation modifications on lysine 27 of histone 3 (H3K27me3) were observed on important immune-related pathways like MAP kinase signaling, several G protein-coupled receptors, and several cancer-related miRNAs (Mitra et al., 2015).

1.2.3 Secondary Cytolytic Infection

After establishment of latency, the virus can reactivate at peripheral sites and establish a time of secondary cytolytic infection (Calnek, 1986). MDV is disseminated throughout the periphery via latently infected T-cells within the infected bird. These T-cells acting as a 'Trojan horse' by which MDV can reactivate and cause secondary infection (Osterrieder et al., 2006). The feather follicle epithelium (FFE) is one of these secondary infection sites. Electron microscopy of lysates of the chicken FFE show fully-enveloped virions present (Calnek, Adldinger, & Kahn, 1970). The cells of the FFE that were infected by MDV, containing fully enveloped viral particles, were stratified squamous epithelium, a cell type that becomes detached along with molted feathers. This allows MDV to re-enter the environment from the infected host to infect a new host.

MDV re-enters cytolytic infection based on the immune response of the host. Latency is initially induced due to the immune response of the host. Aligned with this logic, it is immunosuppression that allows the latent-MDV infection to re-activate (Buscaglia & Calnek, 1988; Buscaglia, Calnek, & Schat, 1988).

1.2.4 Transformation

Lymphoma formation occurs in the host from 4 to 6 weeks post-infection, but with the evolution of vv+MDV strains, lymphomas can occur within 2 weeks (Witter, 1997). Additionally, vv+MDV strains induce stunting, severe dermatitis (red leg), and several neurological symptoms as well as lymphomas and a higher mortality (Witter, 1997). Transformed CD4+ T-cells accumulate within the host, but CD8+ and CD4-CD8- T-cell transformation have also been reported (Schat et al., 1991). T-lymphomas then lodge in the liver, spleen, heart, kidneys, peripheral nerves, and skin (Couteaudier, Courvoisier, Trapp-Fragnet, Denesvre, & Vautherot, 2016). These transformed T-cells are skewed towards a T regulatory (T_{Reg}) – like immunophenotype (Shack, Buza, & Burgess, 2008). These events lead to the permanent immune suppression and death of the host.

1.2.5 Viral Oncoprotein Meq

Meq (Marek's EcoRI-Q-encoded protein) is a viral oncoprotein encoded from repeats flanking the unique long region of the viral genome (IRL, TRL) as a 339-amino-acid protein in vvMDV and vv+MDV strains but is encoded as a longer (398-amino-acids) form in less virulent strains (Shamblin, Greene, Arumugaswami, Dienglewicz, & Parcells, 2004). Meq is a basic leucine zipper (b-ZIP) protein expressed in tumors and cell lines derived from tumors (Jones, Lee, Liu, Kung, &

Tillotson, 1992), and acts as a transcriptional regulator (Qian, Brunovskis, Rauscher, Lee, & Kung, 1995). Furthermore, when both copies of the *meq* gene are deleted, MDV-induced tumor formation significantly decreases, but replication of MDV was not inhibited (Lupiani et al., 2004).

1.2.5.1 Meq as a Transcriptional Regulator

Microarray analysis demonstrates differentially-regulated genes in Meq-transformed chicken embryo fibroblast (DF-1) cells (Levy et al., 2005), several of which were proto-oncogenes themselves (c-Jun, JTAP, JAK, and Hb-EGF). Additionally, Meq is characterized by the traditional hallmarks of a viral oncoprotein (induction of proliferation, blockage of apoptosis, binding to tumor suppressor proteins, etc) (Liu & Kung, 2000). In addition to forming homodimers, Meq also forms heterodimers with other leucine zipper proteins, most notably c-Jun, CREB, ATF-1,-2, and -3, all of which occur through dimerization at the zipper domain (Qian et al., 1995). Furthermore, Meq interacts with host proteins responsible for cell cycle regulation (CDK-2, p53, and Rb) as well as the transcriptional repressor, C-terminal-binding protein (CtBP-1) (Brown et al., 2006; Liu & Kung, 2000).

1.2.5.2 Localization of Meq

Meq localizes to the nucleus and nucleolus in MDV-transformed cells and in Meq over-expressing cells (Liu, Lee, Ye, Qian, & Kung, 1997; M. S. Parcells, Dienglewicz, Anderson, & Morgan, 1999). Utilizing Fluorescence return after photobleaching (FRAP) techniques full-length Meq was demonstrated to have rapid nuclear and nucleolar recovery (15 seconds) (Anobile et al., 2006), indicative of a transcription factor. Localization to the nucleus and nucleolus is mediated by stretches

of basic amino acids known as basic region 1 and 2 (BR1 and BR2) found in the amino terminus of Meq (Liu et al., 1997). BR1 and BR2 are located on the N terminus of Meq, with BR2 containing the primary nuclear localization signal (NLS) and the only nucleolar localization signal (NoLS) (Liu et al., 1997).

1.2.5.3 Meq Splice Variants

During infection *in vivo,* Meq transcriptional regulation is complex, with multiple splice variants being expressed (Peng & Shirazi, 1996). These variants use a common splice donor site within the leucine zipper domain of Meq and splice acceptors in RLORF4, and exons two and three of vIL8 (M.S Parcells et al., 2012). Splice variant-derived proteins (Meq/vIL8 and Meq/vIL8Δexon3) are expressed as MDV establishes latency and are common to lymphomas and cell lines established from lymphomas (M.S Parcells et al., 2012). This was observed via spleens harvested from chickens infected with MDV. Spleen lysates were analyzed at 7, 14, 21, and 38 days post-infection. Expression of Meq and Meq splice-variant protein levels were observed in spleen samples at weeks 3 and 4 post-infection, corresponding to the onset of latency and transformation phases. This pattern of expression indicates that Meq splice-variant proteins are exclusively expressed during latency and during transformation, suggesting that they have an important role in establishing and maintaining the latent state of the viral genome.

Additionally, tumors collected from infected birds along with a cell line established from one of the tumors (MDCC-UD35) both expressed high levels of Meq and Meq splice variant protein (M.S Parcells et al., 2012). These data revealed that Meq splice variants (Meq/vIL8 and Meq/vIL8Δexon3) were highly expressed at weeks 3 and 4 in the spleen, as well as in the primary lymphoma and the UD35 cell line. As

expression of splice variants correlated with the establishment of latency and T-lymphoma formation in chickens, these data suggested that co-expression of Meq and Meq splice variants likely have functions in MDV lytic gene repression and T-cell transformation.

To determine a possible mechanism by which Meq splice-variants may be altering cellular function, chicken macrophage cells (HTCs) were transfected with T7-tagged Meq and Meq/vIL8 expression vectors and immunoprecipitated with anti-T7 antibody-coated beads. These immunoprecipitates were sent to Mississippi State University, where liquid chromatography and tandem mass spectrometry (LC-MS/MS) was performed to identify binding partners, "guilt by association." One prominent peptide identified that was unique to the Meq/vIL8 pull down was the Polycomb complex protein Bmi-1 (peptide = DDY TLM DIA YIY TWR, e = 3.7 x 10-9) (Parcells, unpublished data).

1.3 Polycomb Repressive Complex Proteins

Polycomb repressive complexes (PRCs) were originally discovered and characterized in *Drosophila* and were shown to be silencers of *Hox* (Homeobox) genes, which aid in embryonic development (Ringrose & Paro, 2004). The subunits in *Drosophila* are much simpler than in mammals, which differ slightly from chickens, as well. The increased complexity of these complexes in different organisms presents a challenge when characterizing which subunits are responsible for which biochemical function (Simon & Kingston, 2013).

Both PRCs (PRC1 and PRC2) act cooperatively and sequentially through chromatin remodeling via histone modifications. PRC1 monoubiquitylates histone 2A while PRC2 trimethylates lysine 27 of histone 3. While both modifications have been

reported to be present on multiple silenced genes, it is unclear how these modifications truly work and whether they themselves act as the repressor or are merely indicators of repression (Simon & Kingston, 2013). Polycomb response elements (PREs) in *Drosophila* are responsible for PRC targeting, but this system is characteristically more complex in higher eukaryotes (Kassis & Brown, 2013).

Altered PRC expression levels have been associated with a myriad of human cancers including, but not limited to; Hodgkin's disease (HD) (F. M. Raaphorst et al., 2000), B-cell non-Hodgkin lymphoma (van Kemenade et al., 2001), non-small cell lung cancer (NSCLC) (Zhang, Tian, Sun, Liu, & Fang, 2017), bladder cancer (Liang et al., 2013), diffuse intrinsic pontine glioma (DIGP) (Mohammad et al., 2017), prostate cancer (Varambally et al., 2002), and breast cancer (Kirmizis, Bartley, & Farnham, 2003).

1.3.1 Polycomb Repressive Complex-1 (PRC1)

PRC1 is a regulator of cellular differentiation and development through the targeted modification of histones and chromatin, resulting in the silencing of gene expression (Sparmann & van Lohuizen, 2006). PRC1 genes are located at chromosome 10p11.23 in humans and play a major role in embryogenesis and maintaining adult stem cell renewal (Liang et al., 2013). They are responsible for mediating monoubiquitylation of histone H2A at lysine 119 (H2AK119ub) (Stock et al., 2007), causing compaction of poly-nucleosomes (Simon & Kingston, 2013). PRC1 exists as a multi-protein complex consisting of Bmi-1, RING, CBX, and others (Aloia, Di Stefano, & Di Croce, 2013).

1.3.1.1 B-lymphoma Moloney murine leukemia virus insertion region 1 (Bmi-1)

Bmi-1 was initially identified as a proto-oncogene that interacts with MYC in the generation of B-cell and T-cell lymphomas (Haupt, Alexander, Barri, Klinken, & Adams, 1991). Specifically, Bmi-1 represses expression of $p16^{ink4a}$/p19 ARF, which induces constitutive CDK4/6 activity, and targets p53 for degradation. Constitutive CDK4/6 activity causes an upregulation of the G1 and S phases of the cell cycle by phosphorylating retinoblastoma proteins (Rbs) dissociating them from the transcriptional activator E2F.

Bmi-1 is associated with the repression of p53-mediated apoptosis. This occurs via Bmi-1 inducing the degradation of p53 via repression of *cdkn2a*. This tumor-suppressor locus encodes INK4A and ARF, the latter of the two induces p53 via the inhibition of Mdm2 (Sherr, 2001). Furthermore, Bmi-1 is upregulated and interacts with c-Myc, potentially being the driving factor that is promoting B- and T-cell lymphomas in mice (van Lohuizen, Frasch, Wientjens, & Berns, 1991).

Additionally, Bmi-1 contains a RING (really interesting gene)-finger domain, containing an E3 ubiquitin ligase that is identified to belong to the RAD18 super family (Hemenway, Halligan, & Levy, 1998). Indicating that Bmi-1 plays a functional role in the ubiquitylation of lysine 119 of histone 2A.

1.3.1.2 RING-finger domain proteins

PRC1 contains RING-finger domain proteins Ring1A and Ring1B, both functioning as E3 ubiquitin ligase proteins through their RING-finger domain (Leeb & Wutz, 2007). Aside from this E3 ligase role Ring1B plays in PRC1, it is recruited with the transcriptional repressor E2F6 (Trimarchi, Fairchild, Wen, & Lees, 2001), along with associations with other proteins from PRC1. Interestingly there is a significant

decrease of other PRC1 proteins (Bmi-1 and Ring1 and YY1-binding protein (Rybp)) in *Ring1B* knockout mice, but there is no detectable difference in transcript levels (Leeb & Wutz, 2007).

1.3.1.3 Chromobox protein (CBX)

Chromobox protein (CBX) is a subunit of canonical PRC1 (Aloia et al., 2013). Pc, the *Drosophila* homologue of chromobox protein (Cbx), interacts with the trimethylated ($H3K27Me_3$) marker found on the consensus sequence, AR**K**S, near the N-terminus of histone 3 (Fischle et al., 2003). Indeed, Pc chromodomain had a stronger binding affinity to the $H3k27me_3$ marker than heterochromatin protein 1 (HP1), another conserved chromosomal binding protein associated with gene silencing (Eissenberg & Elgin, 2000; Fischle et al., 2003). Furthermore, colocalization assays reveal a strong interaction between Pc and $H3K27me_3$ but no interaction between Pc and $H3K9Me_3$, and area of the N terminus of histone 3 that shares an identical AR**K**S consensus sequence (Fischle et al., 2003).

1.3.2 Polycomb Repressive Complex-2 (PRC2)

PRC2 regulates gene suppression through the targeted trimethylation of histones regulating certain genes, although the mechanisms of specific gene recognition are still unclear (Aloia et al., 2013). In mammals, enhancer of zeste homolog 2 (EZH2) is responsible for the enzymatic trimethylation activity of PRC2 (Margueron et al., 2008). PRC2 is comprised of other subunits essential for complex assembly and enzymatic activity as well, including; Suz12, and EED (embryonic ectodermal development) (Aloia et al., 2013).

1.3.2.1 Enhancer of Zeste Homolog 2 (EZH2)

Part of PRC-2, EZH2 interacts with lysine 27 on histone 3, trimethylating at the AR**K**S consensus sequence, creating a binding site for PRC1 proteins (Cao et al., 2002). EZH2 is expression is associated exclusively with proliferating tissues (Margueron et al., 2008). Alternatively, EZH1 (functioning in a mutually exclusive form of PRC2), does not exhibit any methyl-transferase activity, but is still responsible for transcriptional repression and interacts with other proteins from PRC2 (Suz12 and EED) (Margueron et al., 2008). Interestingly, both EZH2 and -1 have a SET domain (domain common to Su(var) 3-9, EZH, and Trithorax), which houses the enzymatic active site for methyltransferase activity (Margueron et al., 2008). EZH2 is inactive when independent and can only act enzymatically when assembled with the Suz12 and EED subunits (Pasini, Bracken, Jensen, Lazzerini Denchi, & Helin, 2004).

EZH2 over-expression has been associated with multiple forms of human malignancies. Microarray analysis identified EZH2 being one of many genes upregulated in prostate cancer (Varambally et al., 2002). Confirmatory analysis of protein expression levels of EZH2 in metastatic prostate cancer (METs) compared to benign prostate samples supported these data (Varambally et al., 2002) providing a significant correlation between EZH2 expression levels and reoccurrence in prostate cancer patients. EZH2 is also implemented in diffuse intrinsic pontine glioma (DIPG). Indeed, lysine 27 mutation to methionine on histone 3 (H3K27M) causes a stark decrease in trimethylation activity, presumably due to EZH2 SET domain being unable to properly methylate the methionine (Mohammad et al., 2017). Additionally, GSK343 (a selective EZH2 inhibitor)-treatments leads to a significant decrease in cellular proliferation and colony-forming activity (Mohammad et al., 2017).

Additionally, EZH2 (along with Bmi-1) deregulation is associated with B-cell non-Hodgkin lymphomas (B-NKLs) and is found to be co-expressed with Bmi-1 in Hodgkin-Reed-Sternberg (HRS) cells (van Kemenade et al., 2001). Co-expression of Bmi-1 and EZH2 in follicular B-cells is a rarity, so observing this in HRS cells in Hodgkin lymphoma provides strong evidence that the deregulation of these PRC proteins gives rise to lymphoma formation (van Kemenade et al., 2001). This finding is particularly relevant to MDV-induced lymphomas, as the transformed component of the T-lymphomas are $CD30^{HI}$ expressing (Burgess & Davison, 2002; Burgess et al., 2004).

1.3.2.2 SUZ12

SUZ12 is an integral subunit in PRC2, being required for EZH2 methyltransferase activity to occur (Cao & Zhang, 2004). Furthermore, *Suz12* is necessary for early embryonic development in mice, with *Suz12* mutant mice dying during early stages post-implantation and displaying severe developmental defects (Pasini et al., 2004).

In human gastric cancer (GC) tissues, SUZ12 mRNA and protein expression levels were significantly upregulated in patients with GC compared to normal patients (Xia et al., 2015). High expression of SUZ12 is correlated to poor survival. Additionally, SUZ12 knock-downs using siRNAs led to decreased cell viability and decreased proliferation in two separate GC cell lines (Xia et al., 2015).

1.3.2.3 Embryonic Ectoderm Development (EED)

EED is a core subunit in PRC2, contributing to the trimethylation of H3 (Obier et al., 2015). Indeed, in *Eed* knock-out embryonic stem (ES) cells and trophoblast stem (TS) cells, a stark reduction in H3K27me$_3$ was observed (Montgomery et al., 2005), as well as a reduction in mono- and di-methylated lysine 27 of H3 (H3K27me$_1$ and H3K27me$_2$, respectively). These results were further confirmed through EED rescue experiments, where *Eed* transfection in knock-out cell lines restored H3K27 methylation defects (Montgomery et al., 2005). Furthermore, EED knock-out cell lines also exhibited a decrease in EZH2 protein levels, but not a decrease in *Ezh2* mRNA expression levels, indicating that EED may act in a way to stabilize EZH2 (Montgomery et al., 2005).

EED provides a positive feedback loop for PRC2 through binding H3K27me$_3$ and activating the enzymatic methyltransferase activity of EZH2 (Obier et al., 2015). Knockout of EED in embryonic stem cells (ESCs) shows a drastic difference in pluripotency gene expression compared to the WT ESCs (Obier et al., 2015).

1.3.3 PRCs and MDV-Mediated Transformation

The transformed component of MDV-induced lymphomas are CD30^{HI}-expressing T-cells with a T$_{REG}$-like immunophenotype (Burgess & Davison, 2002; Shack et al., 2008). In the targeted proteomic examination of CD30^{HI} cells fro RB-1B-induced lymphomas, there was a statistically significant increase in PRC-2-associated proteins: EED (7-fold increase), EZH2 (2-fold increase), JARID2 (5-fold), and RBBP7 (1.5-fold), while PRC-1 was largely unrepresented (Shack et al., 2008). This finding was not surprising, as Meq splice variant proteins are tightly-bound to

chromatin (as are PRC-1 proteins), and require nuclease treatment to solubilize these (Parcells M.S, 2012).

The study of the importance of PRCs to cancer biology has been greatly facilitated by the identification of pharmacological inhibitors for Bmi-1 and EZH2 (PTC-209 and GSK-126, respectively).

1.4 Chemical Inhibitors PTC-209 and GSK-126

PTC-209 is a Bmi-1 chemical inhibitor (Kreso et al., 2014), while GSK-126 is the chemical inhibitor for EZH2 (McCabe et al., 2012). Their mechanisms of action are described, briefly, below:

1.4.1 PTC-209

PTC-209 is a small molecule Bmi-1 inhibitor that acts by lowering Bmi-1 transcript levels (Kreso et al., 2014), by a currently unidentified mechanism. Indeed, treatment with PTC-209 shows a decrease in luciferase activity, in vectors containing luciferase open reading frames (ORFs) flanked by areas under post-transcriptional control of Bmi-1. Additionally, PTC-209 lowered Bmi-1 protein levels in a dose-dependent manner in human colorectal cells and human fibrosarcoma cell lines, but not human embryonic kidney cells (HEK293) (Kreso et al., 2014).

Furthermore, PTC-209 has been shown to be a potential treatment for biliary tract cancer (BTC) (Mayr et al., 2016). PTC-209 treatments negatively affect cellular viability in a dosage dependent manner, along with Bmi-1 protein and mRNA expression levels (Mayr et al., 2016). Lysine 119 ubiquitylation markers on histone 2A were also shown to be decreased post-PTC-209 treatments (Mayr et al., 2016). OF relevance to the present work, is the finding that PTC-209 induces apoptosis in a

spectrum of human lymphoid and myeloid cell lines and cells-derived from leukemia patients (Nishida et al., 2015).

1.4.2 GSK-126

GSK-126 is an *S*-adenosyl-methionine (SAM)-competitive small molecule inhibitor of EZH2 methyltransferase activity (Takeshima, Wakabayashi, Hattori, Yamashita, & Ushijima, 2015). Treatments with GSK126 showed marked decrease in tumor volume, this phenomenon being increased with the addition of DNA demethylating agent 5-aza-2'-deoxycytidine (Takeshima et al., 2015). Evidence further points to GSK126's ability to inhibit EZH2 via measurements of reactivation of silenced PRC2 target genes through decreasing global H3K27me$_3$ levels (McCabe et al., 2012). GSK126 is highly selective for EZH2 and shows non-selectivity towards other methyltransferases, indicating that it is an attractive option for targeted EZH2 down-regulation (McCabe et al., 2012). In diffuse large B-cell lymphoma (DLBCL) cells GSK126 treatments show a marked decrease in proliferation, providing further evidence that this EZH2 inhibitor could be used as a therapeutic treatment for lymphoma patients (McCabe et al., 2012). Contrary to previous reports from McCabe at al., reports indicating that GSK-126 does not decrease EZH2 protein levels have been published (Takeshima et al., 2015), but H3K27me$_3$ markers have been downregulated due to these GSK-126 treatments at 6μM.

1.5 Hypothesis of Thesis Research

Given the observations that: (a) Meq splice variant-derived protein expression corresponds to MDV latency and transformation phases, (b) that splice variant protein Meq/vIL8 interacts with and co-localizes with PRC-1 protein, Bmi-1, (c) PRC-2

proteins, which lead to recruitment and tight-binding of PRC-1 proteins to chromatin are upregulated in the transformed component of MDV-induced lymphomas, and (d) dyregulation of PRC proteins are clinically relevant in a host of human malignancies, especially leukemias and lymphomas, I hypothesize that:

(1) Meq splice variant-proteins bind PRC proteins specifically and translocate them to specific sites, *in vivo*.

(2) Pharmacological inhibition of PRCs will result in apoptosis, decreased proliferation and/or reactivation of the MDV genome from latency.

(3) Specific inhibition of PRCs, via siRNAs, will result in induced apoptosis and/or reactivation of the MDV genome from latency.

Completion of this research will tie the MDV establishment of latency directly to its transformation and progression mechanisms, and may ultimately provide a means by which human leukemias and lymphomas may be controlled or prevented through targeting of these pathways.

Chapter 2

MATERIALS AND METHODS

2.1 Cells and Viruses

Chicken macrophage (HTC) cells were used for transfections for co-localization, fluorescence resonance energy transfer (FRET) and fluorescence return after photobleaching (FRAP) experiments (described in 2.11) (Rath, Parcells, Xie, & Santin, 2003). HTC cells were maintained in Dulbecco's modified eagle medium (DMEM), containing 10% fetal bovine serum (FBS), 1X PSN, 4mM L-Glutamine, 2mM sodium pyruvate, and 1X amphotericin. HTC cells were sun-cultured, as needed, using TrypLE express enzyme (1X) (Life Technologies).

Marek's disease cell culture (MDCC) cell lines UA22 (Prigge, Majerciak, Hunt, Dienglewicz, & Parcells, 2004) and UD35 cells (Kumar et al., 2012) were used in siRNA and chemical inhibitor knock-down studies (described in 2.3 and 2.4) and were maintained in Iscove's IITS medium (Iscove's modified Dulbecco medium) supplemented with 20% FBS, 10% chicken serum, 1X Insulin, Transferrin, Selenium, [ITS], 10% tryptose-phosphate broth [TPB], 4mM L-glutamine, 2mM sodium pyruvate, 2μM beta mercaptoethanol [βME], 1X PSN, and 1X amphotericin B.

MDCC-UA22 cell has a soluble-modified green fluorescent protein (smGFP) eopen reading frame downstream of the MDV pp38 gene (Prigge et al., 2004). Assays including UA22 cells were performed with the assumption that smGFP expression was an indicator of pp38 expression, indicating lytic cycle reactivation. Both MDV-

transformed T-cell lines are non-adherent lymphoblastoid cell lines and were sub-cultured by 1:5 to 1:20 dilution into fresh medium.

2.2 Plasmid Construction

To characterize the interactions of Meq and Meq splice-variant proteins with PRC proteins, expression vectors for transfection purposes were constructed. To do this the *meq, meq/vIL8* and *meq/vIL8Δexon3* genes were cloned a cDNAs from RNA purified from RB-1B--transformed T-cell line UD14 (M. S. Parcells et al., 1999). Epitope-tagged (T7, HA, or Myc) versions of Meq, Meq/vIL8 and Meq/vIL8Δexon3, were generated via PCR, confirmed by sequencing and subcloned into expression vectors pBKCMV, peCFP-N1 and peYFP-N1.

Chicken cellular polycomb repressive complex proteins Bmi-1 and EED were cloned as cDNAs from RNA purified from MDV (strain RB-1B)-induced primary lymphomas.

For expression vector construction, high fidelity Taq polymerase was used for polymerase chain reaction (PCR). Amplicons were cloned via Topo-cloning into vector pCR2,1 Topo (Invitrogen). Te primers used for chicken Bmi-1 amplification were *Nhe* I-chBmi-1 for (5'-GCTAGCatg cac cgg acg acc agg atca a-3') and *Eco*RI-stop-*Bam*HI-chBmi-1 rev (5'-gaattc aggatcccc AGC GTA ATC TGG AAC ATC GTC TGG GTC CAT gcc gga cga agt ggc tga gga-3'). These primers inserted unique restriction sites at the 5' (*NheI*) and 3' (*Eco*RI-stop-*Bam*HI) ends, as well as an hemagglutinin (HA)-tag (MYPTDVPDYA) fused in-frame at the C-terminus.

A sequence-confirmed clone was digested with *Nhe*I and *Bam*HI for insertion into pBKCMV and pLVW-IRES-Neo for expressing the epitope-tagged version in a plasmid and lentivirus vector system, respectively. For fluorescent protein expression

ectors, the chBmi-1 gene was inserted into peCFP-N1 and peTFP-N1 after digestion with *Nhe*I – *Eco*RI.

2.3 siRNA assays

To specifically associate changes in cell growth and/or virus reactivation with Bmi-1 and EZH2, we designed siRNAs to knock-down their expression. In using this method of post-transcriptional gene silencing, viral latency maintenance was examined in MDV-transformed T-cells (UD35 and UA22 cells). The siRNAs used were designed by Integrated DNA Technologies (IDTDNA.com) with their sequences given below:

(1) Bmi-1 siRNA (siBmi-1):

5’rCrGrArGrArUrArArUrArArGrCrUrUrArUrCrCrArUrUrGAG

5’rCrUrCrArArUrGrGrArUrArArGrCrUrUrArUrUrArUrCrUrCrGrUrC

(2) EZH2 siRNA (siEZH2):

5’rCrArArArCrArCrCrArArUrArArArGrArUrGrArArGrCrCAA

5’rUrUrGrGrCrUrUrCrArUrCrUrUrUrArUrUrGrGrUrGrUrUrGrArC

(3) Control Scramble RNA (scRNA):

5’rArArUrUrGrUrCrCrArArArCrGrUrGrUrCrArCrGrUrUrUTT

5’rArArArArArCrGrUrGrArCrArCrGrUrUrUrGrGrArCrArArUrUrGrC

Nucleotides denoted with ‘r’ to left of the single letter nomenclature indicate ribose-linked nucleotides, while nucleotide letters with no ‘r’ denotation indicate deoxyribose-linked nucleotides.

All siRNA oligos were received at 2nmole and resuspended to 100μM stock concentration in nuclease-free water. Further dilutions to a 10μM final working

concentration were achieved by adding 90μL of nuclease-free water to 10μL of 100μM stock.

2.4 Transfections

All transfections (both siRNA and plasmid) were conducted using Lipofectamine 2000 transfection reagent (ThermoFisher).

2.4.1 Transfections for Protein Co-Localization, Fluorescence (Forster) Resonance Energy Transfer (FRET), and Fluorescence Return After Photobleaching (FRAP) Analysis.

For co-localization, FRET, FRAP, and high-resolution imaging, transfections were conducted using HTC cells. Meq (pT7-Meq-eYFP), Meq splice-variant (pT7 or Myc-Meq/vIL8-eYFP) and pT7-Meq/vIL8Δexon3-eYFP, and PRC protein vectors (pBmi-1-HA-eCFP and EED-CFP) were transfected at ~100 – 200 ng/well in ether (12)-well dishes or 4-chamber glass slides (Lab-Tek II) using a protocol recommended by the manufacturer (ThermoFisher). Briefly, cells plated at ~70 – 80% confluency had their growth medium removed and replaced with DMEM without antibiotics and antimycotic (transfection medium). DNA/liposomes were generatdd using this medium and were diluted separately, mixed 1:1 (DNA/medium, DNA/Lipofectamine), and dropwise added to cells after mixing. Cells were transfected in transfection medium for 2 – 3 hours, after which complete growth medium was added. Cells were observed 16 – 24 hours post-transfection and either fixed (with 1% paraformaldehyde) or kept alive (for FRET, FRAP, and high-resolution imaging).

In addition to the full-length Meq protein expression vectors (Meq, Meq/vIL8, and Meq/vIL8Δexon3), a number of domain deletion and mutation vefctors were used to establish the domains necessary for interaction with Bmi-1. These were:

(1) pT7-Meq-bZIP-eYFP (YFP fused at *Kpn* I site adjacent to the Meq leucine zipper domain – lacks all of C-terminus)

(2) pT7-Meq/vIL8-bZIP-eYFP, (YFP fused adjacent to the Meq/vIL8 leucine sipper domain which differs from the Meq leucine zipper – lacks exons 2 and 2 of vIL8)

(3) pMeq-AVEFT-eCFP and eYFP (FP fused to form of Meq having a mutated CtBP – interaction domain, *PLDLS*, essential for CtBP-binding, which was changed to the sequence *AVEFT* in the N-terminus) (Brown et al., 2006).

(4) pMeq/vIL8-AVEFT-eCFP and eYFP (FP fused to mutated form of Meq/vIL8, has *PLDLS* mutated to *AVEFT* in N-terminus).

Co-transfections were performed, combining PRC protein vectors with Meq protein expression vectors.

2.4.2 siRNA Transfections

For siRNA assays, transfections were performed using MDCC-UA22 and -UD35 cells using Iscoves transfection medium along with Iscove's IITS medium (as described in 2.1). Both UA22 and UD35 cells were washed through Iscove's IITS complete medium and resuspended in Iscove's transfection media to $2x10^5$cells/mL and plated into either 6-well dish (Falcon) or 12-well dishes (CellTreat) and stored at 41^{o}C while preparing siRNA treatments.

Treatments were prepared using 10μM stock of scRNA, siBmi-1, or siEZH2 and diluting these siRNAs to a final 2x concentration of 60 pmol/mL in Iscove's transfection medium, mixed with an equal amount of Iscove's transfection media + 5μL of Lipofectamine 2000. This mixture sat for 20 min to form liposomes and then

was added to $2x10^5$cells in a 12-well dish. Cells were incubated at 41^{o}C with liposomes for 3-4hrs and then Iscove's transfection media + 20% FBS was added and cells were returned to 41^{o}C for overnight incubation.

Oligo (siRNA) transfections were carried out following the transfection protocol detailed in 2.4 using a working concentration of 30 pmol/mL for Bmi-1, EZH2, scRNA control siRNA, and fluorescent control oligos.

2.5 Chemical Inhibitor Assays

Chemical inhibitor treatments with GSK126 and PTC-209 were conducted in a similar fashion and therefore the common protocol is given. GSK126 was diluted from a 9.5mM stock concentration (in dimethyl sulfoxide, DMSO) to three separate working concentrations to measure dosage response. They were; 10, 20, and 40μM (2x) for final working concentrations of 5, 10, and 20 μM. PTC-209 was diluted from a 0.5mM stock concentration in DMSO to three separate working concentrations, as well (5μM, 10μM, and 20μM as 2x concentrations).

As a control for MDV reactivation, sodium butyrate (NaB), a histone deacetylase (HDAC) inhibitor was used as a positive control at 3mM.

Cells were plated into 12-well dishes in Iscove's IITS growth medium at $1x10^6$cells/mL and placed in 41^{o}C incubator while treatments were prepared. Treatment was added to existing number of cells 1:1, creating the 1x concentration for each dosage treatment group for PTC209, GSK126, and NaB.

2.6 Flow Cytometric Analysis

Flow cytometry samples were prepared for siRNA assays and chemical inhibitor assays by removing 0.5mL of sample at each time point, pelleting cells via

centrifugation, and fixing cells in 4% paraformaldehyde for 30min with agitation. Cells were then washed via the addition of flow cytometry wash buffer (1xPBS, pH 7.4 + 1% BSA + 0.1% NaN_3) and pelleted at 1,500rpm for 5min. After three washes, cells were resuspended in 250μL and stored at 4°C until fluorescence-activated cell sorting (FACS) analysis.

For UD35 intracellular staining, mouse monoclonal anti-EZH2 (DSHB, PCRP-EZH2-1B3), mouse monoclonal anti-Bmi-1 (DSHB, PCRP-BMI1-1G9), and mouse monoclonal anti-pp38(H19.47) antibodies were used at 1:200 in antibody diluent (1xPBS, pH 7.4 + 3% goat serum + 1% BSA + 0.1% saponin + 0.1% NaN_3). Goat anti-mouse Ig ALEXA 488 secondary antibody was used for each primary staining treatment, diluted to 1:200 in antibody diluent.

Intracellular staining was performed on UD35 cells used for siRNA assays to examine EZH2, Bmi-1 and pp38 protein levels. For siRNA treatments, the internal fluorescent siRNA (detectable in FL-3 channel) was used to select for transfected cells. Flow cytometry samples collected (as described previously) were separated into individual tubes and stained with primary and secondary antibodies, as described, above.

Flow cytometry is performed on a Becton-Dickinson FACSCalibur flow cytometer. For each sample, 10,000 events were captured and acquired data was analyzed using CellQuest® software.

2.7 Western Blotting

Protein isolation was performed by taking 0.5mL of sample (same for all cell types/treatment types), pelleting cells and resuspending in radioimmunoprecipitation assay (RIPA) buffer (10mM Tris, pH 7.5, 1mM EDTA, 100mM NaCl, 0.1% SDS, 1%

sodium deoxycholate, 1% NP-40, 1mM DTT, 1x protease inhibitors, 0.1mM Aprotinin, 0.1mM Leupeptin, 0.1mM Pepstatin A, and 0.1mM PMSF). After cells are resuspended in RIPA buffer + inhibitors, cell were lysed via three cycles of freeze/thaw (between liquid nitrogen (LN2) and 37^{o}C bath). After final thaw, cell lysates were subjected to DNAse I treatment (50 µl of 4mg/ml) for 1 hour, with frequent agitation. Following DNAse I treatment cells were pelleted at 14,000rpm for 10 minutes, and supernatant was transferred to a fresh tube where BCA was performed to measure protein concentration.

Protein samples are loaded at 5µg concentrations into NuPAGE^{TM} 4-12% Bis-Tris protein gels, 1.0mm, 12-well (ThermoFisher) and run using NuPAGE SDS MOPS running buffer (ThermoFisher) for 50 minutes at 200 volts. Following protein separation, proteins were transferred onto nitrocellulose membrane in transfer buffer (25mM Tirs, 190mM glycine, 20% methanol, 0.1%SDS) at 20 volts for 150 minutes. Following transfer, the membrane was blocked using SuperBlock^{TM} blocking buffer (ThermoFisher) for 1 hour. Membranes were then washed in 1xPBS + 0.05% Tween (PBST), and probed with Bmi-1, EZH2, or GAPDH (control) primary antibodies at a 1:750 dilution in blocking solution. Blots were incubated at room temperature for 1 hour with agitation, washed 3X with PBST buffer and probed with secondary antibody (HRP-conjugated goat anti-mouse IgG whole molecule), diluted 1: 10,000 in blocking solution for 30 min. Blots were then washed three times with PBST with a final wash in 1XPBS, pH 7.4. For visualization of antibody-binding, Pierce^{TM} enhanced chemiluminescence (ECL) western blotting substrate (ThermoFisher) was added 500µL:500µL to the blots and these were imaged using Bio-Rad Chemidoc^{TM} Imaging System.

2.8 DNA Isolation

At each time point, for both siRNA and chemical treatment assays, 0.5mL of sample was collected and pelleted at 5,000rpm for 30 seconds. This pellet was resuspended in 200uL of 2x proteinase K (PK) solution (20mM tris, pH 7.5, 2mM EDTA, 150mM NaCl, 0.5% SDS, 2mg/mL proteinase K) and incubated at 37^{o}C for 1 hour. Samples were subjected to phenol:chloroform, and chloroform extractions followed by precipitation using isopropanol. DNA was finally pelleted for 10 minutes at 14,000rpm, washed with 70% ethanol, air dried and resuspended in 1X TE, pH 7.5. Final DNA concentrations are measured using Nanodrop ND 1000- spectrophotometer and then stored at 4^{o}C until qPCR analysis.

2.9 RNA Isolation and Reverse Transcriptase

Total RNAs for both siRNA and chemical inhibitor assays were collected using identical protocols. Essentially, 0.5mL of each sample was collected via centrifugation and RNA extraction via the Qiagen RNeasy Plus Mini Kit (Qiagen) with DNAse treatment, according to the manufacturer. All RNA samples were eluted from RNeasy spin columns using 30µL of RNase-free water and final RNA concentrations were measured using Nanodrop ND 1000-spectrophotometer and stored at -80^{o}C until used.

Applied Biosystems MultiScribe^{TM} Reverse Transcriptase (RT) was used to generate random-primed cDNAs for qPCR analysis. For each set of reactions, a Master-mix was made using: 10x RT buffer (2µL per sample), 25x dNTP Mix (0.8µL per sample), 10x RT random primers (2µL per sample), MultiScribe RT (1µL),

Nuclease Free water (depending on RNA sample volume). For each cDNA synthesis, 200ng of total RNA sample was used.

Samples were briefly centrifuged after mixing and placed in an Eppendorf Mastercycler gradient thermocycler using the following program (as recommended by the manufacturer): 10 minutes at 25^{o}C, 120 minutes at 37^{o}C, 5 minutes at 85^{o}C, followed by a hold period at 4^{o}C. All samples were removed from thermocycler immediately after run completion and stored at -20^{o}C until analyzed via qPCR.

2.10 Quantitative PCR

All qPCR analysis was performed on BioRad MyIQ2 real time PCR machine (BioRad). qPCR was used to examine viral genomic copy numbers to assess MDV reactivation from latency. qPCR was also used to quantitate EZH2 and Bmi-1 mRNA expression levels to ensure siRNA knockdown efficiency. DNA samples (described above) were utilized to examine MDV viral genome levels compared to host genome levels to properly assess MDV genomic reactivation.

Primers used to quantitate host genome copy number were for chicken ovotransferrin, a host glycoprotein, with sequences:

Forward – 5'CACTGCCACTGGGCTCTG-3'

Reverse – 5'GCAATGGCAATAAACCTCCAA-3'. Primers used to quantitate viral genome copy number were targeted to gB (Baigent et al., 2005; Neerukonda, Katneni, Bott, Golovan, & Parcells, 2018).

EZH2 and Bmi-1 mRNA levels were quantitated from cDNA, converted from RNA isolated from samples (discussed in 2.9). Bmi-1 and EZH2 expression levels were compared to GAPDH and 18S mRNA expression levels and analyzed through

the delta-delta Ct ($\Delta\Delta C_T$) method (Livak & Schmittgen, 2001). The sequences used for detection of Bmi-1 expression were:

Forward – 5'-ATGCTGCCAATGGCTCTAA-3'

Reverse – 5'-GTTCCAGTCTGTTCTGGTCAA-3'

For EZH2 expression detection, the primers were:

Forward – 5'-GGGTACAGCGGAAGAATTGA-3'

Reverse – 5'-GTGTGCATTCAGGAGGAAGA-3'

The GAPDH primers used were based off a prior publication (Neerukonda, Katneni, Golovan, & Parcells, 2016):

Forward – 5'-GGAGTCCACTGGTGTCTTCA-3'

Reverse – 5'-AGCACCACCCTTCAGATGAG-3'

All qPCR was done using a SYBR green master mix (BioRad). Samples (DNA and cDNA) were loaded (at a 1μL volume) into a 96-well plate format in duplicate, along with 19μL of master mix (SYBR Green, 10μL per sample; Forward primer, 0.4μL per sample; Reverse primer, 0.4μL per sample; nuclease-free water, 8.2μL). Plates were then spun at 3,000rpm for 10 minutes at 15ºC to ensure samples were oriented in the bottom of the wells. Samples were then loaded into MYIQ2 real time PCR machine and run using this program: 3 minutes at 95ºC, 40 cycles of: 10 seconds at 95ºC and 30 seconds at 55ºC, followed by a melt curve: 1 minute of 95ºC and 1 minute of 55ºC. Ct values for genome copy number assays were then analyzed using standard curves generated using the cloned gB and chicken ovotransferrin genes.

2.11 FRET and FRAP Analysis and High-Resolution Localization Images.

All images and microscopy techniques were performed on a Zeiss 710 LSM T-PMT confocal microscope in the bioimaging core facility at the Delaware Biotechnology Institute (DBI). These images were taken using a 40x oil emersion objective lens. Images and FRET and FRAP data were analyzed using Zeiss Zen® analysis software.

2.11.1 Fluorescence Resonance Energy Transfer

Fluorescence (Förster) resonance energy transfer (FRET) is an imaging technique used to determine protein-protein interactions, based on proximity of the fluorophores (Kenworthy, 2001). Essentially, a fluorophore having a fluorescence emission spectrum overlapping the absorption spectrum of a nearby fluorophore (i.e., eCFP and eYFP, respectively) result in the donation of photons from the shorter wavelength fluorophore (eCFP) to the acceptor fluorophore (eYFP), making it appear brighter. In our studies, FRET was measured using the acceptor photo-bleaching method, in which the eYFP-tagged protein is photo-bleached using a high energy laser stimulation (A_{514}), which does not bleach the donor fluorophore (Karpova et al., 2003; Kenworthy, 2001). The intensity of the donor and acceptor are measured over time prior to and after this bleaching event and an increase in the donor signal is an indication of FRET.

Using a CFP-tagged Bmi-1 vector and co-transfecting this with YFP-tagged versions of Meq and Meq-splice-variant vectors, we performed co-localization and protein-protein interactions via acceptor bleaching FRET analysis. Utilizing the 514nm laser line, we measured expression of co-transfected Bmi-1-CFP after photo-bleaching the various co-expressed YFP-tagged Meq proteins.

2.11.2 Fluorescence Return After Photobleaching.

Fluorescence return after photobleaching (FRAP) is a technique utilized to determine the mobility of proteins in an *in vivo* setting (Yguerabide, Schmidt, & Yguerabide, 1982).

In this work FRAP was performed by using a high energy 405nm laser pulse to bleach the CFP-tag of the transfected Bmi-1 protein. Return of fluorescence to the bleached region of interest was then measured over time (3 second intervals) for 2 minutes. This experiment was performed on Bmi-1-CFP single transfection HTC cells as a negative control, as well as co-transfections of Bmi-1-CFP with YFP-tagged versions of Meq, Meq/vIL8, Meq/vIL8Δexon3, Meq-AVEFT, Meq/vIL8-AVEFT, Meq-bZIP, and Meq/vIL8-bZIP (detailed in 2.4.1).

2.11.3 Localization Images.

Images used to analyze co-localization were taken from FRET and FRAP analysis. Co-localization was not specifically measured by any particular metric as this was covered by FRET analysis.

2.12 Statistics.

Analysis of data was done using one-way analysis of variance (ANOVA) and Tukey-Kramer tests adapted from the “Handbook of Biological Statistics” (McDonald, 2014). All significant data was determined with a p-value lower than 0.05.

Chapter 3

RESULTS

3.1 Chemical Inhibition Assays.

Chemical inhibitors PTC-209 and GSK126 are inhibitors of Bmi-1 and EZH2, respectively (Kreso et al., 2014; McCabe et al., 2012). These inhibitors were used to analyze PRC protein involvement in the maintenance of MDV latency. For these studies, chemical inhibitor assays were conducted using UA22 (RB-1Bpp38smGFP-transformed), UD35 (RB-1B transformed) and UA53 (TK, a vv+MDV, transformed) cells. UA22 cells were initially used to assess smGFP downstream of the pp38-coding gene after treatment, with smGFP expression used as an indicator for turning on pp38 gene expression, which is used as a measure of MDV reactivation from latency, as pp38 expression is repressed during latency.

3.1.1 Induction of smGFP-expression in UA22 Cells by PTC-209 and GSK-125.

Chemical inhibitors of Bmi-1 and EZH2 induced significant smGFP expression in UA22 cells compared to vehicle-only control DMSO at both 24 and 48 hrs (Figure 1). Our data showed that GSK-126 induced higher levels of smGFP expression than PTC-209, particularly at 48 hrs, but that neither induced expression to the same level as sodium butyrate (NaB) an inhibitor of histone deacetylase (HDAC) used to induce reactivation of herpesviruses.

3.1.2 Effect of PTC-209 and GSK-126 on MDV Viral Genome Copy Number

To determine if increased smGFP expression was indicative of true MDV reactivation from latency, I performed qPCR analysis on DNA isolated from samples of the cells evaluated for smGFP expression (Figure 2). Our data showed the trend of increased viral genome copy number, particularly by 48 hrs post-treatment, but this was not significant by ANOVA, due to a high level of variation among the individual samples.

3.1.3 Dose Response of PTC-209 and GSK-126 on the Induction of smGFP-expression of UA22 Cells.

Since the concentrations of the inhibitors used was selected based on previous data affecting cell proliferation (data not shown), I performed a dose-response for each treatment to optimize the concentration for each (Figure 3). In this series of studies, I observed that GSK-126 gave consistent, significant, and somewhat dose-dependent induction of smGFP, while PTC-209 did not. These data suggested that 10 μM GSK-126 induced the optimal induction of smGFP, but still did not reach the level of smGFP induction observed for the positive control, NaB (Figure 3).

3.1.4 Dose Response of PTC-209 and GSK-126 on the Induction of MDV Genome Replication in UA22 Cells.

In qPCR analysis of the sample used for smGFP expression induction, I observed that no treatment gave significant induction of MDV genome copy number at 24 hours post-treatment, but that GSK-126 did induce MDV genome copy number by 48 hrs post-treatment. Moreover, the optimal concentration of GSK-126 (10μM) induced viral genome replication to the same extent as NaB-treatment (Figure 4). These data suggest that EZH2, and thereby PRC-2, is involved in the repression of the MDV viral genome during latency.

There is a slight, but significant induction of MDV genome copy number at 48hrs with 5μM PTC-209, suggesting that Bmi-1 may be contributing to this repression. Consequently, I extended these analyses to include dual treatments (PTC-209 + GSK-126) to further test this hypothesis.

3.1.5 Combined Treatment of Cells with PTC-209 and GSK-126 Does Not Show a Consistent Additive Increase in smGFP Expression in UA22 Cells.

To further analyze the results of dosage dependence we examined the possible additive effect of the chemical inhibitors (Figure 5). Additionally, a 72-hour (T72) time point was collected to better understand the effects these chemical inhibitors have on MDV reactivation from latency.

Following the trend of the previous experiments, only the GSK-126 20 μM treatment was significant in increasing pp38 expression levels in T24 samples (Figure 5A). At T48, all GSK126 concentrations showed significant pp38 upregulation compared to the DMSO negative control (Figure 5B). Intriguingly, all combination treatments (PTC-209 2.5μM + GSK126 5μM, PTC-209 5μM + GSK126 10μM, and PTC-209 10μM + GSK126 20μM) indicated significant differences in pp38 levels compared to DMSO but did not show any significant difference from the respective GSK126 concentrations alone at the T48 mark (Figure 5, panel B). In fact, there is a significant decrease in pp38 expression levels in GSK126 20μM + PTC126 10μM compared to GSK126 20μM alone. Although there was not significance in pp38 expression change at T24 or T48, PTC-209 did show significant change in pp38 expression levels compared to DMSO at T72 (Figure 5, panel C).

PTC-209 5μM and PTC-209 10μM treatments significantly increased pp38 expression levels, measured by GFP fluorescence, compared to DMSO. There is also a

notable increase in pp38 expression for the PTC 5μM + GSK126 10μM treatment compared to the GSK126 10μM treatment alone, although this difference is not significant (Figure 5, panel C).

3.1.6 Chemical Inhibitor Treatments Do Not Affect the Protein Level of EZH2.

The effects of PTC-209 and GSK-126 were examined at the protein level via Western blotting (Figure 6). These data suggest that the inhibitor of EZH2 activity (GSK-126) does not actually function via the downregulation of EZH2 at the protein level. To examine relative differences in expression, two concentrations of protein were loaded (5 and 10μg), and I observed no significant difference at either concentration. These data are consistent with McCabe who demonstrated previously that GSK-126 did not affect EZH2 protein levels but blocked its histone methyltransferase activity (McCabe et al., 2012; Takeshima et al., 2015).

3.2 siRNA Assays.

siRNAs targeted to Bmi-1 and EZH2 were used to interrogate whether these PRC proteins are required for maintenance of MDV latency. All results detailing siRNA assays are discussed below.

3.2.1 Examination of the Effects of siRNA Transfection for EZH2 and Bmi-1 on MDV Reactivation.

To examine more specifically the roles of EZH2 and Bmi-1 on regulation of MDV reactivation from latency, I transfected cells with siRNAs targeting EZH2, Bmi-1 or a scramble control (scRNA) in addition to a fluorescently-tagged RNA (FL-3, red channel) as a control for transfection efficiency (Figure 7).

The UD35 cell line was used to assess pp38 expression via intracellular antibody staining, as the fluorescence of smGFP interfered with that ability to screen cells for transfection efficiency via the fluorescent RNA. UD35 cells were stained and examined via flow cytometry. These data show that none of the treatments significantly upregulated pp38 protein expression, but there was a general trend of increased expression of pp38 in cells transfected with the siRNA for EZH2 at 48hrs post-transfection (Figure 7A) and the siRNA for Bmi-1 at 72hrs post-transfection (Figure 7B).

3.2.2 Examination of the Effects of siRNA Transfection for EZH2 and Bmi-1 on EZH2 and Bmi-1 Protein Levels.

In looking at the EZH2 and Bmi-1 expression levels (Figures 8 and 9, respectively) there was no significant difference in the amount of expression of these proteins, comparing the respective siRNA treatments to the protein expression levels. Yet, while not significant, there was still a similar trend to our observation for pp38 expression (Figure 7), in that an effect on pp38 induction was observed at 48hrs post-EZH2 siRNA treatment and this did correlate with a decrease in EZH2 expression at this time (Figure 8).

Indeed, in delving further into the visual analysis of these graphs, one can note a discernable decrease in pp38 expression in scRNA treatments compared to siRNA (both EZH2 and Bmi-1) (Figures 7, panel A and panel B). This observation is compounded by the fact that both EZH2 and Bmi-1 expression levels are notably higher in scRNA treatments as well (Figures 8 and 9).

3.2.3 Effect of siRNA Transfection on MDV Genome Copy Number and Expression Levels.

In UA22 cells, at 48 hrs post-transfection, the siRNA targeting EZH2 resulted in a significant increase in viral genome copy number (Figure 11, panel A), but does not result in a significant downregulation of EZH2 expression at the RNA level (Figure 11, panel B). The siRNA to Bmi-1 showed a similar increase in genome copy number, however, this was not significant. Transfection of cells with the siRNA to Bmi-1 resulted in a slight, but not significant increase in its expression at the RNA level. Consequently, these data suggest that the effects of siRNA transfection would be seen post-transcriptionally.

I observed a similar effect of siRNA transfection using UD35 cells, in that siRNAs for EZH2 and Bmi-1 increase the genome copy number in UD35 cells at 24 and 48 hrs post-transfection, respectively; however, these data were not significantly different from the scramble siRNA control (Figure 12).

3.3 Meq Splice Variant-derived Proteins Show Increased Localization and Interaction with Chicken Bmi-1.

Fluorescent protein fusions of chicken Bmi-1, Meq and Meq/vIL8, showed that all proteins were nuclear in their localization, with Meq and Meq/vIL8 showing increased nucleolar localization (Figure 13, panel B and C), as detailed previously (Anobile et al., 2006). Chicken Bmi-1 was primarily nucleoplasmic in its localization (Figure 13, panel A), consistent with previous reports for the human Bmi-1 protein (Dutton et al., 2007; Liang et al., 2013; Frank M. Raaphorst et al., 2000; van Kemenade et al., 2001; Weng, Li, Feng, & Hong, 2012).

When proteins were co-expressed in HTC cells, there was a notable co-localization of Bmi-1 with Meq splice variant proteins (Figure 14), and this co-

localization, which was primarily nucleolar, was not affected by mutation of the CtBP-bind consensus (PLDLS -> AVEFT; Figure 14, panels D and E). These data indicated that Meq/vIL8-binding of Bmi-1 was not dependent on interaction with CtBP, a scaffold for many chromatin remodeling enzymes. Moreover, these data supported the specific immunoprecipitation of Bmi-1 with Meq/vIL8 and not with Meq (see Introduction).

To further characterize the interactions of these proteins *in vivo*, transfected and co-transfected HTC cells were subjected to fluorescence resonance energy transfer (FRET) and fluorescence return after photo-bleaching (FRAP) analyses (Figures 15 and 16). FRET analysis permits the direct assessment of the proximity of proteins, with the transfer of photons from a donor fluorophore (in this case, eCFP) to an acceptor fluorophore (in this case, eYFP), requiring an intermolecular distance of 10nm or less. FRET occurs due to the proximity and the overlap of the emission spectrum of the one fluorophore (eCFP) with the excitation spectrum of the other (eYFP). FRET can be assessed by several methods; however, the most commonly used method is the acceptor-bleaching method (ABM). In ABM, the acceptor fluorophore is bleached (ideally ~50%) with a high-energy laser pulse at or near its absorption peak (in this case, 514nm). The destruction of this fluorophore blocks FRET from the donor fluorophore and hence, the donor emission increases in intensity. ABM FRET is measured using the formula:

(Dpost – Dpre)/Dpre x 100

Where Dpost = donor fluorescence intensity post acceptor bleaching and Dpre = donor fluorescence intensity pre-bleach.

In FRET analysis, I found very weak interaction between full length Meq and Bmi-1 (0.13265%) whereas there was a significant increase in FRET efficiency with splice-variant proteins Meq/vIL8 and Meq/vIL8Δexon3 (22.37738% and 8.35105%, respectively). The increased interaction with these proteins corresponded to the increased nucleolar localization of Bmi-1, suggesting that Meq/vIL8 and Meq/vIL8Δexon3 (to a somewhat lesser extent), induce nucleolar localization of Bmi-1, while full-length Meq does not. This interaction is further confirmed with FRET efficiency data from Bmi-1 interacting weakly with Meq-AVEFT (2.86654%) and having an increase in FRET efficiency with Meq/vIL8-AVEFT when photobleached in the nucleolus (42.41046%).

In FRAP analysis, which provides a measure of protein motility, we found that Bmi-1 was highly motile in the nucleoplasm, but had its motility decrease, although not consistently, when translocated to the nucleolus with Meq/vIL8 (Figure 20). This somewhat inconsistent decrease in motility suggests that Bmi-1 may be in several fractions within the nucleus and nucleolus, one form bound to DNA directly, and one form bound to Meq/vIL8. These data therefore suggest that the MDV splice variant proteins co-localize and physically interact with Bmi-1, but that a portion are found in low-mobility complexes with Meq/vIL8. As the DNA-binding portion of Meq proteins is found in the N-terminus, these data suggest that Bmi-1 is recruited to specific chromosomal locations by the splice-variant proteins, as well as binding DNA on its own as part of PRC-1.

Chapter 4

DISCUSSION

4.1 Influence of Bmi-1 in Maintenance of MDV Latency.

Based on our results, PRC proteins EZH2 and Bmi-1 appear to be essential in maintaining MDV latency, as chemicals that disrupt their function (GSK-126 and PTC-209, respectively) induce not only cell cycle arrest, but also induce expression of pp38 and increased MDV genome copy number in UA22 cells.

Chemical inhibitor PTC-209 is described as a small-molecule-mediated inhibitor of Bmi-1 that is designed to reduce Bmi-1 at the transcriptional level (Kreso et al., 2014). Indeed, PTC-209 was demonstrated to decrease endogenous Bmi-1 levels and reduced global ubiquitinated histone H2A (uH2A) levels (Kreso et al., 2014).

The data presented in this work demonstrates the ability of PTC-209 to increase pp38 levels in the MDV-transformed cell line UA22, thus indicating an increase in MDV reactivation (Fig. 1 and Fig. 5C). These results suggest that Bmi-1 plays a role in the maintenance of MDV's latency phase. This is highlighted by figure 5, panel C, which shows Bmi-1 expression is affecting the latent phase of the MDV genome in a dose-dependent manner, indicated via pp38 expression levels. Furthermore, through qPCR analysis MDV genome copy numbers showed a significant increase at the T48 time point when treated with PTC-209 at 5μM (Figure 4, panel B). Both flow analysis of pp38 expression levels and qPCR data analyzing MDV genome copy numbers showed some significance in increase in MDV, indicating reactivation of viral genome.

4.1.1 Role of EZH2 in Latency and Transformation.

EZH2 is a methyltransferase associated as a subunit of PRC-2, known for trimethylation of lysine 27 on histone 3 ($H3K27me_3$) (Cao et al., 2002). This protein became a target of interest not only due to the co-operative nature of the PRCs 1 and 2 (Fischle et al., 2003), but also due to the specific mark it places ($H3K27me_3$). This mark is associated with transcriptional repression and found on the MDV genome of tumor-bearing birds, located around the origin of lytic replication (Ori_{Lyt}) (Brown et al., 2012). Furthermore, interactions between CtBP, a Meq binding protein (Liu & Kung, 2000), and PRC proteins (Sewalt, Gunster, van der Vlag, Satijn, & Otte, 1999) provide strong evidence that EZH2 is a potential player in maintaining viral latency of MDV (Brown et al., 2006).

GSK-126 is a small molecular chemical inhibitor used for reduction of the enzymatic effects of EZH2 methyltransferase activity (McCabe et al., 2012). This is demonstrated by a decrease in global $H3K27me_3$ markers when treated as low as 150 nM of GSK-126 (McCabe et al., 2012). Furthermore GSK-126 treatments indicated a significant decrease in PC3 (a prostate cancer cell line) and MCF7 (A breast cancer cell line) cell counts at 6μM (Takeshima et al., 2015). This decrease in proliferation was observed in a chicken macrophage cell line (HTC) when treated with 5, 10, and 15μM of GSK-126, acting in a dosage-dependent manner (Parcells, unpublished data).

Not only does GSK-126 inhibition of EZH2 cause a decrease in cellular proliferation, it dramatically increases pp38 levels of MDV (Fig. 1, 3, 4B, and 5). Indeed, GSK-126 was shown to work not only in a time dependent manner but also a dosage dependent one. Interestingly, while there is a significant increase in pp38 expression levels due to increased dosages of GSK126 (Figures 3 and 5), there is not additive effect of PTC-209 and GSK126 (Figure 5). In fact, there is a significant

decrease in MDV reactivation, measured by pp38 expression levels, when PTC-209 treatments are added in concert with GSK126 (Figure 5).

Unsurprisingly, protein levels of EZH2 remained unchanged regardless of GSK126 concentration levels (Figure 6). EZH2 protein levels being unaffected, of course, was noted in the original publication featuring GSK-126 (McCabe et al., 2012). Future work detailing the effects of GSK-126 in this system will have to be done through measuring H3K27me_3 levels, as a decrease in this marker was noted globally in (McCabe et al., 2012).

Regarding UD35 cells, there is a notable increase in MDV genome copy numbers in siEZH2 treatments, but these data are not deemed significant through ANOVA analysis (Figure 10, panel A and Figure 12, panel A). For both UD35 and UA22 siRNA knockdown experiments there is only a small decrease in EZH2 mRNA expression levels (Figure 10, panel B and Figure 11, panel B). This could provide reasoning for the low MDV reactivation numbers in relation to scramble RNA treatments. Additionally, as mentioned prior, qPCR analysis does not account for transfection efficiency. This could offer insight as to why there is insignificant MDV genome copy differences between siRNA treatment and scramble. Furthermore, qPCR is measuring full genome copies, while flow cytometric analysis only measures pp38 protein levels. This could explain the discrepancies between the two data sets, regardless of the samples being obtained from the same source.

Regarding the flow cytometry data, there is no significant relationship between EZH2 siRNA treatment and MDV genome reactivation, although there is a notable trend of pp38 expression due to siRNA knock down of EZH2 in UD35 cells at the T48 time point, this relationship is not significant (Figure 7, panel A). Additionally, there

seems to be a relationship between pp38 protein expression levels (Figure 7, panel A) and EZH2 protein expression levels (Figure 8, panel A), but these data are not significant.

Additionally, EZH2 has been identified as a binding partner of a human immunodeficiency virus 1 (HIV-1) long-noncoding RNA (lncRNA) (Zapata et al., 2017). Indeed, antisense transcript ASP is shown to interact with EZH2, recruiting it to the HIV-1 5'LTR, causing the establishment of HIV viral latency through the increase of the suppressive marker $H3K27me_3$ (Zapata et al., 2017).

EZH2 has also been associated with increased proliferation and tumor formation in a myriad of other systems (Sparmann & van Lohuizen, 2006). Furthermore, EZH2 upregulation has been detected in lymphomas collected from MDV positive birds along with MDV-transformed T-cell lymphoma cell lines (Shack et al., 2008).

Beyond MDV, EZH2 is associated with other herpes viruses as well. EZH2 has been implicated in HD and has been found to upregulated in Reed-Sternberg cells, an EBV-induced lymphoma cell line (F. M. Raaphorst et al., 2000; van Kemenade et al., 2001). Furthermore, EZH2 is associated with Kaposi's sarcoma-associated herpesvirus (KSHV). Indeed, EZH2 is reported to be upregulated in Kaposi's sarcoma (He et al., 2012). EZH2 is essential not only for KSHV-induced angiogenesis but was shown to upregulated in during KSHV viral latency, mediated through KSHV latency associated proteins vFLIP and LANA via the NK-κB pathway (He et al., 2012).

4.1.2 Role of Bmi-1 in Latency and Transformation.

siRNA silencing of Bmi-1 appears to correlate with MDV genome reactivation. This is seen in both flow and qPCR data (Figures 7, 10, and 11), although none of these results indicate any significant differences as analyzed by ANOVA. While not significant, there is a trend existing between the decrease in Bmi-1 protein levels at the T72 time point sample (Figure 9, panel B) and the increase in pp38 protein levels (Figure 7, panel B) via flow cytometric analysis. Although this could be due to the decrease in EZH2 (Figure 8, panel B), but with such a large standard deviation in the expression of EZH2 it is uncertain whether this is related to pp38 expression levels.

qPCR analysis of MDV genome copy numbers from siRNA treatments, again, indicate a potential relationship between a decrease in Bmi-1 levels and an increase in MDV genome copies for both UA22 cells (Figure 11) and UD35 cells (Figures 10 and Figure 12, panel B), although these relationships are not deemed significant. This trend was also not noted at the T24 hour time point in UD35 cells (Figure 12, panel A). This could be due to the lack of time allotted for MDV genome reactivation, as prior studies looking at reactivation of MDV saw greater effects in reactivation at the T48 time point (Brown et al., 2012). Additionally, results presented here also indicated a time sensitive reactivation effect (Figures 1-5).

Furthermore, all qPCR data analyzed in this work does not take in account for transfection efficiency. Since transfection with lipofectamine 2000 transfection reagent would yield only a 30% efficiency the total MDV genome copy number could be higher in the percent of transfected cells. A way to rectify this problem could be to perform qPCR on cells sorted using Cy5 fluorescence as a transfection indicator. These trends could be more significant if analyzed through that lens.

Bmi-1 is known for its role in epigenetic silencing, specifically due to the presence of a unique zinc-finger domain (van Lohuizen et al., 1991), and for its role as an oncoprotein, interacting c-Myc during lymphoma formation (Haupt et al., 1991). Furthermore, Bmi-1 is associated with poor prognoses in myriad cancer types (F. M. Raaphorst et al., 2000; van Kemenade et al., 2001; Zhang et al., 2017). Additionally, the inhibition of Bmi-1 through siRNA knockdown techniques resulted in a significant decrease in proliferation rates in T24 bladder cancer cells (Liang et al., 2013). This phenomenon is seen in the MDV-induced T-cell lymphoma model using the Bmi-1 chemical inhibitor PTC-209 (Parcells, unpublished data).

Bmi-1 upregulation in Reed-Sternberg tumor cells of Hodgkin's disease (HD) (F. M. Raaphorst et al., 2000) is intriguing, as this would be analogous to the model studied in this work. This is due to the finding that Hodgkin's lymphoma Reed-Sternberg cells are positive for Epstein-Barr virus (EBV) encoded proteins (Murray, Young, Rowe, & Crocker, 1992), and is particularly relevant given that the Reed-Sternberg antigen is CD30, a TNF family receptor upregulated on the transformed component of MDV-induced lymphomas (Burgess et al., 2004).

EBV is a human gammaherpes virus, the initial classification of MDV until it was learned that MDV was, in fact, an alphaherpesvirus, in terms of genome organization (Buckmaster et al., 1988). EBV is prevalent in ~90% of the world adult population, but usually exists as a silent infection (G. Miller, 1990). Furthermore, EBV is the causative agent for infectious mononucleosis, and is a major factor in Burkitt's lymphoma, Hodgkin's lymphoma, cutaneous T-cell lymphoma, and nasopharyngeal carcinoma (Murray et al., 1992).

In Hodgkin's lymphoma cells, EBV encoded latent membrane protein 2A (LMP2A) is associated with Reed-Sternberg tumor cells in EBV-positive HD, being present in over half of the samples collected (Murray et al., 1992; Niedobitek et al., 1997). Similar to MDV, only a small fraction of the genes expressed during replication of EBV are expressed during its latent phase, with LMP-1 and LMP2 being two of them (Ma et al., 2017). Although, reports have indicated that these two proteins are non-essential in EBV-induced B cell lymphoma formation (Ma et al., 2017). Furthermore, Bmi-1 is upregulated through LMP-1 downstream signaling in Hodgkin lymphoma cells (Dutton et al., 2007). This establishes a strong connection between this latently expressed protein and Bmi-1, again providing evidence that the model observed in this report could have potential relevance to human medicine.

4.2 Direct Interaction of MDV Oncoproteins and Bmi-1.

Interactions between Bmi-1:Meq and Bmi-1:Meq-splice-variant proteins were assessed via FRET, FRAP and co-localization assays. Localization of Bmi-1 to the nucleoplasm is a known phenomenon (Dutton et al., 2007; Liang et al., 2013; F. M. Raaphorst et al., 2000; van Kemenade et al., 2001). Confirmation of this in chicken-Bmi-1 was shown in this work (Figure 13, panel A). Interestingly, there is additional movement of Bmi-1 to the nucleolus when co-transfected with Meq/vIL8 (Figure 14, panels B and E), but this is not seen with full length Meq (Figure 14, panels A and D) or Meq/vIL8Δexon3 (Figure 14, panel C). This leads one to surmise that the interaction of Bmi-1 and Meq/vIL8 occurs on the third exon of vIL8.

Indeed, the FRET analysis of Bmi-1 and Meq/vIL8 indicate a strong interaction between these two proteins (Figure 16). With percent fluorescence efficiencies at **22.37738%** for Region 1 is and **22.46762%** Region 2. This is further

supported by the FRET analysis of Bmi-1-CFP + Meq/vIL8-AVEFT-YFP. This mutated version of Meq/vIL8 is only changed at the C-terminal region where binding to CtBP would occur, naturally (Brown et al., 2006). Thus, the exons of vIL8 are no different than non-mutated Meq/vIL8. Again, there is a strong interaction between Bmi-1 and Meq/vIL8-AVEFT determined by FRET analysis (Figure 19). Interestingly, while at Region-1 there is a strong interaction, indicated by a percent fluorescence efficiency of **42.41046%** this is not seen in Region-2, with a percent fluorescence efficiency of **-1.66554%.** This could be due to the location of the photobleaching event of Region-1 occurring in the nucleoplasm rather than the nucleolus (Figure 19, panels A and B), indicating that the interaction between Bmi-1 and Meq/vIL8 is highly dependent on the location of the proteins.

FRAP analysis of Meq/vIL8 and Bmi-1 does not indicate a difference in Bmi-1 mobility when interacting with Meq/vIL8 (Figure 20). Meq and Meq/vIL8 FRAP data has been published, indicating quick mobility of full-length Meq and a much slower movement of Meq/vIL8 (Anobile et al., 2006). This decrease in mobility was not noted in Bmi-1 when co-transfected with Meq/vIL8.

4.3 Follow-up Work.

The present set of data provide a framework for additional studies to identify the biological role of Meq splice variant-derived proteins and their interaction with chromatin remodeling complexes in the pathogenesis of Marek's disease. These data suggest that interactions with the PRCs correlate with latency onset and appear to contribute to transformation. To follow-up on my present work, subsequent students plan to examine the localization of EZH2 with Meq oncoproteins, as well as to examine each of these pathways with more efficient knock-down mechanisms,

potentially with inducible constructs (shRNAs and CRISPR-Cas9 technology). Moreover, I plan to examine the interactions between Bmi-1 and Meq proteins in cell lines and tumors *ex vivo*, to establish these interactions *in vivo*.

4.4 Conclusions.

The present work establishes putative roles of polycomb repressive complexes (PRCs) in the regulation of MDV latency and in MDV oncogenesis. In addition, these data show that forms of Meq expressed in latency and in transformed cells bind and localize Bmi-1 into the nucleolus of co-expressing cells. The importance of this localization is not clear, however, as chromosome 16 contains a major nucleolar organizing region (NOR) as well the MHC locus of the chicken (M. M. Miller & Taylor, 2016), this translocation may be important to mediating immune-regulation during MDV-mediated transformation.

Chapter 5

FIGURES

Figure 1. Flow Cytometric Analysis of Chemical Inhibitor Treatments Effect on Viral Reactivation Based on pp38-GFP Expression in UA22 Cells.

Panel A +B: 24-hour time point (T24) (A) and 48-hour time point (T48) (B) were both collected for flow cytometry analysis (sample collection detailed in 2.6) and compared based on percent fluorescence of GFP expression. GSK126 treatments used were adjusted to 10μM. PTC-209 treatments were adjusted to 5μM. Chemical treatments were compared to DMSO negative control, along with sodium butyrate (NaB) as a positive control (adjusted to 2mM). All chemical inhibitors were diluted in Iscove's IITS complete medium. Data was analyzed based on percent expression in gated 'M1' (marker 1) area. M1 was determined based on time point zero (T0) and 24-hour time point (T24) GFP fluorescence expression levels in untreated samples. Treatment samples from T48 collection were taken from the same wells as the respective T24 samples. Significance indicated by asterisks, two asterisks (**) indicates p-value less than 0.001. Significance was determined using ANOVA (detailed in 2.12). Error bars indicate standard deviation of triplicate samples.

Panel A.

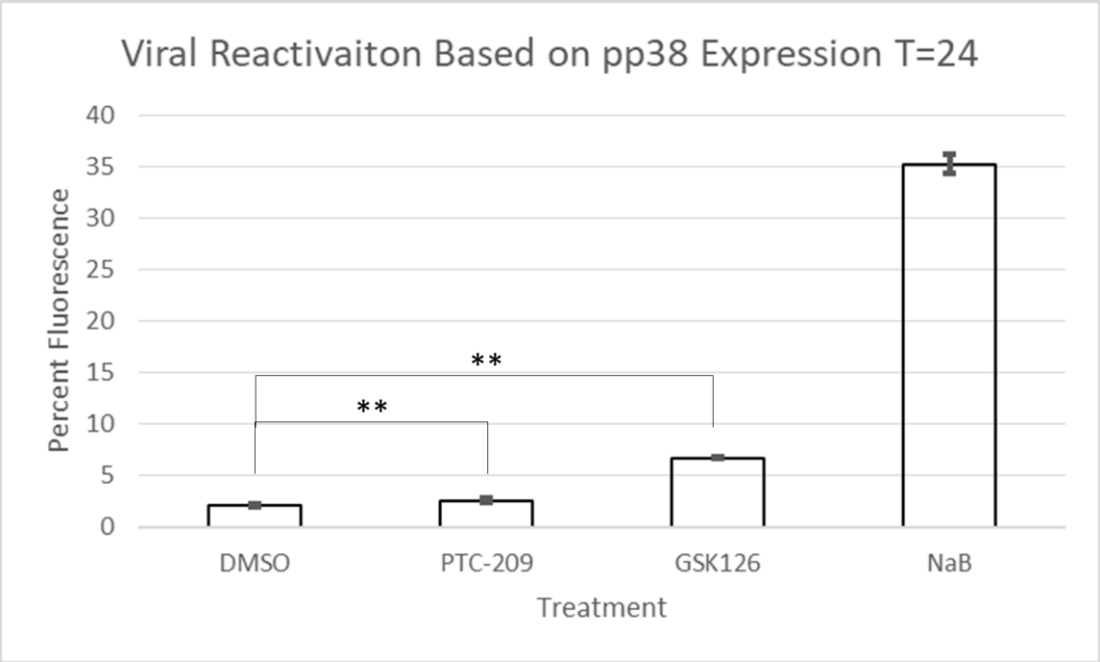

Panel B.

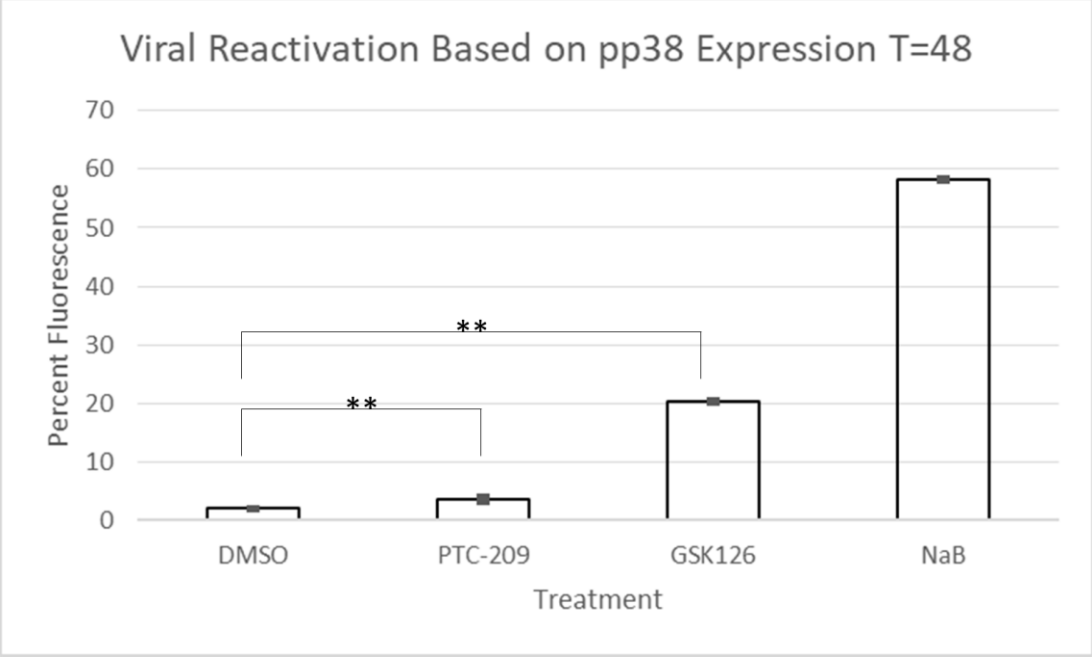

Figure 2. **qPCR Analysis of Chemical Inhibitor Affects on Viral Reactivation in UA22 cells.**

Panel (A + B) T24 (A) and T48 (B) of chemical inhibitor treatment assay, analyzed via qPCR. PTC-209 chemical inhibitor was adjusted to 5μM, GSK126 chemical inhibitor was used at a 10μM concentration. Sodium butyrate (NaB) was used as a positive control, adjusted to 2mM. Primers used to quantify MDV genome expression levels are targeted to gB (detailed in 2.10). Primers targeted to ovotransferrin (2.10) were used to quantify host genome copy number. Triplicate samples were analyzed each in duplicate on 96-well plate and average Ct values were used for statistical analysis. There was no significant difference in MDV genome copy numbers between treatments based on ANOVA (2.12). Error bars denote standard deviation of triplicate samples.

Panel A.

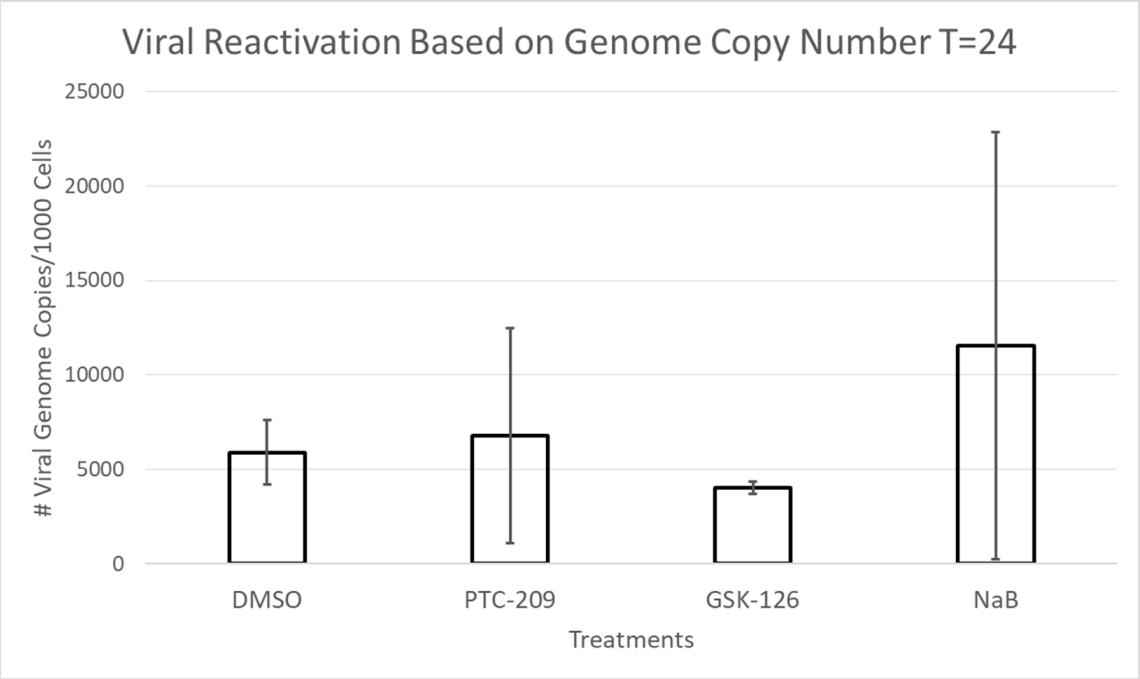

Panel B.

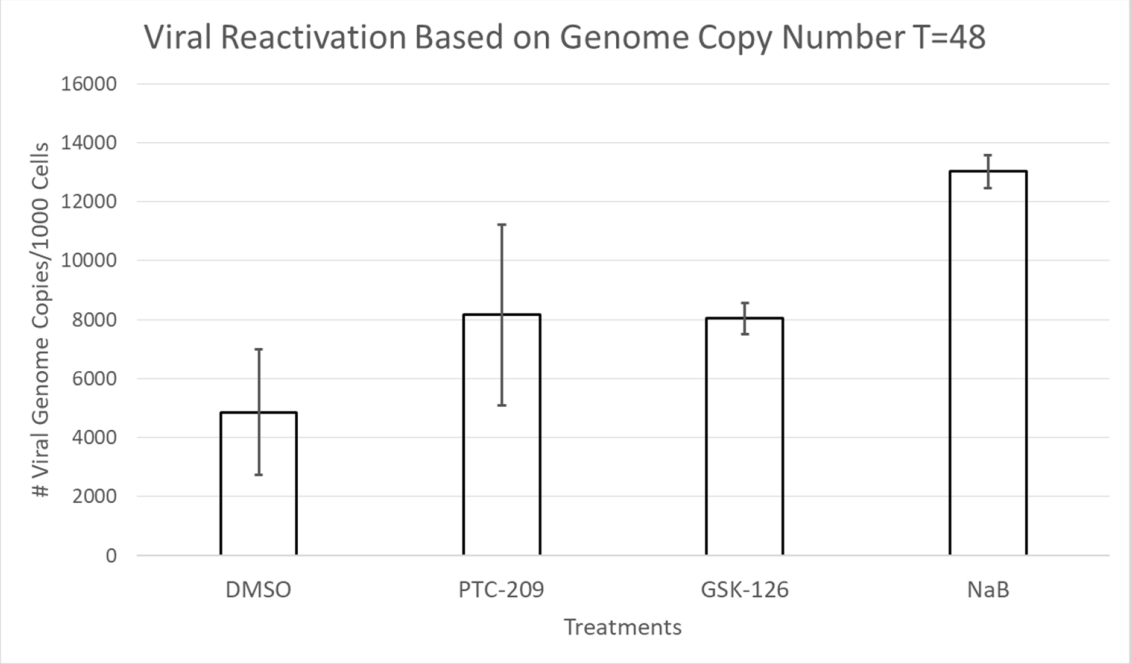

Figure 3. Flow Cytometric Analysis of Chemical Inhibition of EZH2 is Dose Dependent in MDV Reactivation of UA22.

Panel A + B: T24 (A) and T48 (B) flow cytometry samples were collected as described in 2.6. Dose dependent samples were analyzed via flow cytometry in triplicate for percent GFP fluorescence levels. Varying concentrations of chemical inhibitors (denoted on figure x-axis) were diluted in Iscove's IITS complete medium. NaB (positive control) was diluted to a 2mM concentration, while DMSO was used as a negative control. Data was analyzed based on percent expression in gated M1 area. M1 was determined based on T0 and T24 GFP fluorescence expression levels in untreated samples. Significance is indicated by asterisks, three asterisks (***) to signify a p-value less than 0.001. Error bars denote standard deviation of triplicate samples.

Panel A.

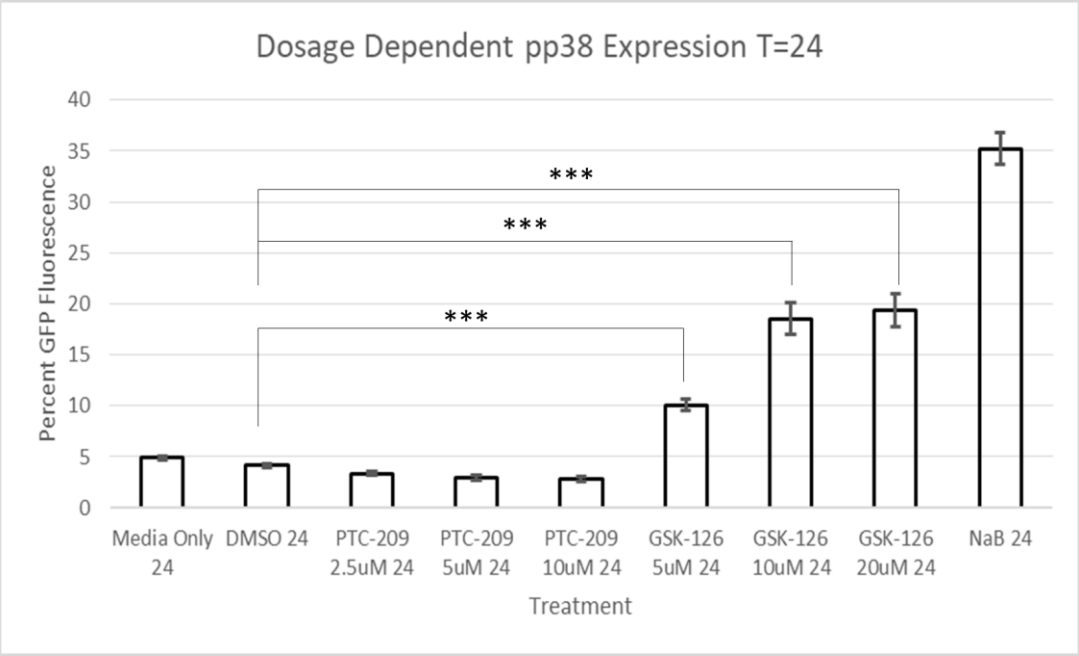

Panel B.

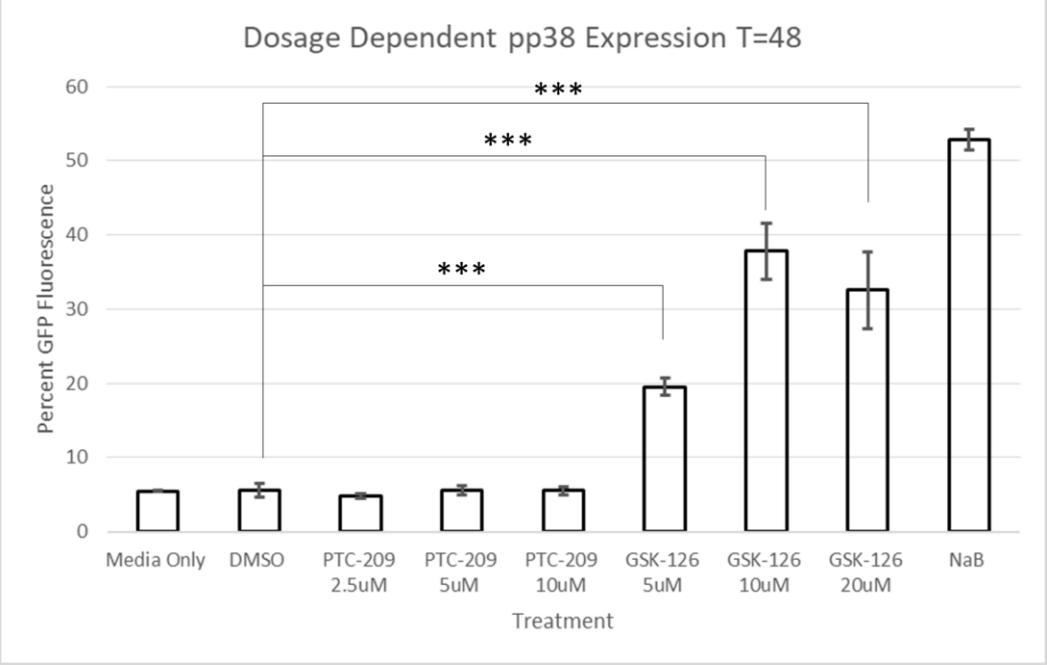

Figure 4. qPCR Analysis of MDV Reactivation Shows Dosage Dependence via Chemical Inhibitor Assays in UA22 Cells.

Panel A+B: 24-hour (A) and 48-hour (B) time points were collected as described in 2.8. Primers used to quantify MDV genome expression levels are targeted to gB (detailed in 2.10). Primers targeted to ovotransferrin (2.10) were used to quantify host genome copy number. Triplicate samples were analyzed each in duplicate on 96-well plate and average Ct values were used for statistical analysis. Significance is denoted with an asterisk, a single asterisk ('*') indicating a p-value less than 0.05. Significance was determined by ANOVA analysis detailed in 2.12. Error bars are used to signify standard deviation.

Panel A.

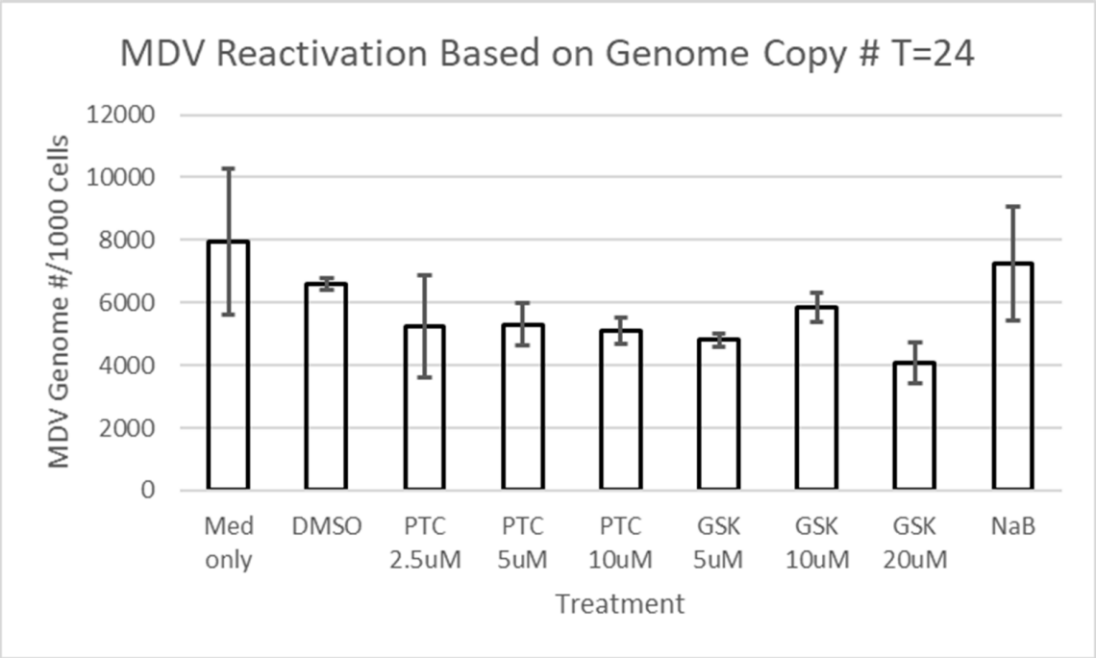

Panel B.

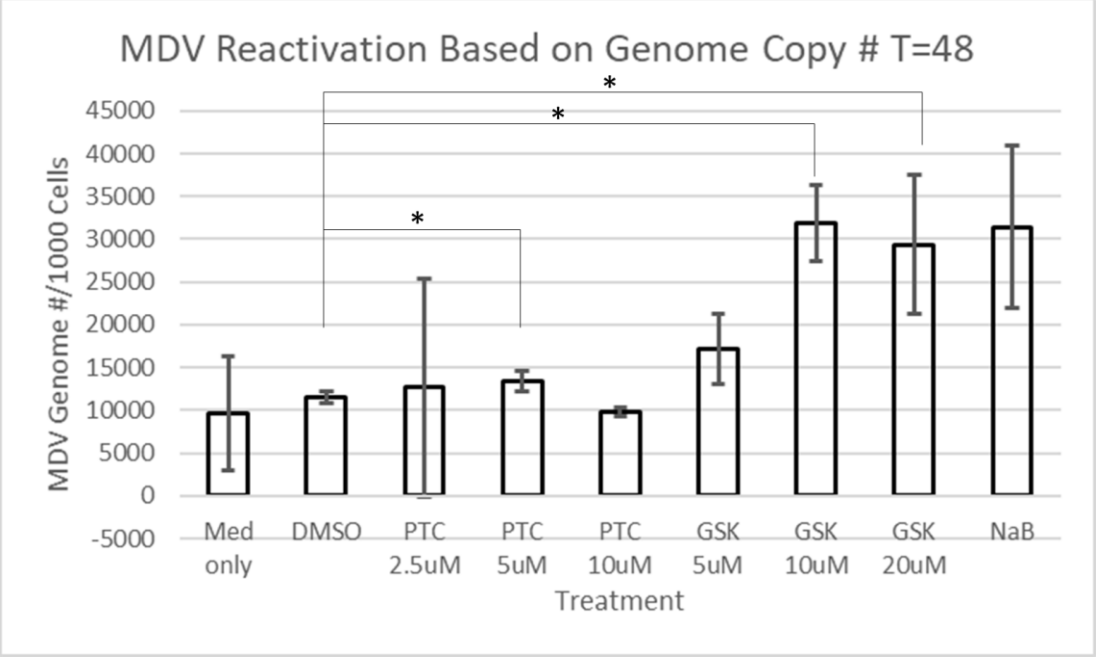

Figure 5. Flow Cytometry Analysis of Additive Affect Chemical Inhibitors Have on MDV Reactivation in UA22 Cells.

Panel A, B, and C: T24 (A), T48 (B), and T72 (C) samples were all collected following procedure detailed in 2.6. Treatment samples from T72, T48, and T24 were all taken from the same treatment wells (e.g. PTC-209 10μM A T48 was collected from the same well as T24). All samples were diluted to the appropriate concentration (as denoted on figure x-axis) in Iscove's IITS complete medium. NaB (positive control) was adjusted to a 2mM concentration, and DMSO was used as a negative control. Data was analyzed based on percent expression in gated M1 area. M1 was determined based on T0 and T24 GFP fluorescence expression levels in untreated samples. Significance was determined using ANOVA analysis (2.12). A p-value of less than 0.001 is denoted as (***). Samples 'grouped' under one significance bar all shared a p-value of less than 0.001. Error bars indicate standard deviation of triplicate samples.

Panel A.

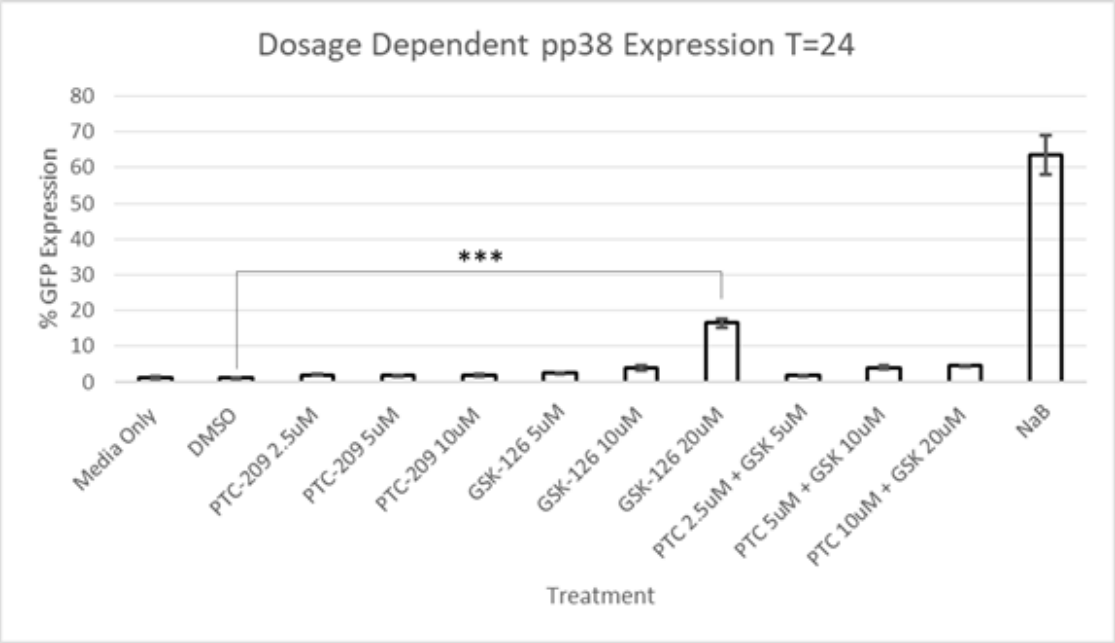

Panel B.

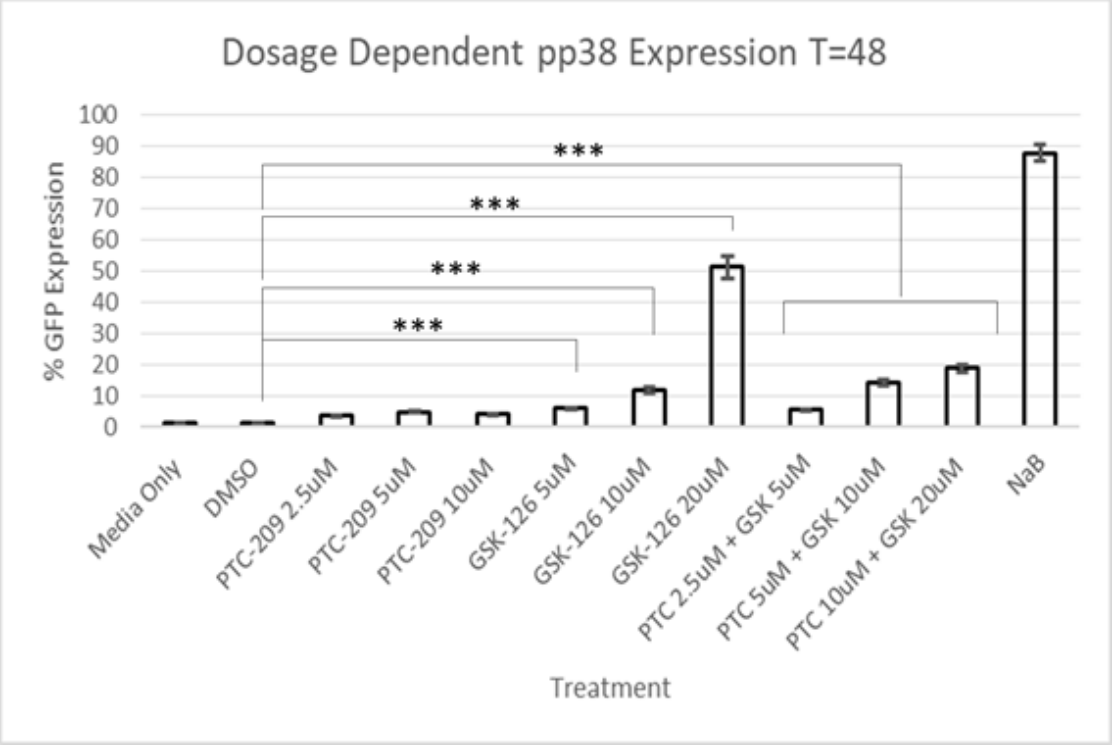

Panel C.

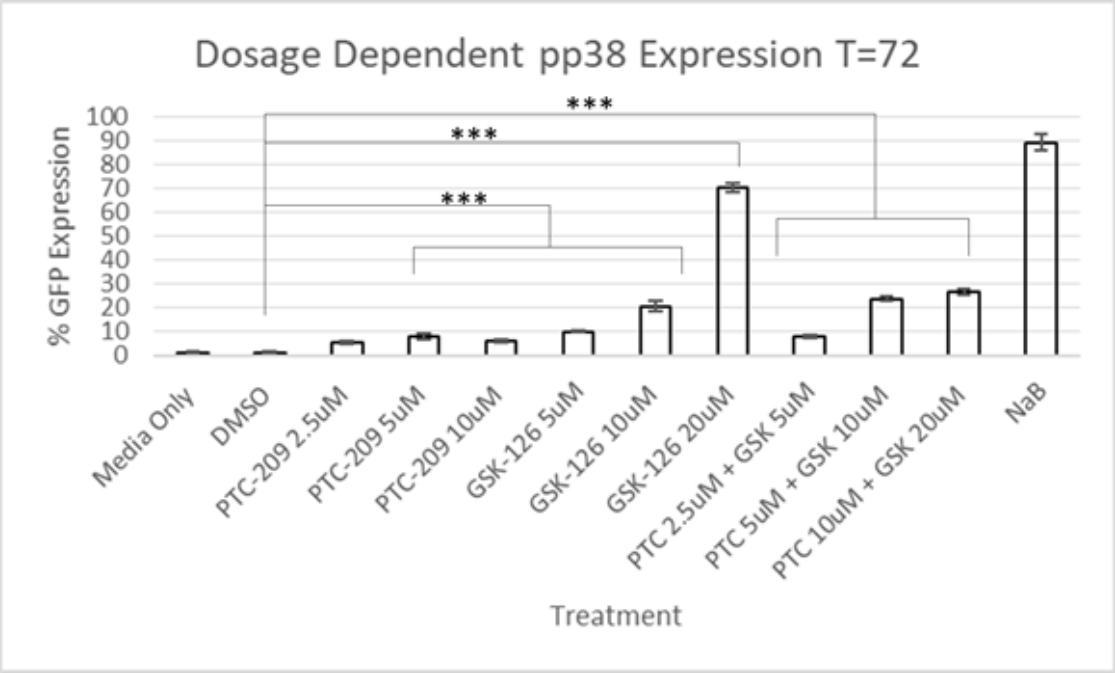
Dosage Dependent pp38 Expression T=72
% GFP Expression
100
90
80
70
60
50
40
30
20
10
0
***
***
***
Media Only
DMSO
PTC-209 2.5uM
PTC-209 5uM
PTC-209 10uM
GSK-126 5uM
GSK-126 10uM
GSK-126 20uM
PTC 2.5uM + GSK 5uM
PTC 5uM + GSK 10uM
PTC 10uM + GSK 20uM
NaB
Treatment

Figure 6. Western Blot Analysis of EZH2 Protein Concentrations After Chemical Inhibitor Treatments.

For Western blots, each sample was loaded at 5µg (left well for each sample) or 10µg (right well for each sample). The 'Marker' in the far left well is PageRuler™ Plus (ThermoFisher, prod#: 26619) and was loaded at a 5µL volume. Western blots were done following procedure outlined in 2.7. NuPAGE™ 4-12% Bis-Tris protein gels were used for protein separation. Protein was then transferred to a nitrocellulose membrane, stained with primary and secondary antibody. Mouse anti-EZH2 antibody was used as the primary, diluted 1:750. Goat ant-mouse HRP-conjugate antibody was used as the secondary, diluted to 1:10,000. Pierce™ enhanced chemiluminescence (ECL) western blotting substrate was then used as substrate to visualize bands. This image was taken on Bio-Rad Chemidoc™ Imaging System.

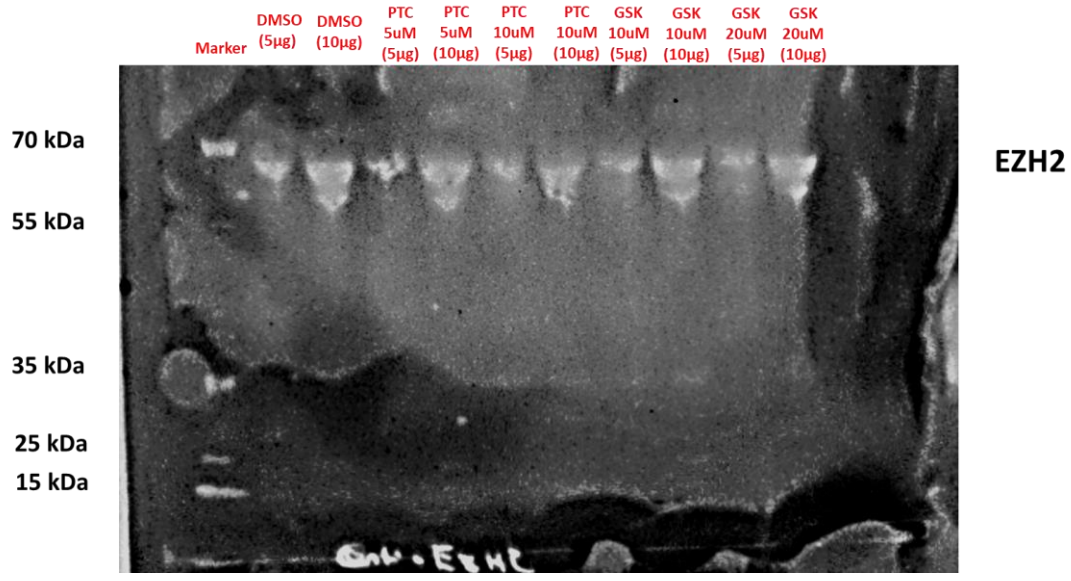

Figure 7. Flow Cytometry Analysis of pp38 Expression in UD35 Cells After siRNA Treatments.

Panel A + B: Time points T48 (A) and T72 (B) were stained following intracellular staining procedure outlined in 2.6. Mouse monoclonal anti-pp38 antibody was used for primary staining, diluted to 1:200. Secondary staining was done utilizing goat anti-mouse ALEXA 488. Flow cytometric analysis was done by taking the events recorded for FL1-H (as denoted by falling into M1 range) and dividing these events by the events recorded in the M1 range of FL3-H. M1 for both FL3-H and FL1-H were determined based on T0 and T48 unstained FITC expression measurements. Significance was determined by ANOVA analysis (2.12). Error bars represent standard deviations of duplicate samples.

Panel A.

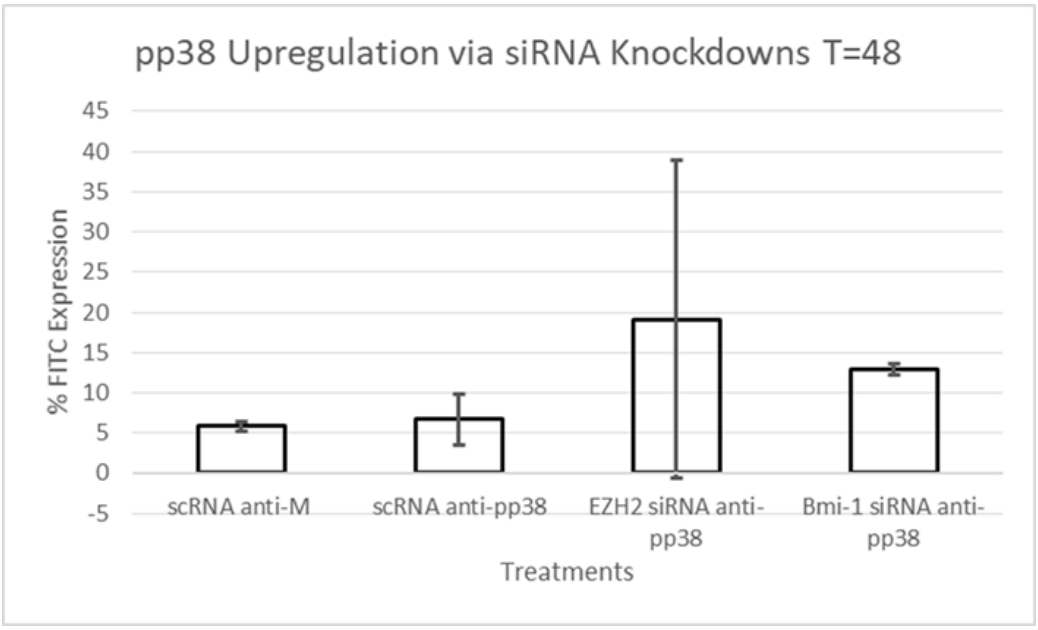

Panel B.

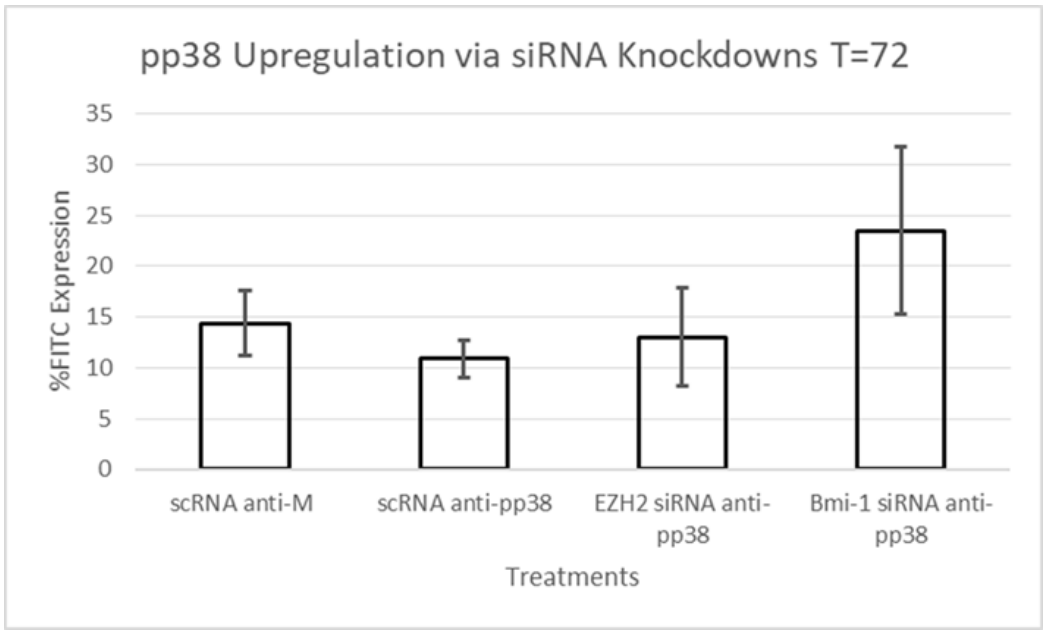

Figure 8. Flow Cytometry Analysis of EZH2 Expression Levels for siRNA Knockdown Assay.

Panel A+B: T48 (A) and T72 (B) time-points were collected and stained intracellularly based on procedure detailed in 2.6. Mouse monoclonal anti-EZH2 antibody was used for primary staining, diluted to 1:200. Secondary staining was done utilizing goat anti-mouse ALEXA 488. Flow cytometric analysis was done by taking the events recorded for FL1-H (as denoted by falling into M1 range) and dividing these events by the events recorded in the M1 range of FL3-H. M1 for both FL3-H and FL1-H were determined based on T0 and T48 unstained FITC expression measurements. Significance was determined by ANOVA analysis (2.12). Error bars represent standard deviations of duplicate samples.

Panel A.

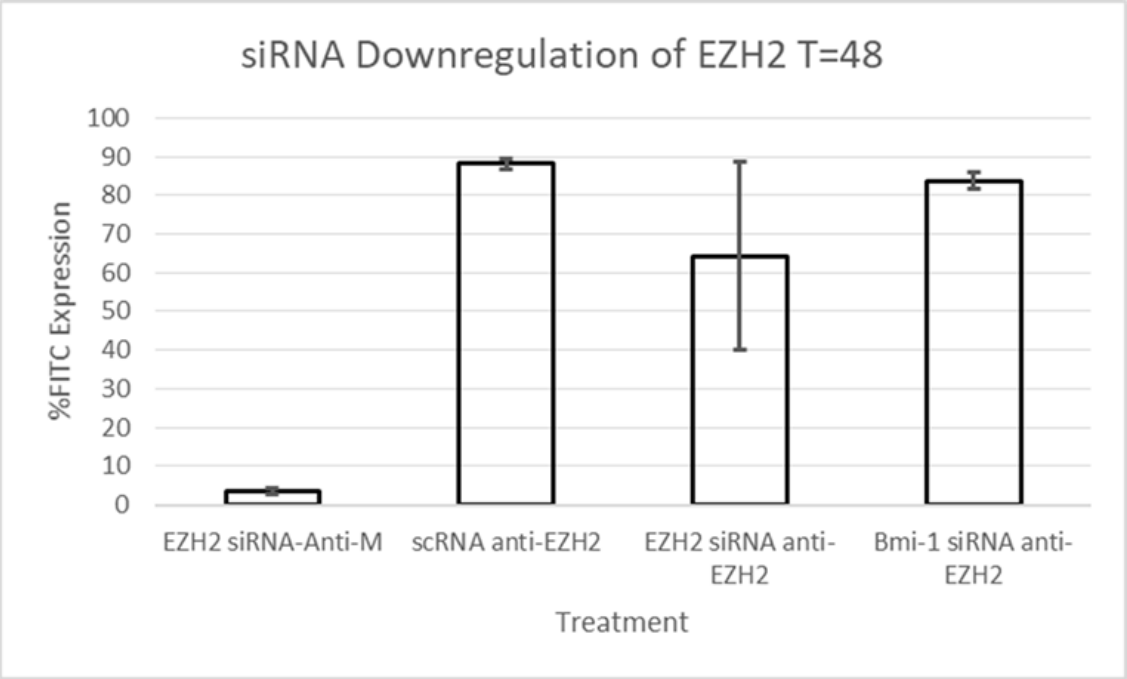

Panel B.

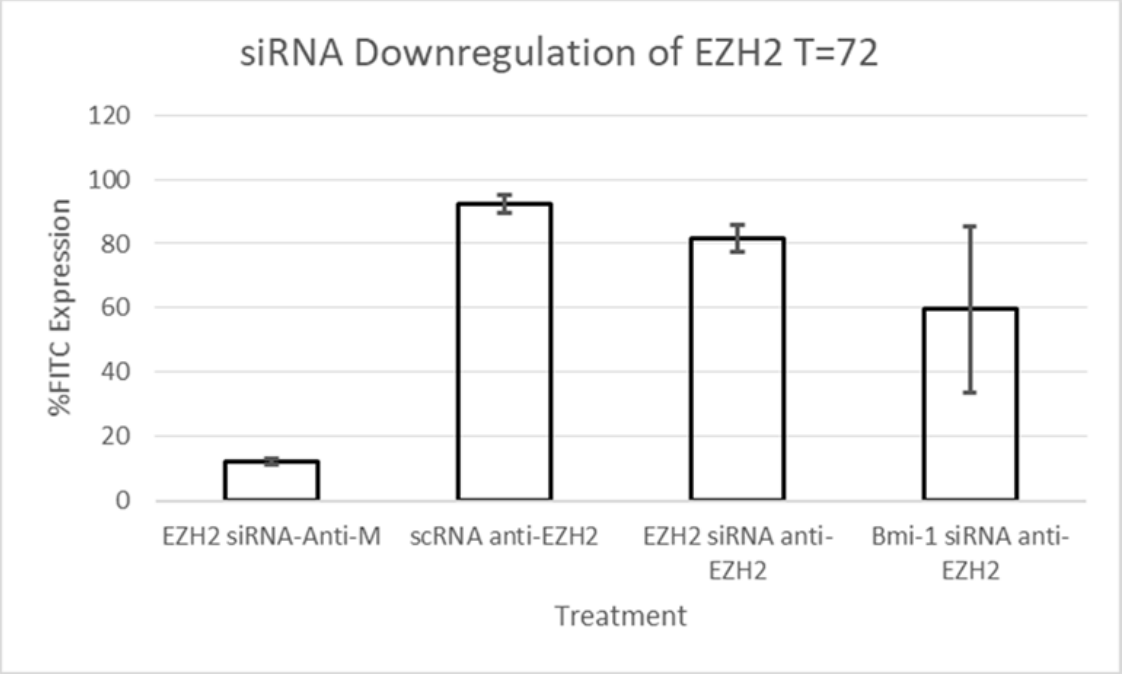

Figure 9. Flow Cytometry Analysis of Bmi-1 Expression Levels for siRNA Knockdown Assay.

Panel A+B: T48 (A) and T72 (B) time-points were collected and stained intracellularly based on procedure detailed in 2.6. Mouse monoclonal anti-EZH2 antibody was used for primary staining, diluted to 1:200. Secondary staining was done utilizing goat anti-mouse ALEXA 488. Flow cytometric analysis was done by taking the events recorded for FL1-H (as denoted by falling into M1 range) and dividing these events by the events recorded in the M1 range of FL3-H. M1 for both FL3-H and FL1-H were determined based on T0 and T48 unstained FITC expression measurements. Significance was determined by ANOVA analysis (2.12). Error bars represent standard deviations of duplicate samples.

Panel A.

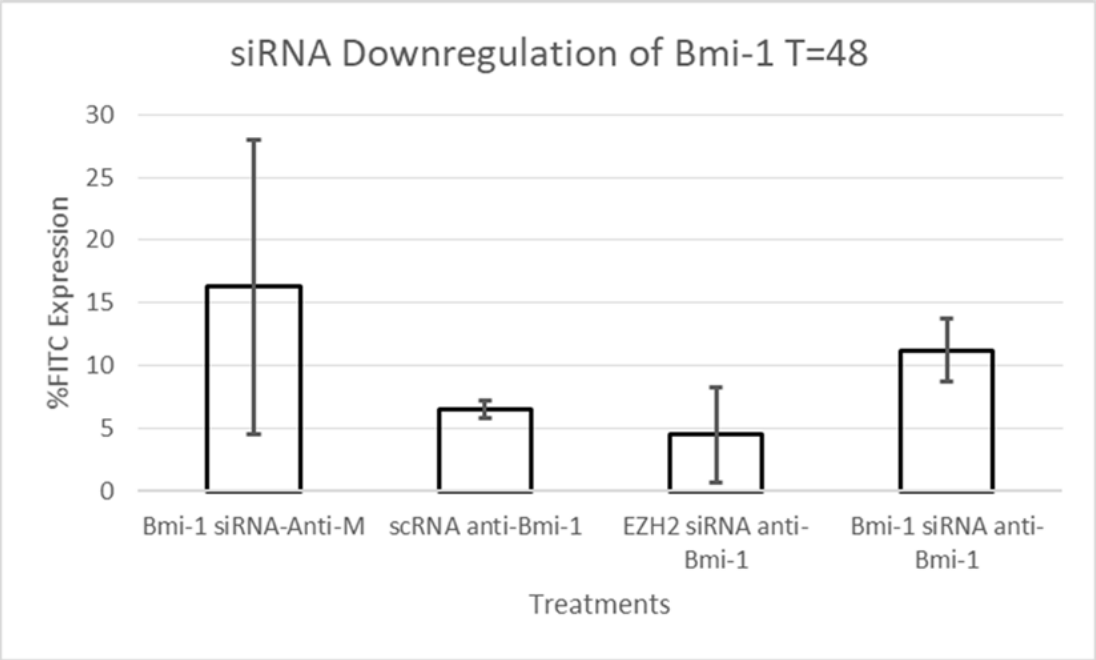

Panel B.

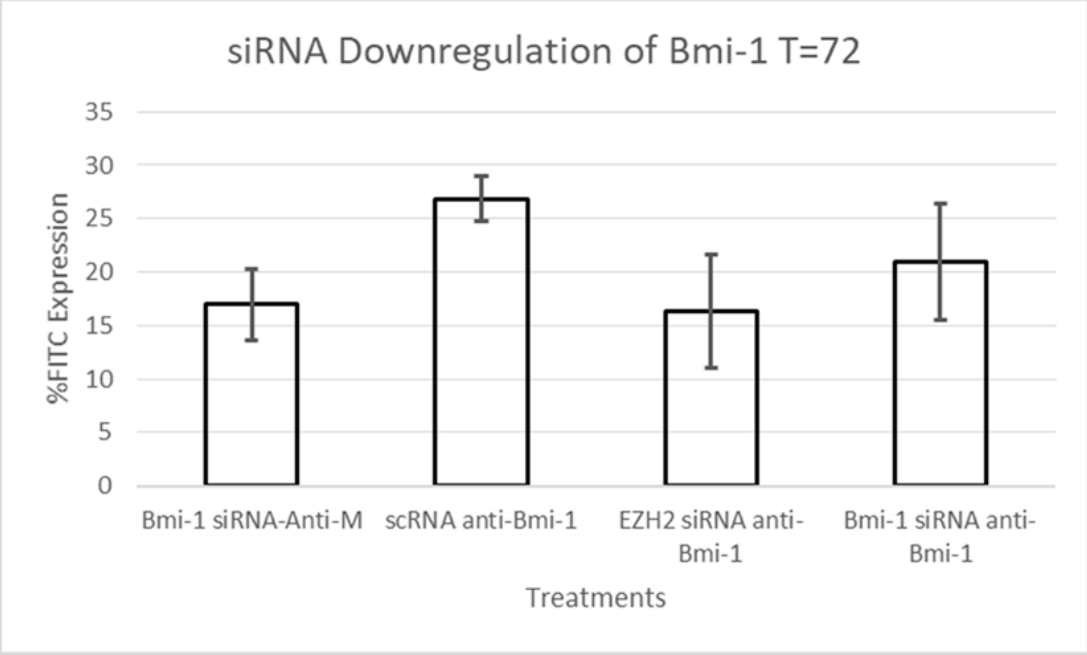

Figure 10. qPCR Analysis of MDV Genome Reactivation Through Targeted siRNA Knockdowns in UD35 cells.

Panel A: Targeted knockdowns of Bmi-1 and EZH2 were conducted following the procedure outlined in 2.4.2. Primers used to quantify MDV genome expression levels are targeted to gB (2.10). Primers targeted to ovotransferrin (2.10) were used to quantify host genome copy number. Duplicate samples (e.g. siEZH2 A and B) were each examined in duplicate (e.g. siEZH2 A-1 and A-2) on 96-well plate and the average of these two Ct values were used in statistical analysis. Significance was determined using ANOVA analysis. There were no significant differences between any of the siRNA treatments samples.

Panel B: Targeted knockdowns of Bmi-1 and EZH2 were conducted following 2.4.2. Reverse transcriptase was performed following procedure outlined in. Primers used to quantify Bmi-1 and EZH2 mRNA expression levels are detailed in 2.10. Bmi-1 and EZH2 mRNA expression levels were measured for their respective siRNA treatment and compared to scRNA. Ct values were analyzed via the delta-delta Ct method (Livak & Schmittgen, 2001).

Panel A.

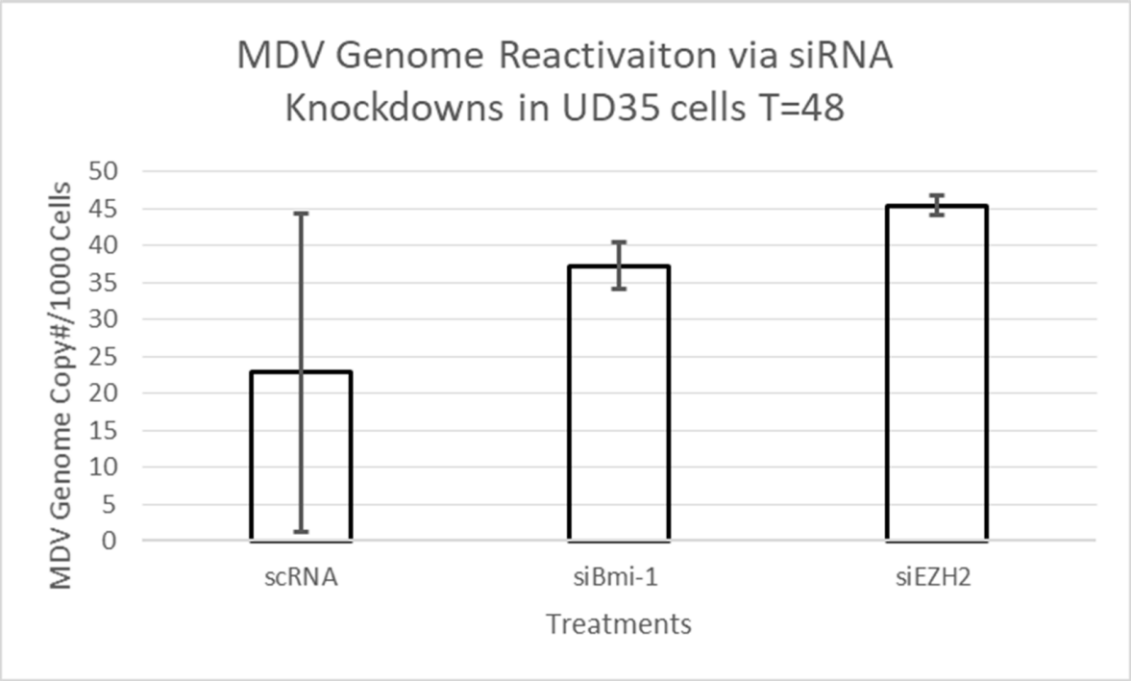

Panel B.

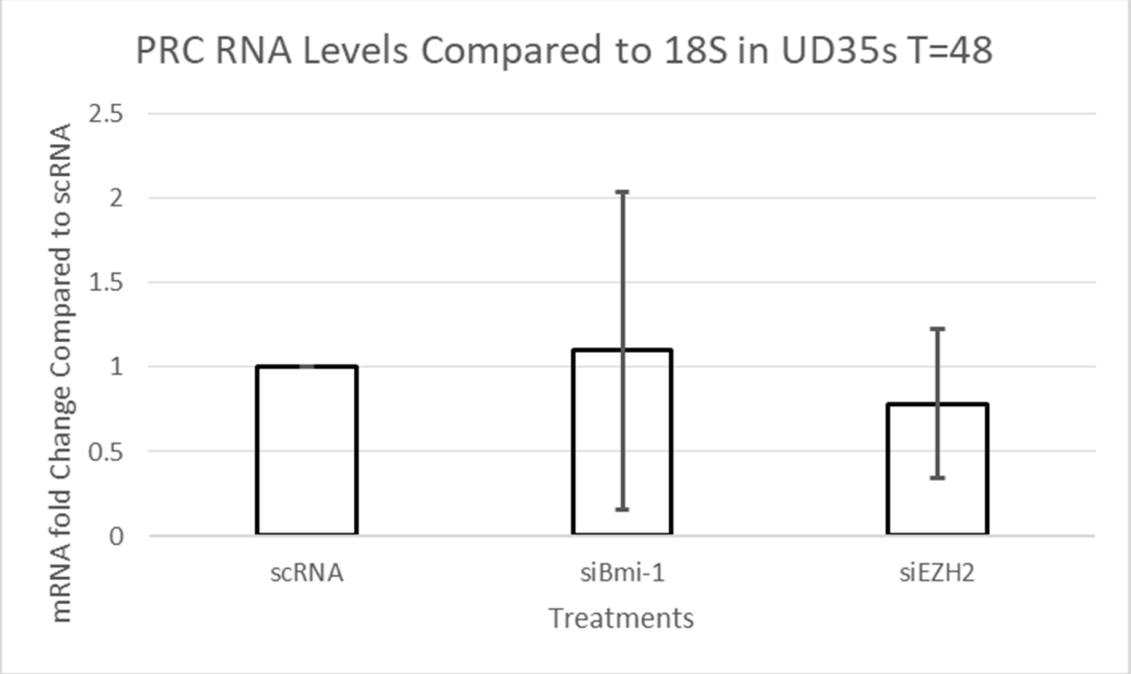

Figure 11. qPCR Analysis of MDV Genome Reactivation Through Targeted siRNA Knockdowns in UA22 cells.

Panel A: Targeted knockdowns of Bmi-1 and EZH2 were conducted following the procedure outlined in 2.4.2. Primers used to quantify MDV genome expression levels are targeted to gB (2.10). Primers targeted to ovotransferrin (2.10) were used to quantify host genome copy number. Duplicate samples (e.g. siEZH2 A and B) were each examined in duplicate (e.g. siEZH2 A-1 and A-2) on 96-well plate and the average of these two Ct values were used in statistical analysis. Significance was determined using ANOVA analysis. Significance of $p<0.05$ is denoted by '*' above siEZH2 and scRNA.

Panel B: Targeted knockdowns of Bmi-1 and EZH2 were conducted following 2.4.2. Reverse transcriptase was performed following procedure outlined in. Primers used to quantify Bmi-1 and EZH2 mRNA expression levels are detailed in 2.10. Bmi-1 and EZH2 mRNA expression levels were measured for their respective siRNA treatment and compared to scRNA. Ct values were analyzed via the delta-delta Ct method (Livak & Schmittgen, 2001).

Panel A.

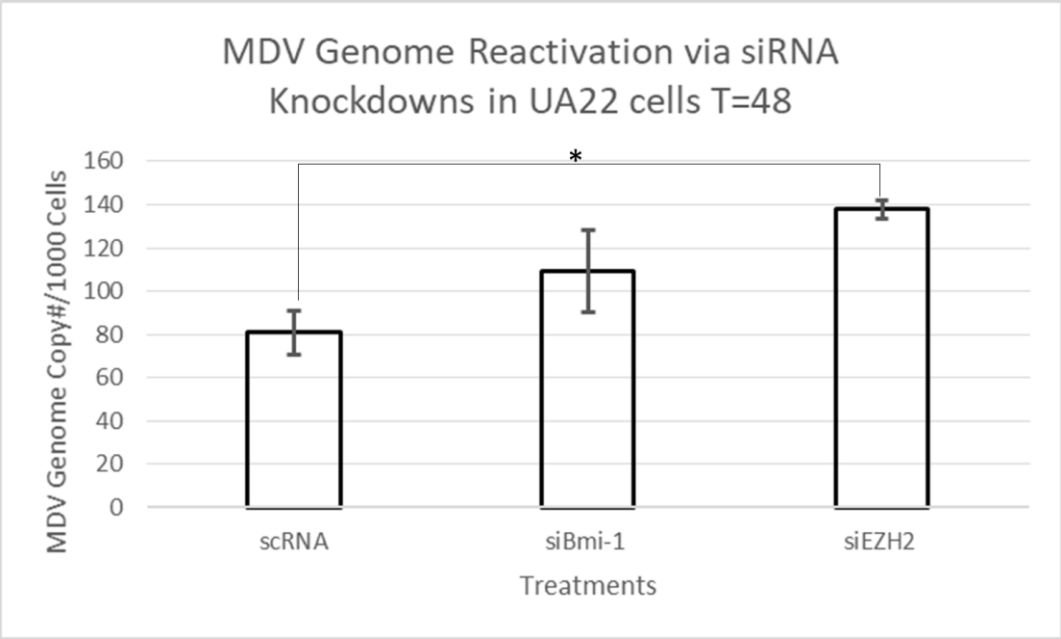

Panel B.

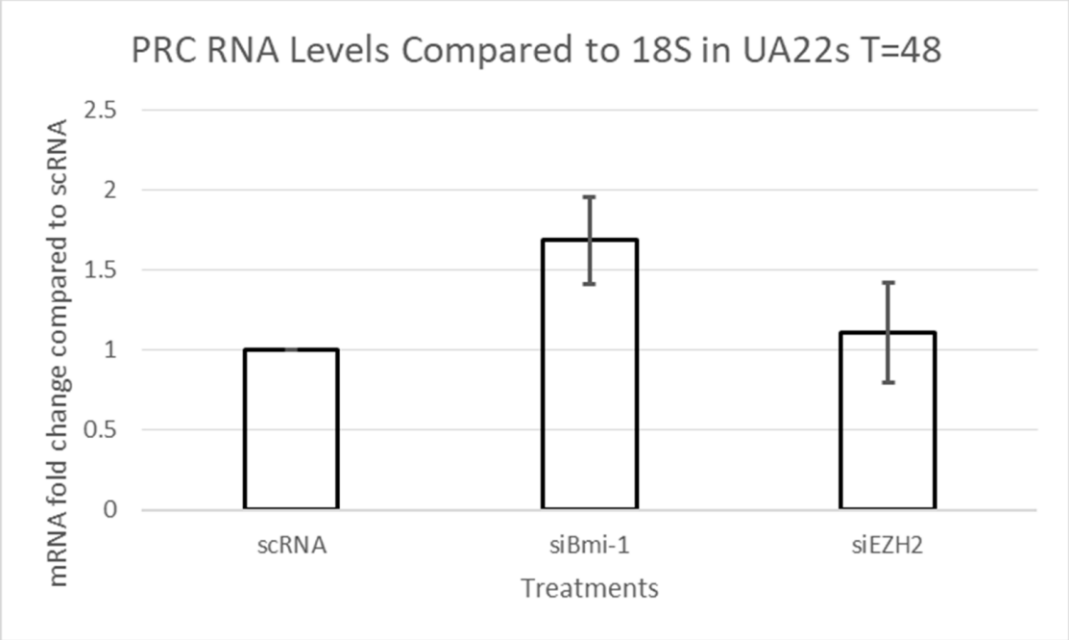

Figure 12. qPCR Analysis of MDV Genome Reactivation Through Targeted siRNA Knockdowns in UD35 cells.

Panel A+B: T24 (A) and T48(B) time points were collected following procedure outlined in 2.8. Targeted knockdowns of Bmi-1 and EZH2 were conducted following protocol detailed in 2.4.2. Primers used to quantify MDV genome expression levels are targeted to gB (2.10). Primers targeted to ovotransferrin (2.10) were used to quantify host genome copy number. Triplicate samples (were each examined in duplicate (e.g. siEZH2 A-1 and A-2) on 96-well plate and the average of these two Ct values were used in statistical analysis. Ct values were converted to genome copy numbers using a standard curve. No significance was determined using ANOVA analysis. Error bars indicate standard deviation of triplicate samples.

Panel A.

Panel B.

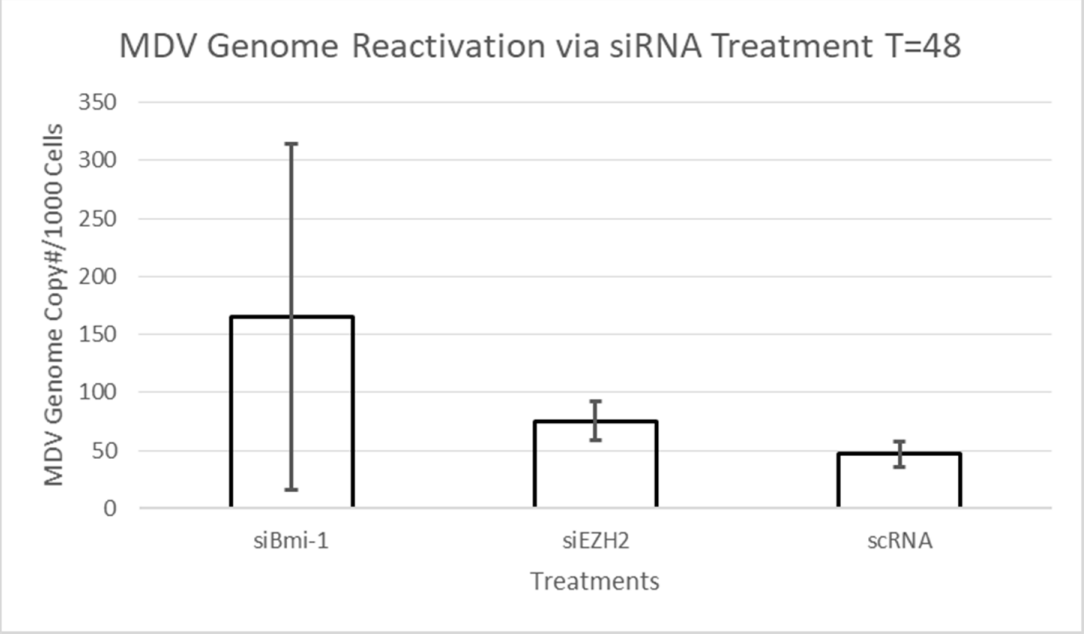

Figure 13. Localization Images of Fluorescent-Tagged Bmi-1, Meq, and Meq Variant Proteins.

Images taken were done so by a Zeiss 710 LSM T-PMT confocal microscope. These images were taken using a 40x oil emersion objective lens. Images taken were analyzed via Zen Lite software. All transfections were done so following procedure detailed in 2.4.1.

Panel A: Single transfection of peCFP-Bmi-1. Bmi-1-CFP is seen localized to the nucleus specifically. 'Merged' indicates a merged image of both Bmi-1-CFP and Bright-Field images.

Panel B: Single transfection of peYFP-Meq. Full length Meq with YFP tag is localized to nucleus and, more specifically, the nucleolus in both 'Meq-YFP' and 'Merged' panels. 'Merged' indicates a merged image of both Meq-YFP and Bright-Field images.

Panel C: Single transfection of peYFP-Meq/vIL8. YFP-tagged Meq-splice-variant is seen here localized to the nucleolus in both 'Meq/vIL8' and 'Merged' panels. 'Merged' indicates a merged image of both Meq/vIL8-YFP and Bright-Field images.

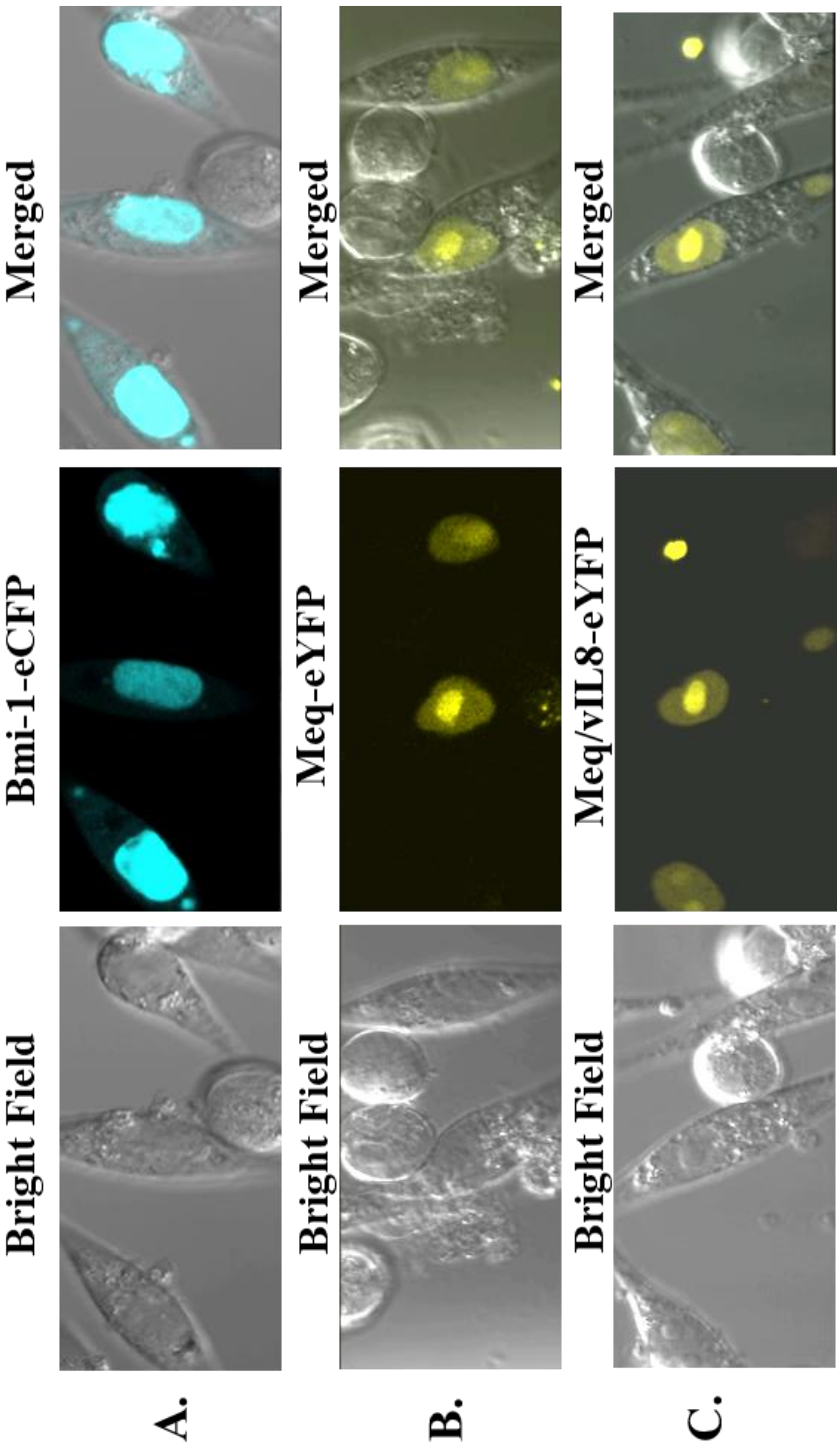
Bright Field
Bmi-1-eCFP
Merged
Bright Field
Meq-eYFP
Merged
Bright Field
Meq/vIL8-eYFP
Merged
A.
B.
C.

Figure 14. Co-Localization Images of Fluorescent-Tagged Bmi-1, Meq, and Meq Vairant Proteins.

Images taken were done so by a Zeiss 710 LSM T-PMT confocal microscope. These images were taken using a 40x oil emersion objective lens. Images taken were analyzed via Zen Lite software. All co-transfections were done so following procedure detailed in 2.4.1.

Panel A: Co-transfection of peCFP-Bmi-1 and peYFP-Meq. Image is taken from the T0 time-point of corresponding FRET experiment. 'Merged' panel indicates a merged image of 'Meq-YFP', 'Bmi-1-CFP', and 'Bright-Field' panels.

Panel B: Co-transfection of pBKCMV-Bmi-1-CFP and peYFP-Meq/vIL8. Image is taken from the T0 time-point of corresponding FRAP experiment. 'Merged' panel indicates a merged image of all other panels.

Panel C: Co-transfection of peCFP-Bmi-1 and peYFP-Meq/vIL8Δexon3. Image is taken from the T0 time-point of corresponding FRET experiment. 'Merged' panel indicates a merged image of all other panels.

Panel D: Co-transfection of peYFP-Bmi-1 and peCFP-Meq-AVEFT. Image is taken from the T0 time-point of corresponding FRET experiment. 'Merged' panel indicates a merged image of all other panels.

Panel E: Co-transfection of peCFP-Bmi-1 and peYFP-Meq/vIL8-AVEFT. Image is taken from the T0 time-point of corresponding FRET experiment. 'Merged' panel indicates a merged image of all other panels.

Bright Field
Bmi-1-eCFP
Meq-eYFP
Merged
A.
Bright Field
Bmi-1-eCFP
Meq/vIL8-eYFP
Merged
B.
Bright Field
Bmi-1-eCFP
Meq/vIL8Δexon3-eYFP
Merged
C.
Bright Field
Bmi-1-eYFP
Meq-AVEFT-eCFP
Merged
D.
Bright Field
Bmi-1-eCFP
Meq/vIL8-AVEFT-eYFP
Merged
E.

Figure 15. FRET Analysis of Bmi-1-CFP and Meq-YFP Co-Transfections.

FRET analysis and images of corresponding transfection images were taken using a Zeiss 710 LSM T-PMT confocal microscope. These images were taken using a 40x oil emersion objective lens. All co-transfections were done so following procedure detailed in 2.4.1. FRET experiments were done following procedure detailed in 2.11.1.

Panel A: Cropped image of peCFP-Bmi-1 and peYFP-Meq co-transfection, taken at T4, directly prior to photobleaching event of YFP. Red circle indicates area of photobleaching event.

Panel B: Cropped image of peCFP-Bmi-1 and peYFP-Meq co-transfection, taken at T5, directly after photobleaching event of YFP. Red circle indicates area of photobleaching event.

Panel C: Graph showing the progression of Fluorescence intensity over time. Bmi-CFP intensity is depicted in blue, while Meq-YFP intensity is shown in yellow. Photobleach occurs between 5.99 and 11.97 second time frames. Percent fluorescence efficiency equals 0.13265 analyzed via Zen 2011 FRET analysis software.

Panel A.

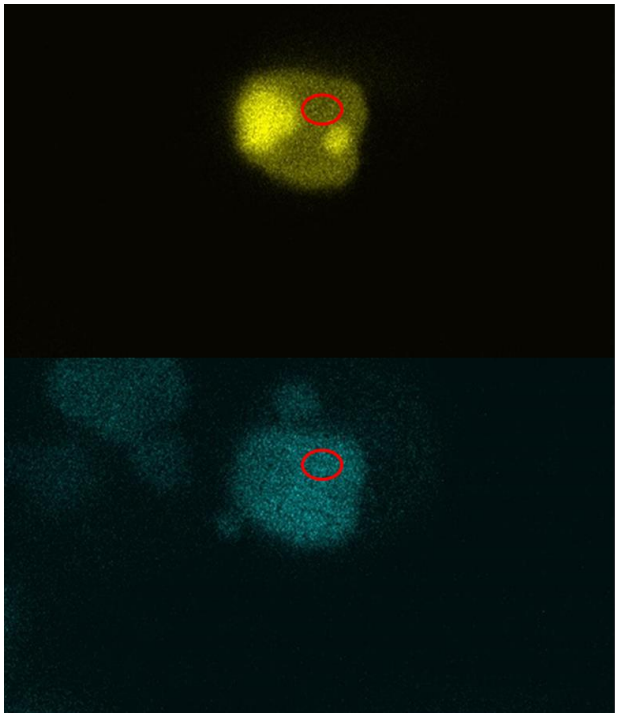

Panel B.

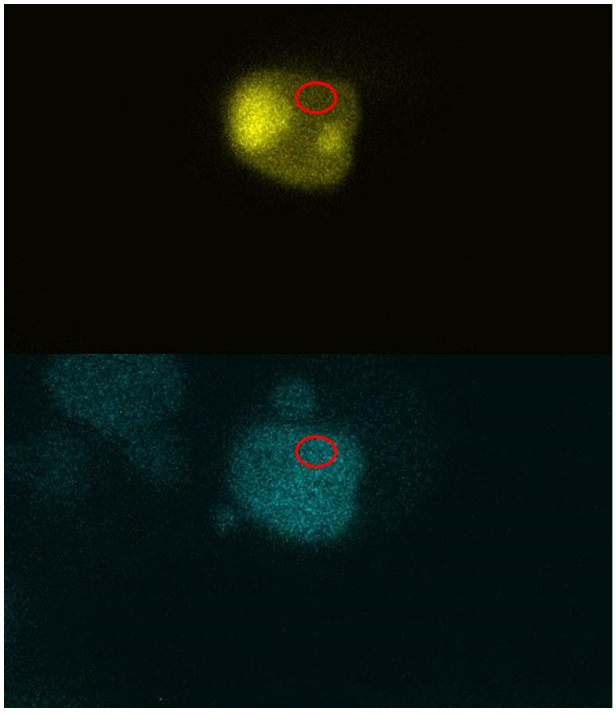

Panel C.

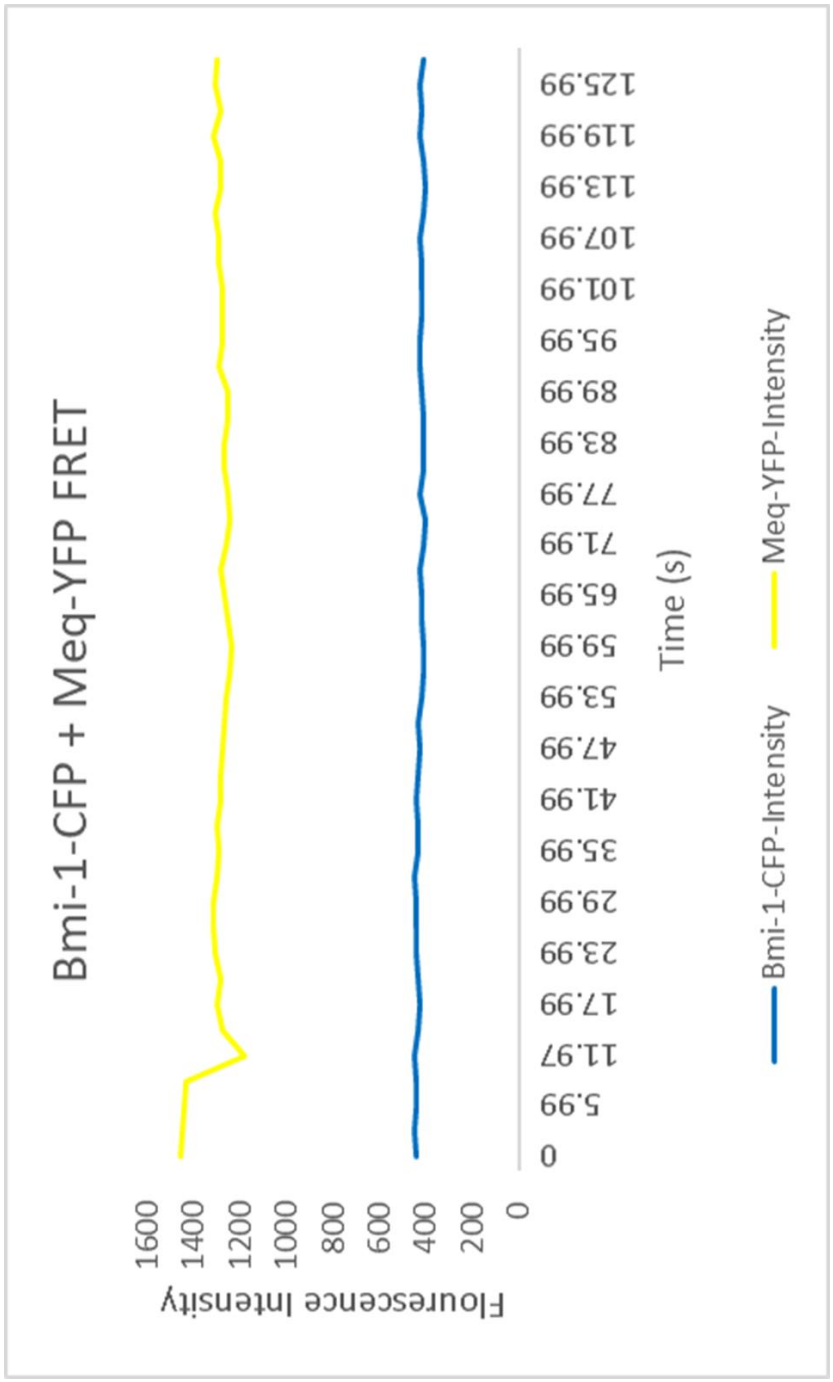
Bmi-1-CFP + Meq-YFP FRET
Fluorescence Intensity
1600
1400
1200
1000
800
600
400
200
0
Time (s)
0
5.99
11.97
17.99
23.99
29.99
35.99
41.99
47.99
53.99
59.99
65.99
71.99
77.99
83.99
89.99
95.99
101.99
107.99
113.99
119.99
125.99
Bmi-1-CFP-Intensity
Meq-YFP-Intensity

Figure 16. FRET Analysis of Bmi-1-CFP and Meq/vIL8-YFP Co-Transfections.

FRET analysis and images of corresponding transfection images were taken using a Zeiss 710 LSM T-PMT confocal microscope. These images were taken using a 40x oil emersion objective lens. All co-transfections were done so following procedure detailed in 2.4.1. FRET experiments were done following procedure detailed in 2.11.1.

Panel A: Cropped image of peCFP-Bmi-1 and peYFP-Meq/vIL8 co-transfection, taken at T4, directly prior to photobleaching event of YFP. Red circle indicates where photobleaching event occurs.

Panel B: Cropped image of peCFP-Bmi-1 and peYFP-Meq/vIL8 co-transfection, taken at T5, directly after photobleaching event of YFP. Red circle indicates where photobleaching event occurs.

Panel C: Graph depicting the progression of fluorescence over time. Region-1: Bmi-1-CFP shown in light blue, with Meq/vIL8-YFP shown in gold. Region-2: Bmi-1-CFP shown in dark blue, while Meq/vIL8-YFP is graphed in orange. Region-3: is a control region, with fluorescence taken from an area with no cell. Photobleaching event occurs in-between 6 second and 11.99 second time points. Percent fluorescence efficiency for Region 1 is 22.37738 and Region 2 equals 22.46762 based on Zen 2011 FRET analysis software.

Panel A.

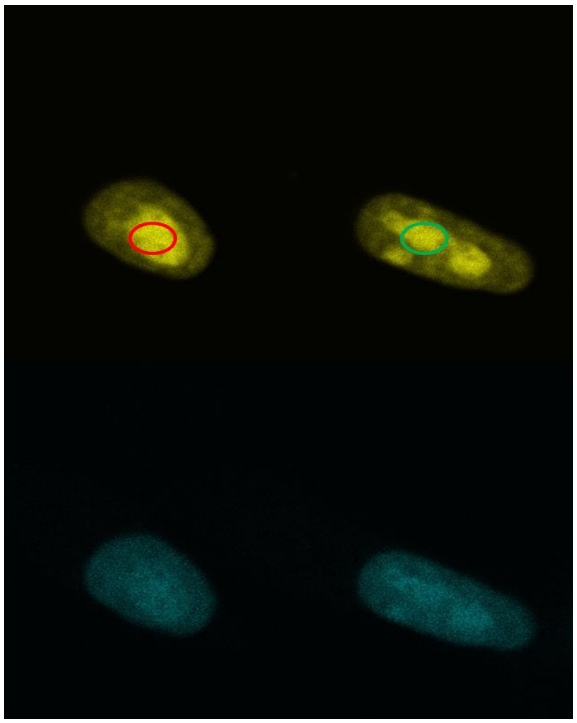

Panel B.

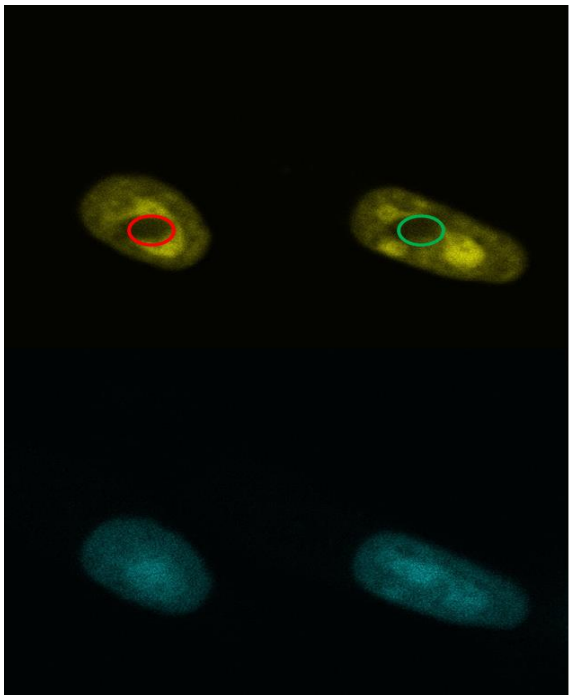

Panel C.

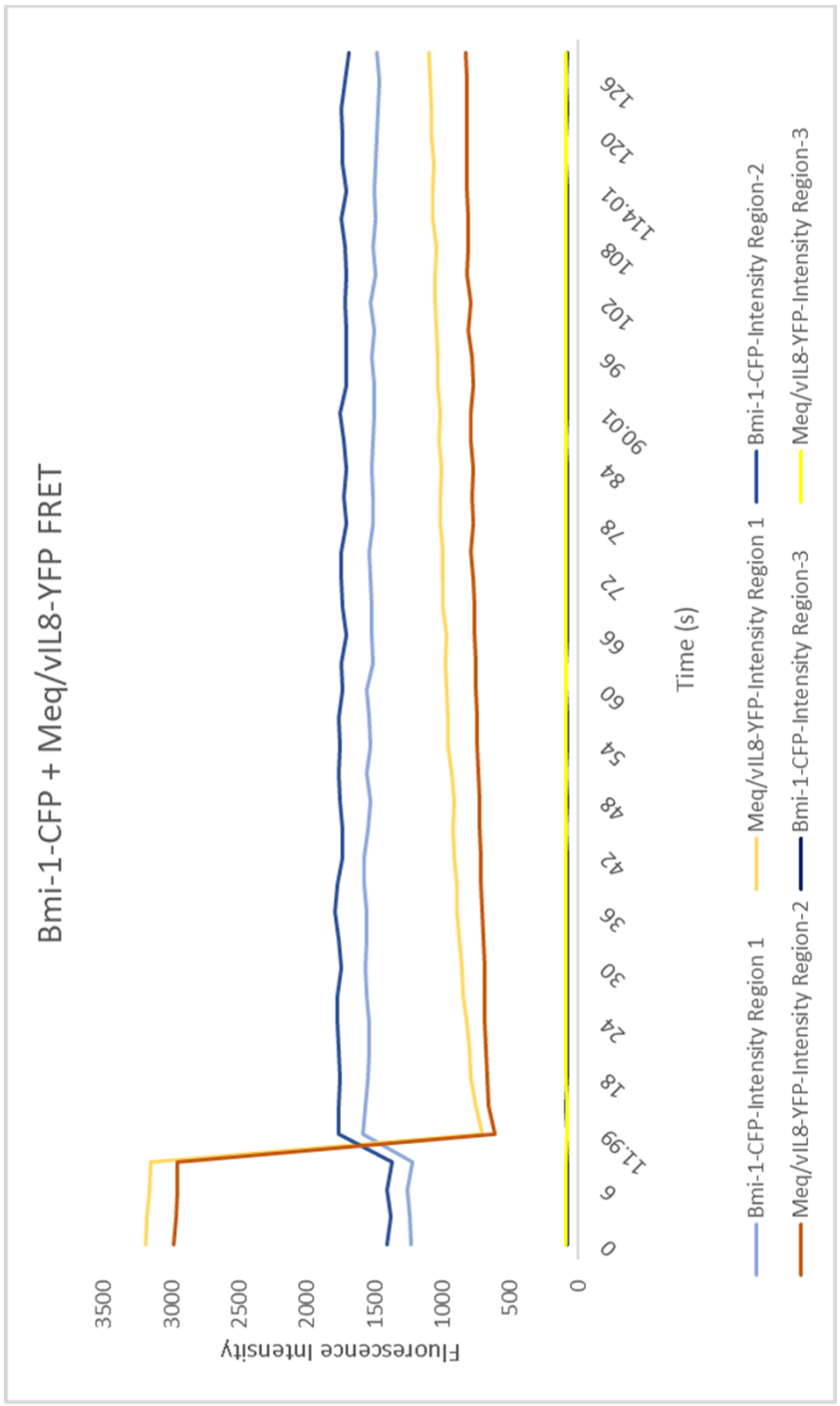
Bmi-1-CFP + Meq/vIL8-YFP FRET
Fluorescence Intensity
3500
3000
2500
2000
1500
1000
500
0
0
6
11.99
18
24
30
36
42
48
54
60
66
72
78
84
90.01
96
102
108
114.01
120
126
Time (s)
Bmi-1-CFP-Intensity Region 1
Meq/vIL8-YFP-Intensity Region 1
Bmi-1-CFP-Intensity Region-2
Meq/vIL8-YFP-Intensity Region-2
Bmi-1-CFP-Intensity Region-3
Meq/vIL8-YFP-Intensity Region-3

Figure 17. **FRET Analysis of Bmi-1-CFP and Meq/vIL8Δexon3-YFP Co-Transfections.**

FRET analysis and images of corresponding transfection images were taken using a Zeiss 710 LSM T-PMT confocal microscope. These images were taken using a 40x oil emersion objective lens. All co-transfections were done so following procedure detailed in 2.4.1. FRET experiments were done following procedure detailed in 2.11.1.

Panel A: Cropped image of peCFP-Bmi-1 and peYFP-Meq/vIL8Δexon3 co-transfection, taken at T4, directly prior to photobleaching event of YFP.

Panel B: Cropped image of peCFP-Bmi-1 and peYFP-Meq/vIL8Δexon3 co-transfection, taken at T5, directly after photobleaching event of YFP.

Panel C: Graph showing the progression of fluorescence over time. Region 1: Bmi-1-CFP is indicated by the dark blue line, while Meq/vIL8Δexon3-YFP is shown in gold. Region 2: Bmi-CFP expression is shown in light blue and Meq/vIL8Δexon3-YFP is depicted in orange. Photobleaching event occurs from the 6.01 second and 12.98 second time points. Percent fluorescence efficiency is 3.99861 for Region 1 and 8.65311 for Region 2. Efficiency measurements were obtained through Zen 2011 FRET analysis software.

Panel A.

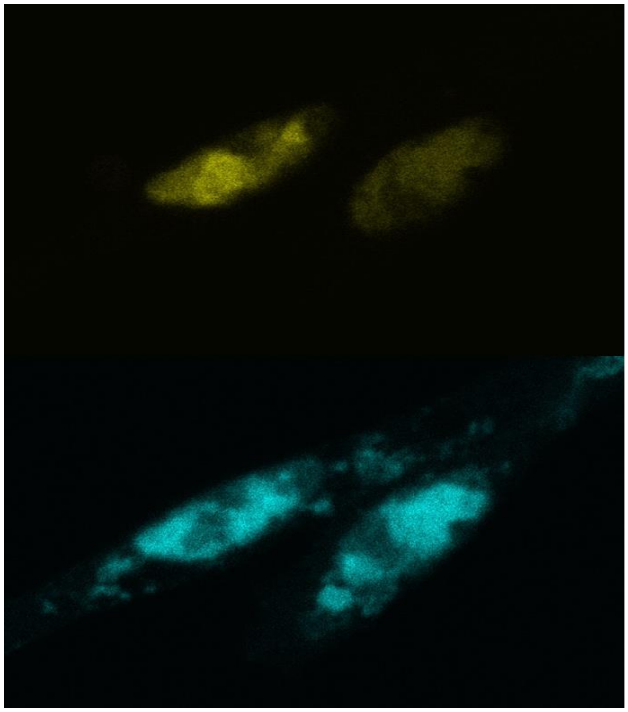

Panel B.

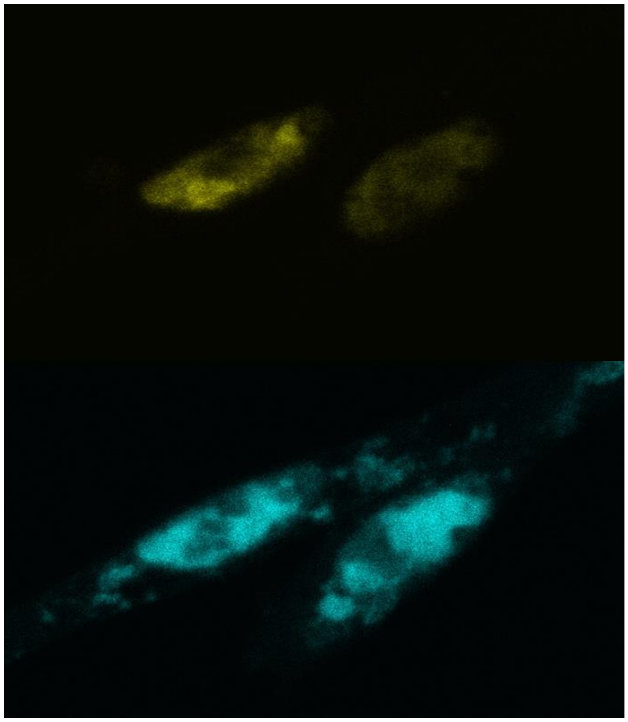

Panel C.

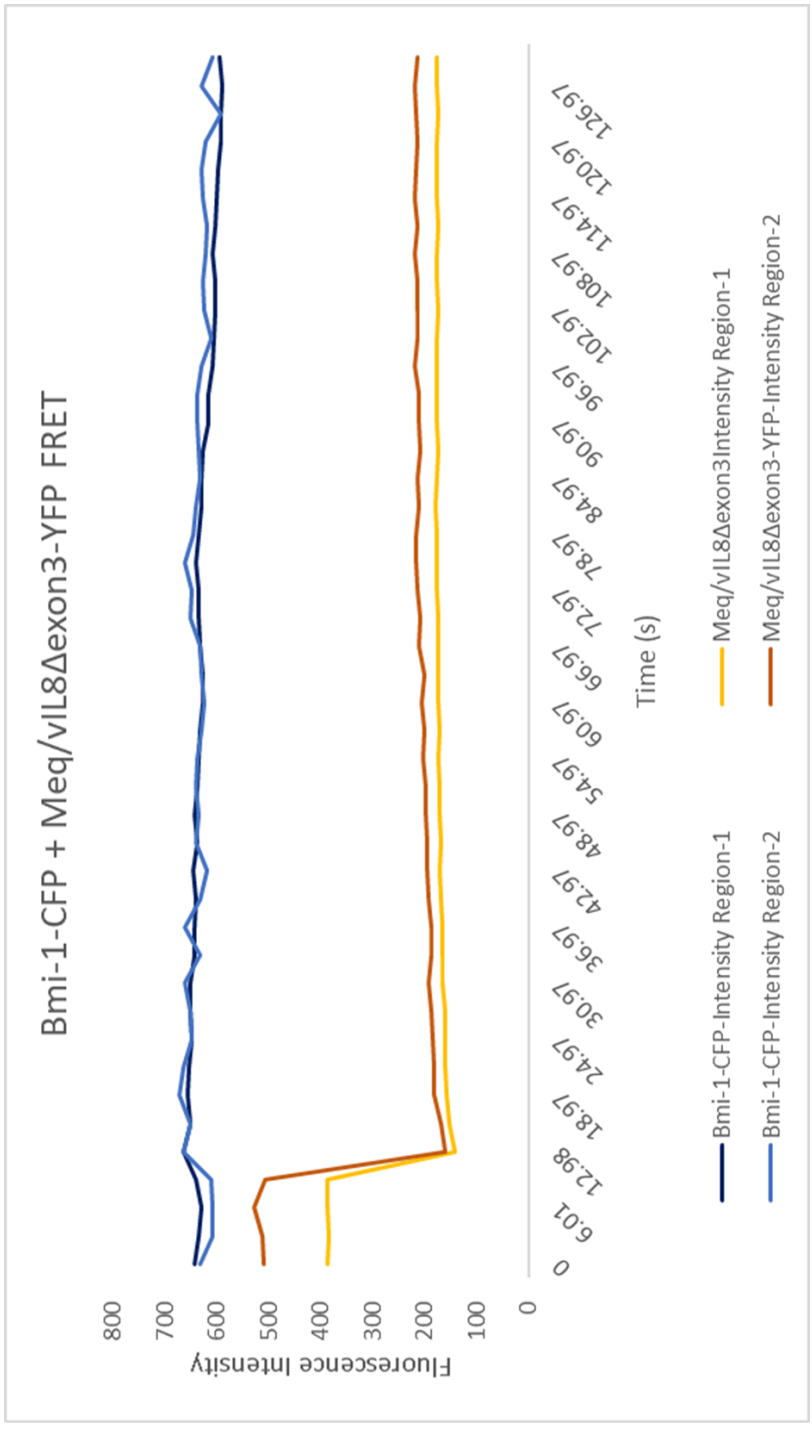
Bmi-1-CFP + Meq/vIL8Δexon3-YFP FRET
Fluorescence Intensity
800
700
600
500
400
300
200
100
0
Time (s)
0
6.01
12.98
18.97
24.97
30.97
36.97
42.97
48.97
54.97
60.97
66.97
72.97
78.97
84.97
90.97
96.97
102.97
108.97
114.97
120.97
126.97
Bmi-1-CFP-Intensity Region-1
Bmi-1-CFP-Intensity Region-2
Meq/vIL8Δexon3Intensity Region-1
Meq/vIL8Δexon3-YFP-Intensity Region-2

Figure 18. FRET Analysis of Bmi-1-YFP and Meq-AVEFT-CFP Co-Transfections**.**

FRET analysis and images of corresponding transfection images were taken using a Zeiss 710 LSM T-PMT confocal microscope. These images were taken using a 40x oil emersion objective lens. All co-transfections were done so following procedure detailed in 2.4.1. FRET experiments were done following procedure detailed in 2.11.1.

Panel A: Cropped image of peYFP-Bmi-1 and peCFP-Meq-AVEFT co-transfection, taken at T4, directly prior to photobleaching event of YFP.

Panel B: Cropped image of pBKCMV-Bmi-1-YFP and peCFP-Meq-AVEFT co-transfection, taken at T5, directly after photobleaching event of YFP.

Panel C: Graph portraying fluorescence intensity over the course of 130 seconds. Region 1: Bmi-1-YFP is represented in gold and Meq-AVEFT-CFP in light blue. Region 0 shows an area with no cells to be used as a negative control. Photobleaching occurs between 6 seconds and 12.29 seconds. Fluorescence percent efficiency for Region 1 is 2.86654.

Panel A.

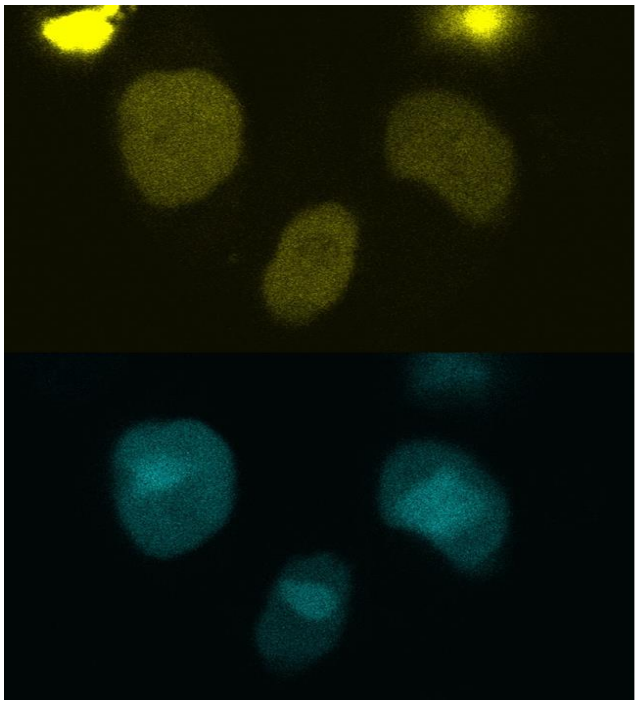

Panel B.

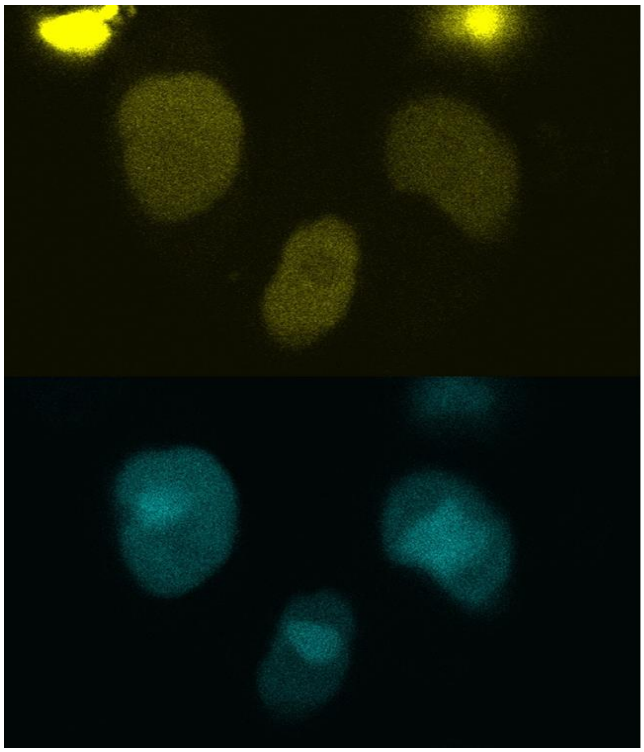

Panel C.

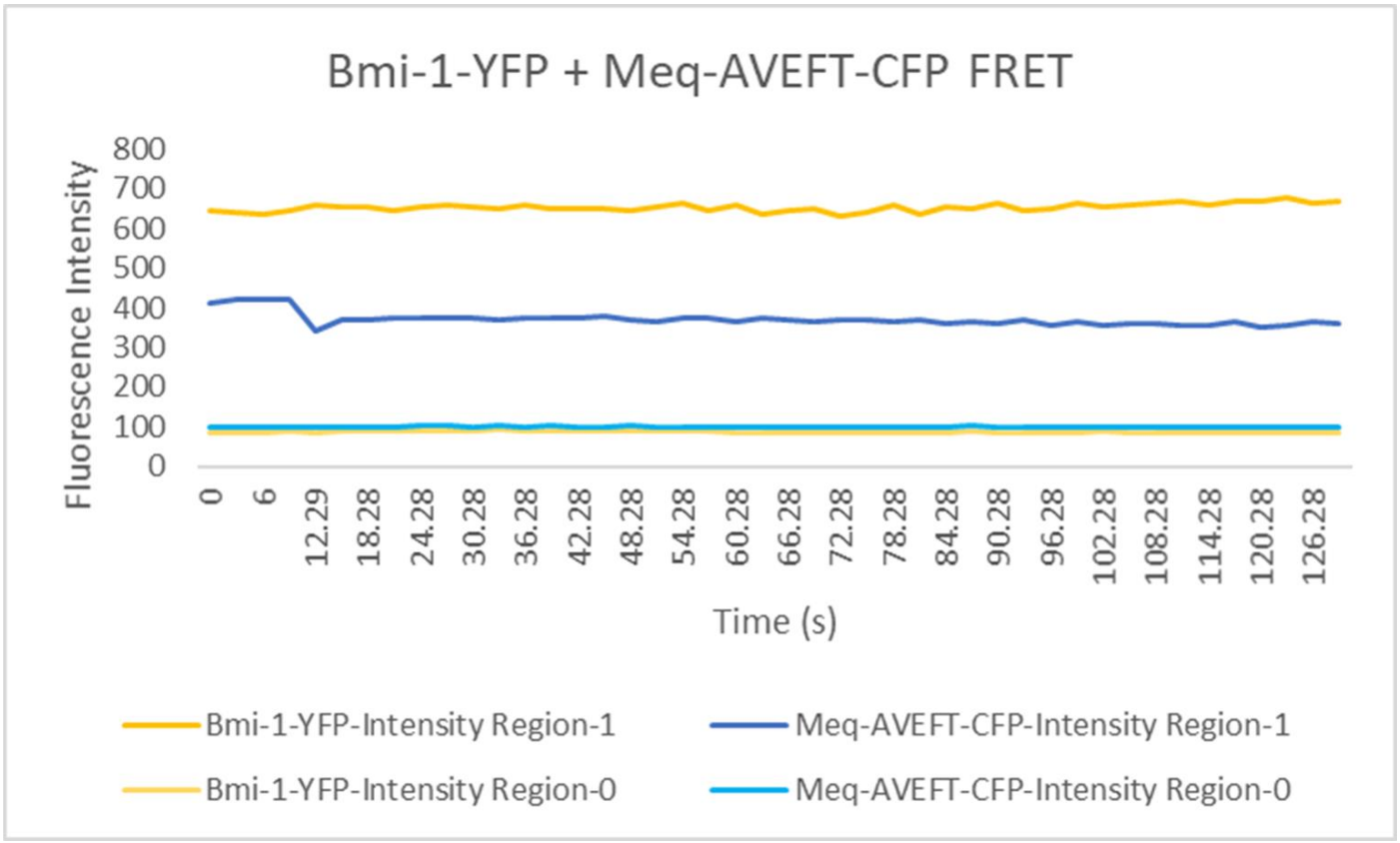
Bmi-1-YFP + Meq-AVEFT-CFP FRET
Fluorescence Intensity
800
700
600
500
400
300
200
100
0
0
6
12.29
18.28
24.28
30.28
36.28
42.28
48.28
54.28
60.28
66.28
72.28
78.28
84.28
90.28
96.28
102.28
108.28
114.28
120.28
126.28
Time (s)
Bmi-1-YFP-Intensity Region-1
Meq-AVEFT-CFP-Intensity Region-1
Bmi-1-YFP-Intensity Region-0
Meq-AVEFT-CFP-Intensity Region-0

Figure 19. FRET Analysis of Bmi-1-CFP and Meq/vIL8-AVEFT-YFP Co-Transfections.

FRET analysis and images of corresponding transfection images were taken using a Zeiss 710 LSM T-PMT confocal microscope. These images were taken using a 40x oil emersion objective lens. All co-transfections were done so following procedure detailed in 2.4.1. FRET experiments were done following procedure detailed in 2.11.1.

Panel A: Cropped image of peCFP-Bmi-1 and peYFP-Meq/vIL8-AVEFT co-transfection, taken at T4, directly prior to photobleaching event of YFP.

Panel B: Cropped image of peCFP-Bmi-1 and peYFP-Meq/vIL8-AVEFT co-transfection, taken at T5, directly after photobleaching event of YFP.

Panel C: Graph representing fluorescence expression over time. Region 1: Bmi-1-CFP is depicted in dark blue with Meq/vIL8-AVEFT-YFP shown in gold. Region 2: Bmi-1-CFP is shown in light blue with Meq/vIL8-AVEFT-YFP is shown in orange. Region 3 is a negative control region. Photobleaching event occurs between the 5.99 and 11.98 second mark. Percent fluorescence efficiency (determined by Zen 2011 FRET analysis software) for Region 1 is 42.41046, while Region 2 is -1.66554.

Panel A.

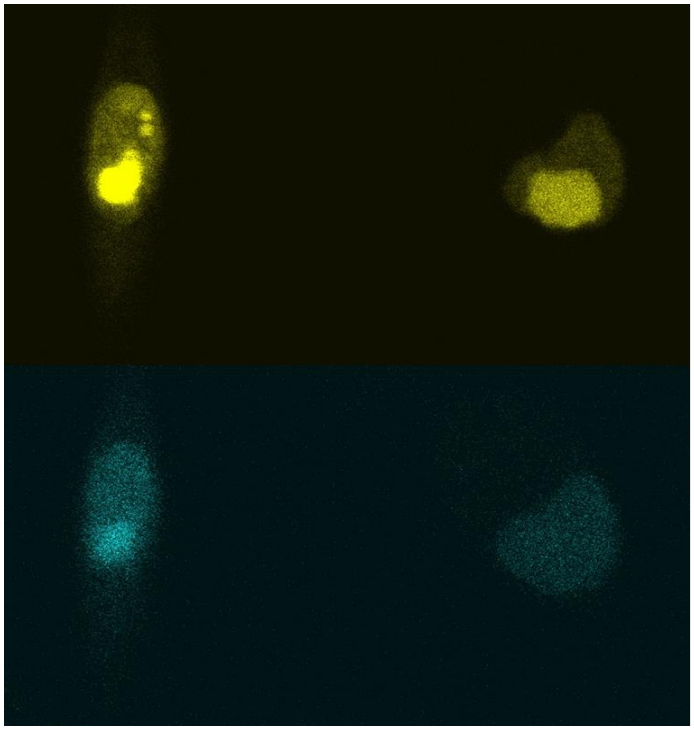

Panel B.

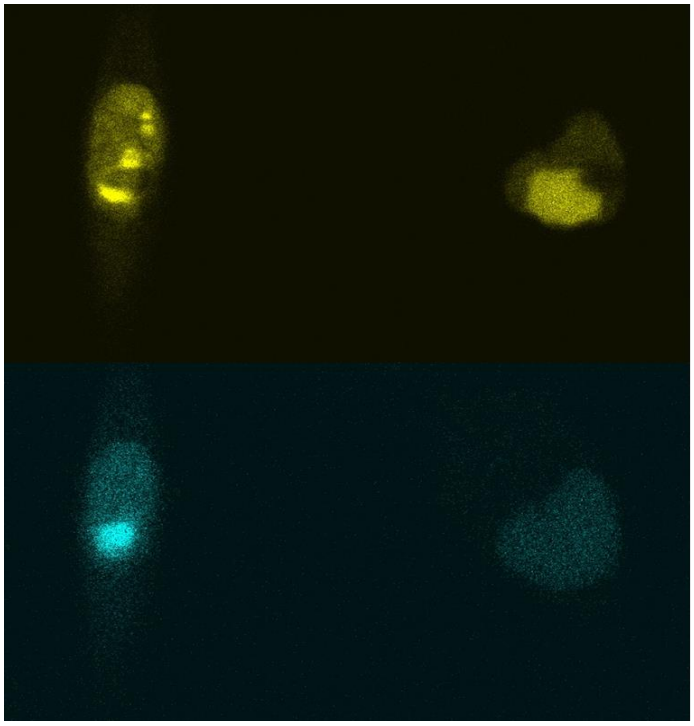

Panel C.

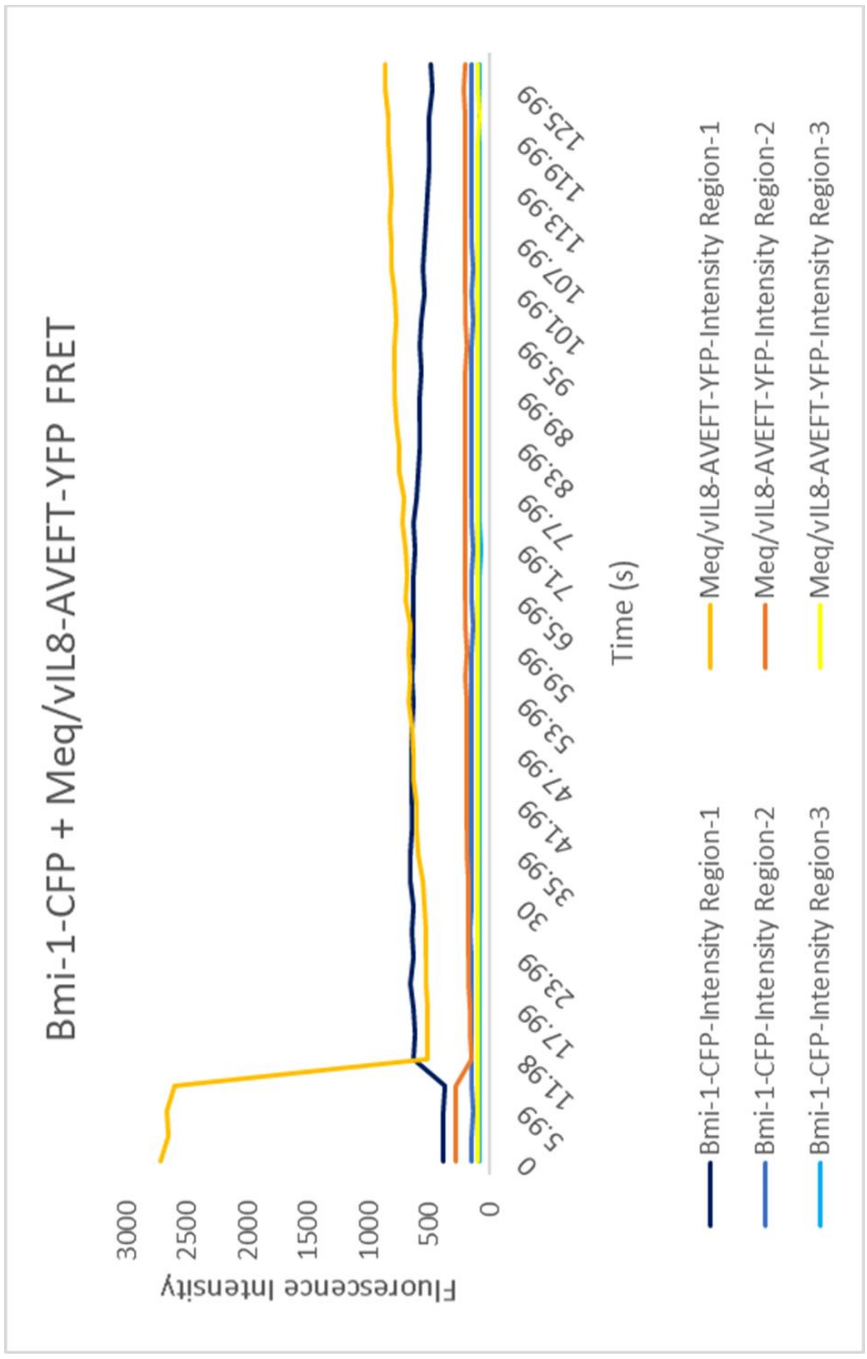
Bmi-1-CFP + Meq/vIL8-AVEFT-YFP FRET
Fluorescence Intensity
3000
2500
2000
1500
1000
500
0
0
5.99
11.98
17.99
23.99
30
35.99
41.99
47.99
53.99
59.99
65.99
71.99
77.99
83.99
89.99
95.99
101.99
107.99
113.99
119.99
125.99
Time (s)
Bmi-1-CFP-Intensity Region-1
Bmi-1-CFP-Intensity Region-2
Bmi-1-CFP-Intensity Region-3
Meq/vIL8-AVEFT-YFP-Intensity Region-1
Meq/vIL8-AVEFT-YFP-Intensity Region-2
Meq/vIL8-AVEFT-YFP-Intensity Region-3

Figure 20. FRET Efficiencies for Each Co-Transfection.

Bar graph depicting the percent FRET efficiencies for each of the co-transfected images. FRET efficiencies were determined by the formula (Dpost – Dpre)/Dpre x 100. Numbers following co-transfection sample name on *x-axis* indicate the Region of photobleaching for that sample.

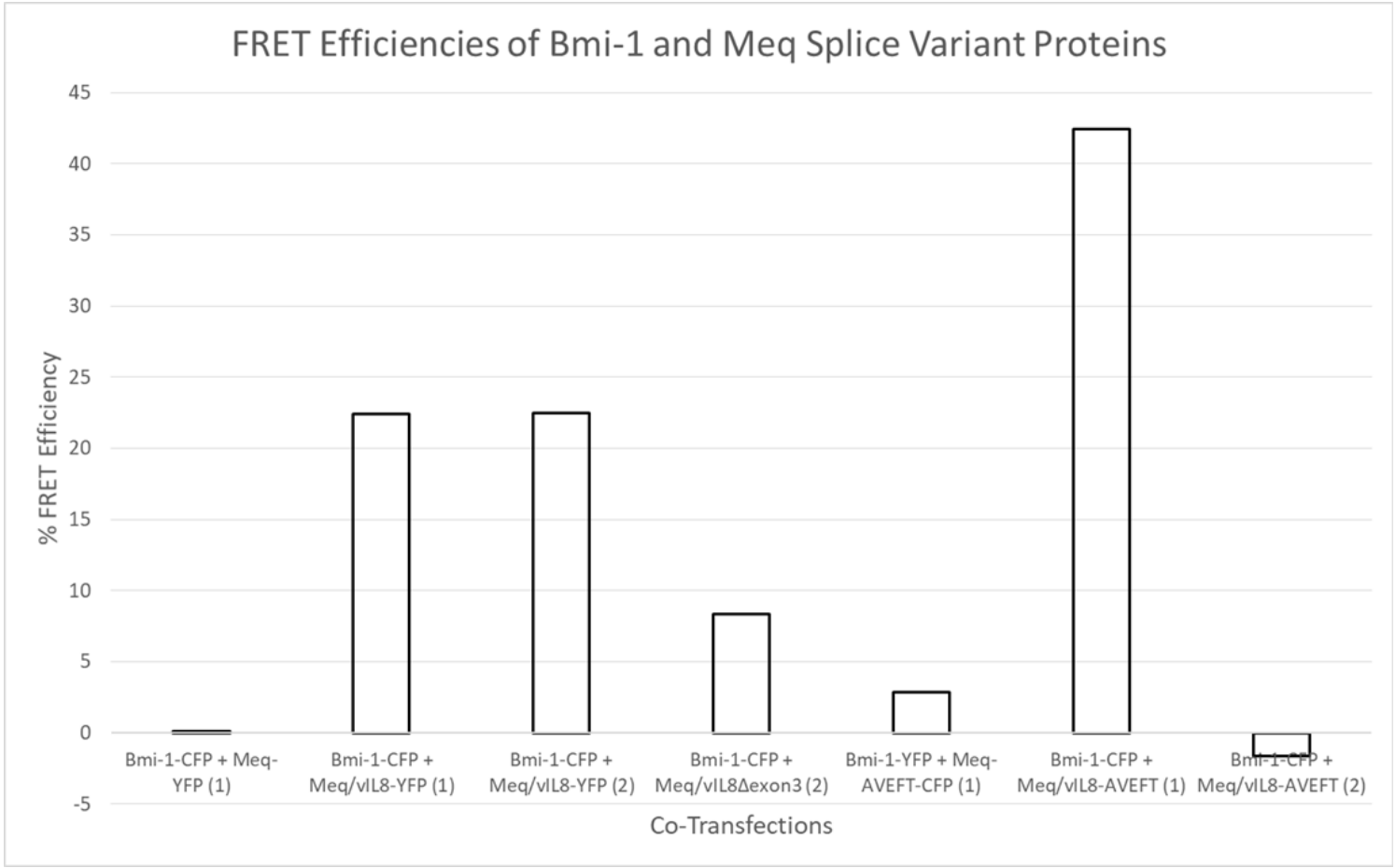
FRET Efficiencies of Bmi-1 and Meq Splice Variant Proteins
% FRET Efficiency
45
40
35
30
25
20
15
10
5
0
-5
Bmi-1-CFP + Meq-YFP (1)
Bmi-1-CFP + Meq/vIL8-YFP (1)
Bmi-1-CFP + Meq/vIL8-YFP (2)
Bmi-1-CFP + Meq/vIL8Δexon3 (2)
Bmi-1-YFP + Meq-AVEFT-CFP (1)
Bmi-1-CFP + Meq/vIL8-AVEFT (1)
Bmi-1-CFP + Meq/vIL8-AVEFT (2)
Co-Transfections

Figure 21. FRAP Analysis of Bmi-1 When Transfected Alone and When Co-Transfected With Meq or Meq-Splice-Variants.

Panel A: Graph depicting FRAP of Bmi-1-CFP from a single transfection in HTC cells. Bmi-1 is shown in dark blue in Region-1 and light blue in Region-2. BF-control is used as a non-photobleached negative control. Photobleaching event occurs between 6 and 10.67 seconds. Half-life time for Region-1 is 2.8371s and 2.2989s for Region-2.

Panel B: Graph showing FRAP of Bmi-1-CFP when co-transfected with Meq-YFP in HTC cells. Bmi-1 is shown in dark blue for Region-1, purple for Region-2 and light blue for Region-3 (a region that was not photobleached, to be used as a negative control). Photobleaching occurs between 8.98 and 12.38 seconds. Half-life time for Bmi-1-CFP-Region-1 is 1.6865s, while Region-2 is 42.0847.

Panel C: Graph showing FRAP of Bmi-1-CFP when co-transfected with Meq/vIL8-YFP in HTC cells. Bmi-1 is shown in dark blue for Region-1, light blue for Region-2 and turquoise for the negative control Region-3. Photobleach event occurs between 9.01 and 12 seconds. The half-life time for Bmi-1-CFP-Region-1 is 2.5932s, while the half-life time for Bmi-1-CFP-Region 2 is 3.8481.

Panel A.

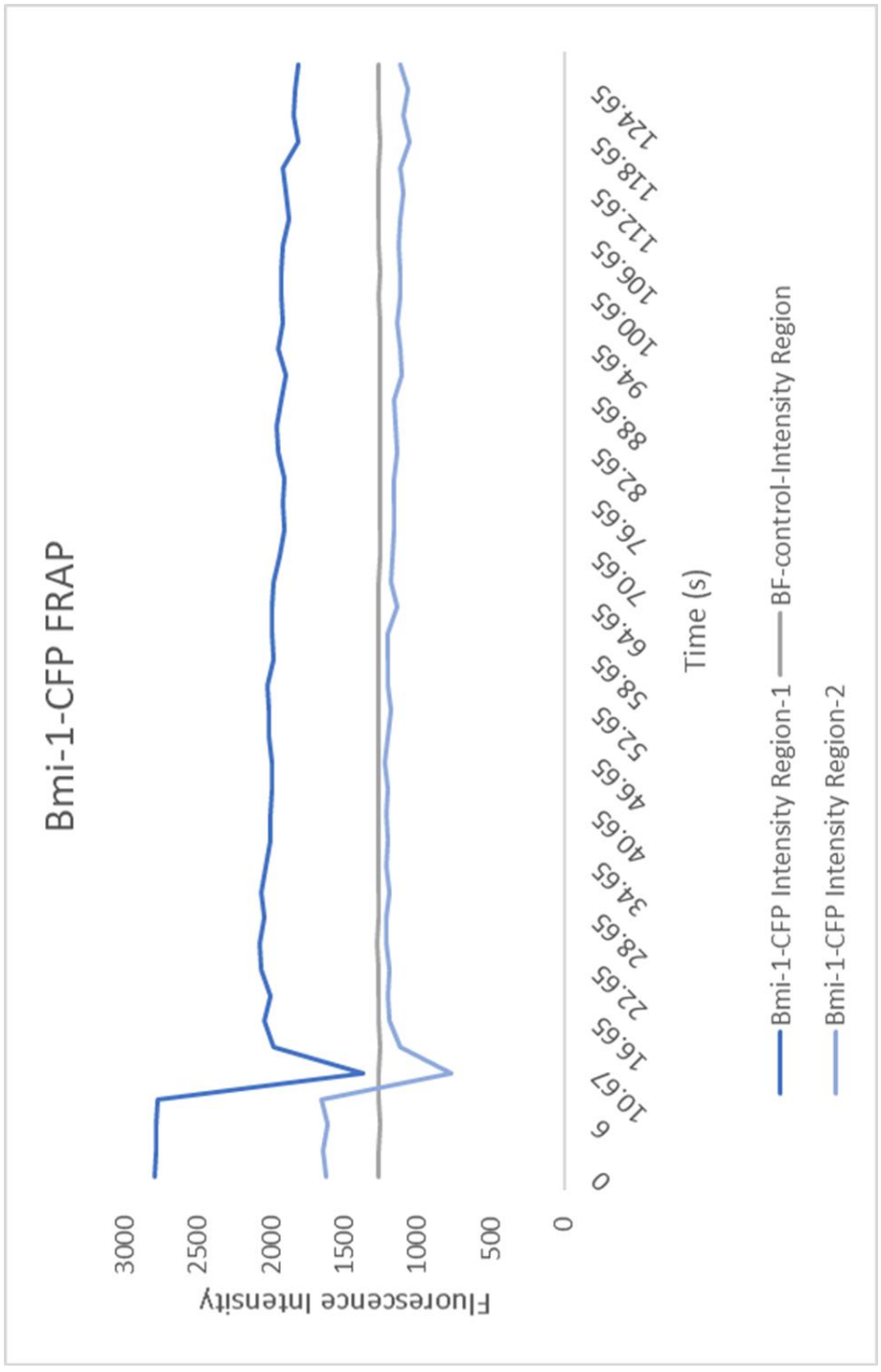
Bmi-1-CFP FRAP
Fluorescence Intensity
3000
2500
2000
1500
1000
500
0
0
6
10.67
16.65
22.65
28.65
34.65
40.65
46.65
52.65
58.65
64.65
70.65
76.65
82.65
88.65
94.65
100.65
106.65
112.65
118.65
124.65
Time (s)
Bmi-1-CFP Intensity Region-1
BF-control-Intensity Region
Bmi-1-CFP Intensity Region-2

Panel B.

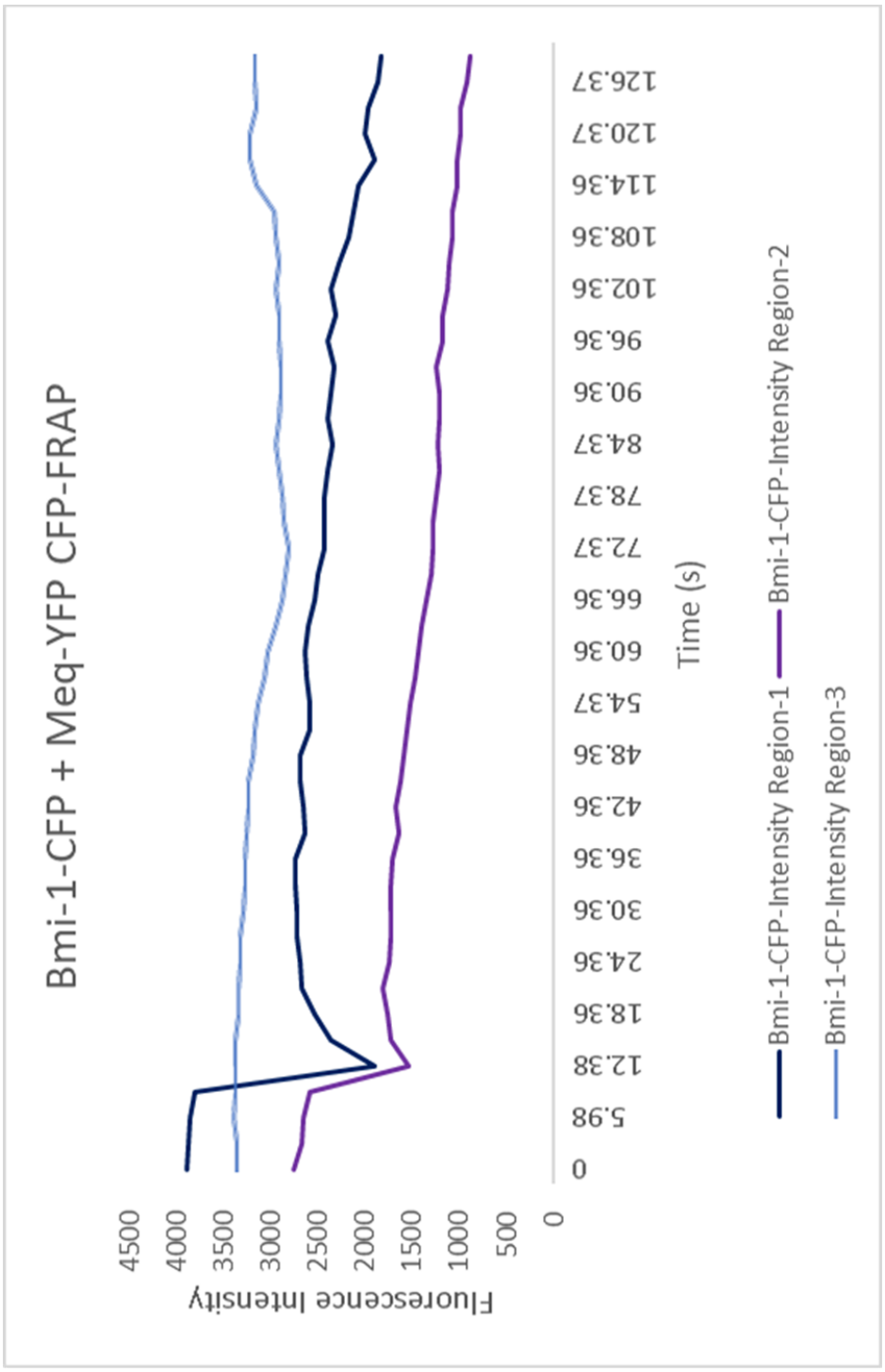
Bmi-1-CFP + Meq-YFP CFP-FRAP
Fluorescence Intensity
4500
4000
3500
3000
2500
2000
1500
1000
500
0
Time (s)
0
5.98
12.38
18.36
24.36
30.36
36.36
42.36
48.36
54.37
60.36
66.36
72.37
78.37
84.37
90.36
96.36
102.36
108.36
114.36
120.37
126.37
Bmi-1-CFP-Intensity Region-1
Bmi-1-CFP-Intensity Region-2
Bmi-1-CFP-Intensity Region-3

Panel C.

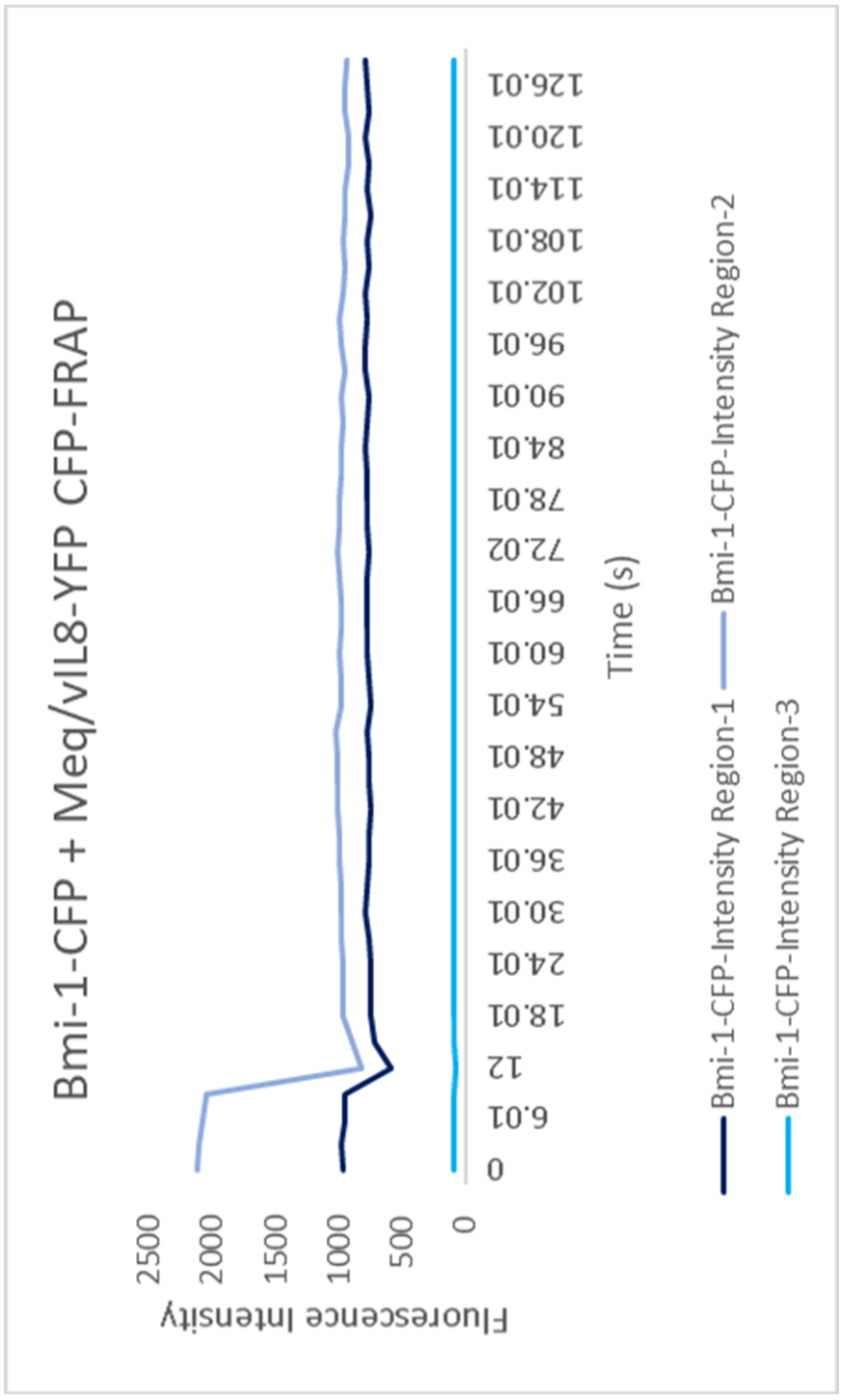
Bmi-1-CFP + Meq/vIL8-YFP CFP-FRAP
Fluorescence Intensity
2500
2000
1500
1000
500
0
Time (s)
0
6.01
12
18.01
24.01
30.01
36.01
42.01
48.01
54.01
60.01
66.01
72.02
78.01
84.01
90.01
96.01
102.01
108.01
114.01
120.01
126.01
Bmi-1-CFP-Intensity Region-1
Bmi-1-CFP-Intensity Region-2
Bmi-1-CFP-Intensity Region-3

REFERENCES

Afonso, C. L., Tulman, E. R., Lu, Z., Zsak, L., Rock, D. L., & Kutish, G. F. (2001). The genome of turkey herpesvirus. *J Virol, 75*(2), 971-978. doi:10.1128/jvi.75.2.971-978.2001

Aloia, L., Di Stefano, B., & Di Croce, L. (2013). Polycomb complexes in stem cells and embryonic development. *Development, 140*(12), 2525-2534. doi:10.1242/dev.091553

Anobile, J. M., Arumugaswami, V., Downs, D., Czymmek, K., Parcells, M., & Schmidt, C. J. (2006). Nuclear localization and dynamic properties of the Marek's disease virus oncogene products Meq and Meq/vIL8. *J Virol, 80*(3), 1160-1166. doi:10.1128/jvi.80.3.1160-1166.2006

Arumugaswami, V., Kumar, P. M., Konjufca, V., Dienglewicz, R. L., Reddy, S. M., & Parcells, M. S. (2009). Latency of Marek's disease virus (MDV) in a reticuloendotheliosis virus-transformed T-cell line. I: uptake and structure of the latent MDV genome. *Avian Dis, 53*(2), 149-155. doi:10.1637/8383-062308-Reg.1

Atkins, K. E., Read, A. F., Savill, N. J., Renz, K. G., Islam, A. F., Walkden-Brown, S. W., & Woolhouse, M. E. (2013). Vaccination and reduced cohort duration can drive virulence evolution: Marek's disease virus and industrialized agriculture. *Evolution, 67*(3), 851-860. doi:10.1111/j.1558-5646.2012.01803.x

Baaten, B. J., Staines, K. A., Smith, L. P., Skinner, H., Davison, T. F., & Butter, C. (2009). Early replication in pulmonary B cells after infection with Marek's disease herpesvirus by the respiratory route. *Viral Immunol, 22*(6), 431-444. doi:10.1089/vim.2009.0047

Baigent S. J., D. F. (2004). Marek’s Disease Virus: Biology and Life Cycle. *Elsevier Academic Press, vol.1*(Marek’s disease, an evolving problem), 62-76.

Baigent, S. J., Petherbridge, L. J., Howes, K., Smith, L. P., Currie, R. J., & Nair, V. K. (2005). Absolute quantitation of Marek's disease virus genome copy number in chicken feather and lymphocyte samples using real-time PCR. *J Virol Methods, 123*(1), 53-64. doi:10.1016/j.jviromet.2004.08.019

Baigent, S. J., Ross, L. J., & Davison, T. F. (1998). Differential susceptibility to Marek's disease is associated with differences in number, but not phenotype or location, of pp38+ lymphocytes. *J Gen Virol, 79 (Pt 11)*, 2795-2802. doi:10.1099/0022-1317-79-11-2795

Brown, A. C., Baigent, S. J., Smith, L. P., Chattoo, J. P., Petherbridge, L. J., Hawes, P., . . . Nair, V. (2006). Interaction of MEQ protein and C-terminal-binding protein is critical for induction of lymphomas by Marek's disease virus. *Proc Natl Acad Sci U S A, 103*(6), 1687-1692. doi:10.1073/pnas.0507595103

Brown, A. C., Nair, V., & Allday, M. J. (2012). Epigenetic regulation of the latency-associated region of Marek's disease virus in tumor-derived T-cell lines and primary lymphoma. *J Virol, 86*(3), 1683-1695. doi:10.1128/jvi.06113-11

Buckmaster, A. E., Scott, S. D., Sanderson, M. J., Boursnell, M. E., Ross, N. L., & Binns, M. M. (1988). Gene sequence and mapping data from Marek's disease virus and herpesvirus of turkeys: implications for herpesvirus classification. *J Gen Virol, 69 (Pt 8)*, 2033-2042. doi:10.1099/0022-1317-69-8-2033

Bulow, V. V., & Biggs, P. M. (1975). Differentiation between strains of Marek's disease virus and turkey herpesvirus by immunofluorescence assays. *Avian Pathol, 4*(2), 133-146. doi:10.1080/03079457509353859

Burgess, S. C., & Davison, T. F. (2002). Identification of the neoplastically transformed cells in Marek's disease herpesvirus-induced lymphomas: recognition by the monoclonal antibody AV37. *J Virol, 76*(14), 7276-7292.

Burgess, S. C., Young, J. R., Baaten, B. J., Hunt, L., Ross, L. N., Parcells, M. S., . . . Davison, T. F. (2004). Marek's disease is a natural model for lymphomas overexpressing Hodgkin's disease antigen (CD30). *Proc Natl Acad Sci U S A, 101*(38), 13879-13884. doi:10.1073/pnas.0305789101

Buscaglia, C., & Calnek, B. W. (1988). Maintenance of Marek's disease herpesvirus latency in vitro by a factor found in conditioned medium. *J Gen Virol, 69 (Pt 11)*, 2809-2818. doi:10.1099/0022-1317-69-11-2809

Buscaglia, C., Calnek, B. W., & Schat, K. A. (1988). Effect of immunocompetence on the establishment and maintenance of latency with Marek's disease herpesvirus. *J Gen Virol, 69 (Pt 5)*, 1067-1077. doi:10.1099/0022-1317-69-5-1067

Calnek, B. W. (1986). Marek's disease--a model for herpesvirus oncology. *Crit Rev Microbiol, 12*(4), 293-320.

Calnek, B. W. (2001). Pathogenesis of Marek's disease virus infection. *Curr Top Microbiol Immunol, 255*, 25-55.

Calnek, B. W., Adldinger, H. K., & Kahn, D. E. (1970). Feather follicle epithelium: a source of enveloped and infectious cell-free herpesvirus from Marek's disease. *Avian Dis, 14*(2), 219-233.

Calnek, B. W., Schat, K. A., Peckham, M. C., & Fabricant, J. (1983). Field trials with a bivalent vaccine (HVT and SB-1) against Marek's disease. *Avian Dis, 27*(3), 844-849.

Cao, R., Wang, L., Wang, H., Xia, L., Erdjument-Bromage, H., Tempst, P., . . . Zhang, Y. (2002). Role of histone H3 lysine 27 methylation in Polycomb-group silencing. *Science, 298*(5595), 1039-1043. doi:10.1126/science.1076997

Cao, R., & Zhang, Y. (2004). SUZ12 is required for both the histone methyltransferase activity and the silencing function of the EED-EZH2 complex. *Mol Cell, 15*(1), 57-67. doi:10.1016/j.molcel.2004.06.020

Cebrian, J., Kaschka-Dierich, C., Berthelot, N., & Sheldrick, P. (1982). Inverted repeat nucleotide sequences in the genomes of Marek disease virus and the herpesvirus of the turkey. *Proc Natl Acad Sci U S A, 79*(2), 555-558.

Churchill, A. E., & Biggs, P. M. (1968). Herpes-type virus isolated in cell culture from tumors of chickens with Marek's disease. II. Studies in vivo. *J Natl Cancer Inst, 41*(4), 951-956.

Couteaudier, M., Courvoisier, K., Trapp-Fragnet, L., Denesvre, C., & Vautherot, J. F. (2016). Keratinocytes derived from chicken embryonic stem cells support Marek's disease virus infection: a highly differentiated cell model to study viral replication and morphogenesis. *Virol J, 13*, 7. doi:10.1186/s12985-015-0458-2

Davidson, I., Malkinson, M., & Weisman, Y. (2002). Marek's disease in turkeys. I. A seven-year survey of commercial flocks and experimental infection using two field isolates. *Avian Dis, 46*(2), 314-321. doi:10.1637/0005-2086(2002)046[0314:Msditi]2.0.Co;2

Delecluse, H. J., Schuller, S., & Hammerschmidt, W. (1993). Latent Marek's disease virus can be activated from its chromosomally integrated state in herpesvirus-transformed lymphoma cells. *Embo j, 12*(8), 3277-3286.

Dutton, A., Woodman, C. B., Chukwuma, M. B., Last, J. I., Wei, W., Vockerodt, M., . . . Murray, P. G. (2007). Bmi-1 is induced by the Epstein-Barr virus oncogene LMP1 and regulates the expression of viral target genes in Hodgkin lymphoma cells. *Blood, 109*(6), 2597-2603. doi:10.1182/blood-2006-05-020545

Eissenberg, J. C., & Elgin, S. C. (2000). The HP1 protein family: getting a grip on chromatin. *Curr Opin Genet Dev, 10*(2), 204-210.

Fischle, W., Wang, Y., Jacobs, S. A., Kim, Y., Allis, C. D., & Khorasanizadeh, S. (2003). Molecular basis for the discrimination of repressive methyl-lysine marks in histone H3 by Polycomb and HP1 chromodomains. *Genes Dev, 17*(15), 1870-1881. doi:10.1101/gad.1110503

Haupt, Y., Alexander, W. S., Barri, G., Klinken, S. P., & Adams, J. M. (1991). Novel zinc finger gene implicated as myc collaborator by retrovirally accelerated lymphomagenesis in E mu-myc transgenic mice. *Cell, 65*(5), 753-763.

He, M., Zhang, W., Bakken, T., Schutten, M., Toth, Z., Jung, J. U., . . . Gao, S. J. (2012). Cancer angiogenesis induced by Kaposi sarcoma-associated herpesvirus is mediated by EZH2. *Cancer Res, 72*(14), 3582-3592. doi:10.1158/0008-5472.Can-11-2876

Hemenway, C. S., Halligan, B. W., & Levy, L. S. (1998). The Bmi-1 oncoprotein interacts with dinG and MPh2: the role of RING finger domains. *Oncogene, 16*(19), 2541-2547. doi:10.1038/sj.onc.1202042

Hunt, H. D., Lupiani, B., Miller, M. M., Gimeno, I., Lee, L. F., & Parcells, M. S. (2001). Marek's disease virus down-regulates surface expression of MHC (B Complex) Class I (BF) glycoproteins during active but not latent infection of chicken cells. *Virology, 282*(1), 198-205. doi:10.1006/viro.2000.0797

Izumiya, Y., Jang, H. K., Ono, M., & Mikami, T. (2001). A complete genomic DNA sequence of Marek's disease virus type 2, strain HPRS24. *Curr Top Microbiol Immunol, 255*, 191-221.

Jones, D., Lee, L., Liu, J. L., Kung, H. J., & Tillotson, J. K. (1992). Marek disease virus encodes a basic-leucine zipper gene resembling the fos/jun oncogenes that is highly expressed in lymphoblastoid tumors. *Proc Natl Acad Sci U S A, 89*(9), 4042-4046.

Kaiser, P., Underwood, G., & Davison, F. (2003). Differential cytokine responses following Marek's disease virus infection of chickens differing in resistance to Marek's disease. *J Virol, 77*(1), 762-768.

Karpova, T. S., Baumann, C. T., He, L., Wu, X., Grammer, A., Lipsky, P., . . . McNally, J. G. (2003). Fluorescence resonance energy transfer from cyan to yellow fluorescent protein detected by acceptor photobleaching using confocal microscopy and a single laser. *J Microsc, 209*(Pt 1), 56-70.

Kassis, J. A., & Brown, J. L. (2013). Polycomb Group Response Elements in Drosophila and Vertebrates. *Advances in genetics, 81*, 83-118. doi:10.1016/B978-0-12-407677-8.00003-8

Kenworthy, A. K. (2001). Imaging protein-protein interactions using fluorescence resonance energy transfer microscopy. *Methods, 24*(3), 289-296. doi:10.1006/meth.2001.1189

Kim, T., Hunt, H. D., Parcells, M. S., van Santen, V., & Ewald, S. J. (2018). Two class I genes of the chicken MHC have different functions: BF1 is recognized by NK cells while BF2 is recognized by CTLs. *Immunogenetics*. doi:10.1007/s00251-018-1066-2

Kingham, B. F., Zelnik, V., Kopacek, J., Majerciak, V., Ney, E., & Schmidt, C. J. (2001). The genome of herpesvirus of turkeys: comparative analysis with Marek's disease viruses. *J Gen Virol, 82*(Pt 5), 1123-1135. doi:10.1099/0022-1317-82-5-1123

Kirmizis, A., Bartley, S. M., & Farnham, P. J. (2003). Identification of the polycomb group protein SU(Z)12 as a potential molecular target for human cancer therapy. *Mol Cancer Ther, 2*(1), 113-121.

Kreso, A., van Galen, P., Pedley, N. M., Lima-Fernandes, E., Frelin, C., Davis, T., . . . O'Brien, C. A. (2014). Self-renewal as a therapeutic target in human colorectal cancer. *Nat Med, 20*(1), 29-36. doi:10.1038/nm.3418

Kumar, P., Dong, H., Lenihan, D., Gaddamanugu, S., Katneni, U., Shaikh, S., . . . Parcells, M. S. (2012). Selection of a recombinant Marek's disease virus in vivo through expression of the Marek's EcoRI-Q (Meq)-encoded oncoprotein: characterization of an rMd5-based mutant expressing the Meq of strain RB-1B. *Avian Dis, 56*(2), 328-340. doi:10.1637/9955-100611-Reg.1

Lee, L. F., Liu, J. L., Cui, X. P., & Kung, H. J. (2003). Marek's disease virus latent protein MEQ: delineation of an epitope in the BR1 domain involved in nuclear localization. *Virus Genes, 27*(3), 211-218.

Leeb, M., & Wutz, A. (2007). Ring1B is crucial for the regulation of developmental control genes and PRC1 proteins but not X inactivation in embryonic cells. *J Cell Biol, 178*(2), 219-229. doi:10.1083/jcb.200612127

Levy, A. M., Gilad, O., Xia, L., Izumiya, Y., Choi, J., Tsalenko, A., . . . Kung, H. J. (2005). Marek's disease virus Meq transforms chicken cells via the v-Jun transcriptional cascade: a converging transforming pathway for avian oncoviruses. *Proc Natl Acad Sci U S A, 102*(41), 14831-14836. doi:10.1073/pnas.0506849102

Liang, W., Zhu, D., Cui, X., Su, J., Liu, H., Han, J., . . . Xie, W. (2013). Knockdown BMI1 expression inhibits proliferation and invasion in human bladder cancer T24 cells. *Mol Cell Biochem, 382*(1-2), 283-291. doi:10.1007/s11010-013-1745-0

Liu, J. L., & Kung, H. J. (2000). Marek's disease herpesvirus transforming protein MEQ: a c-Jun analogue with an alternative life style. *Virus Genes, 21*(1-2), 51-64.

Liu, J. L., Lee, L. F., Ye, Y., Qian, Z., & Kung, H. J. (1997). Nucleolar and nuclear localization properties of a herpesvirus bZIP oncoprotein, MEQ. *J Virol, 71*(4), 3188-3196.

Livak, K. J., & Schmittgen, T. D. (2001). Analysis of relative gene expression data using real-time quantitative PCR and the 2(-Delta Delta C(T)) Method. *Methods, 25*(4), 402-408. doi:10.1006/meth.2001.1262

Lupiani, B., Lee, L. F., Cui, X., Gimeno, I., Anderson, A., Morgan, R. W., . . . Reddy, S. M. (2004). Marek's disease virus-encoded Meq gene is involved in transformation of lymphocytes but is dispensable for replication. *Proc Natl Acad Sci U S A, 101*(32), 11815-11820. doi:10.1073/pnas.0404508101

Ma, S. D., Tsai, M. H., Romero-Masters, J. C., Ranheim, E. A., Huebner, S. M., Bristol, J. A., . . . Kenney, S. C. (2017). Latent Membrane Protein 1 (LMP1) and LMP2A Collaborate To Promote Epstein-Barr Virus-Induced B Cell Lymphomas in a Cord Blood-Humanized Mouse Model but Are Not Essential. *J Virol, 91*(7). doi:10.1128/jvi.01928-16

Marek. (1907). Multiple Nervenentzündung (Polyneuritis) bei Hühnern. *Dtsch Tierarztl Wochenschr, 15:417–421*.

Margueron, R., Li, G., Sarma, K., Blais, A., Zavadil, J., Woodcock, C. L., . . . Reinberg, D. (2008). Ezh1 and Ezh2 maintain repressive chromatin through different mechanisms. *Mol Cell, 32*(4), 503-518. doi:10.1016/j.molcel.2008.11.004

Mayr, C., Wagner, A., Loeffelberger, M., Bruckner, D., Jakab, M., Berr, F., . . . Kiesslich, T. (2016). The BMI1 inhibitor PTC-209 is a potential compound to halt cellular growth in biliary tract cancer cells. *Oncotarget, 7*(1), 745-758. doi:10.18632/oncotarget.6378

McCabe, M. T., Ott, H. M., Ganji, G., Korenchuk, S., Thompson, C., Van Aller, G. S., . . . Creasy, C. L. (2012). EZH2 inhibition as a therapeutic strategy for lymphoma with EZH2-activating mutations. *Nature, 492*(7427), 108-112. doi:10.1038/nature11606

Miller, G. (1990). Epstein-Barr virus ; biology, pathogenesis, and medical aspect. *Virology*.

Miller, M. M., & Taylor, R. L., Jr. (2016). Brief review of the chicken Major Histocompatibility Complex: the genes, their distribution on chromosome 16, and their contributions to disease resistance. *Poult Sci, 95*(2), 375-392. doi:10.3382/ps/pev379

Mitra, A., Luo, J., He, Y., Gu, Y., Zhang, H., Zhao, K., . . . Song, J. (2015). Histone modifications induced by MDV infection at early cytolytic and latency phases. *BMC Genomics, 16*, 311. doi:10.1186/s12864-015-1492-6

Mohammad, F., Weissmann, S., Leblanc, B., Pandey, D. P., Hojfeldt, J. W., Comet, I., . . . Helin, K. (2017). EZH2 is a potential therapeutic target for H3K27M-mutant pediatric gliomas. *Nat Med, 23*(4), 483-492. doi:10.1038/nm.4293

Montgomery, N. D., Yee, D., Chen, A., Kalantry, S., Chamberlain, S. J., Otte, A. P., & Magnuson, T. (2005). The murine polycomb group protein Eed is required for global histone H3 lysine-27 methylation. *Curr Biol, 15*(10), 942-947. doi:10.1016/j.cub.2005.04.051

Morimura, T., Hattori, M., Ohashi, K., Sugimoto, C., & Onuma, M. (1995). Immunomodulation of peripheral T cells in chickens infected with Marek's disease virus: involvement in immunosuppression. *J Gen Virol, 76 (Pt 12)*, 2979-2985. doi:10.1099/0022-1317-76-12-2979

Murray, P. G., Young, L. S., Rowe, M., & Crocker, J. (1992). Immunohistochemical demonstration of the Epstein-Barr virus-encoded latent membrane protein in paraffin sections of Hodgkin's disease. *J Pathol, 166*(1), 1-5. doi:10.1002/path.1711660102

Neerukonda, S. N., Katneni, U. K., Bott, M., Golovan, S. P., & Parcells, M. S. (2018). Induction of the unfolded protein response (UPR) during Marek's disease virus (MDV) infection. *Virology, 522*, 1-12. doi:10.1016/j.virol.2018.06.016

Neerukonda, S. N., Katneni, U. K., Golovan, S., & Parcells, M. S. (2016). Evaluation and validation of reference gene stability during Marek's disease virus (MDV) infection. *J Virol Methods, 236*, 111-116. doi:10.1016/j.jviromet.2016.07.017

Niedobitek, G., Kremmer, E., Herbst, H., Whitehead, L., Dawson, C. W., Niedobitek, E., . . . Young, L. S. (1997). Immunohistochemical detection of the Epstein-Barr virus-encoded latent membrane protein 2A in Hodgkin's disease and infectious mononucleosis. *Blood, 90*(4), 1664-1672.

Nishida, Y., Maeda, A., Chachad, D., Ishizawa, J., Qiu, Y. H., Kornblau, S. M., . . . Kojima, K. (2015). Preclinical activity of the novel B-cell-specific Moloney murine leukemia virus integration site 1 inhibitor PTC-209 in acute myeloid leukemia: Implications for leukemia therapy. *Cancer Sci, 106*(12), 1705-1713. doi:10.1111/cas.12833

Obier, N., Lin, Q., Cauchy, P., Hornich, V., Zenke, M., Becker, M., & Muller, A. M. (2015). Polycomb protein EED is required for silencing of pluripotency genes upon ESC differentiation. *Stem Cell Rev, 11*(1), 50-61. doi:10.1007/s12015-014-9550-z

Okazaki, W., Purchase, H. G., & Burmester, B. R. (1970). Protection against Marek's disease by vaccination with a herpesvirus of turkeys. *Avian Dis, 14*(2), 413-429.

Osterrieder, N. (2004). The genome content of Marek's disease-like virus. *Biology of Animal Infections, Marek's Disease An Evolving Problem*, 17-31.

Osterrieder, N., Kamil, J. P., Schumacher, D., Tischer, B. K., & Trapp, S. (2006). Marek's disease virus: from miasma to model. *Nat Rev Microbiol, 4*(4), 283-294. doi:10.1038/nrmicro1382

Pappenheimer, A. M., Dunn, L. C., & Seidlin, S. M. (1929). STUDIES ON FOWL PARALYSIS (NEUROLYMPHOMATOSIS GALLINARUM) : II. TRANSMISSION EXPERIMENTS. *J Exp Med, 49*(1), 87-102.

Parcells M.S, B. J., Morgan R.W. (2012). Marek's Disease Virus-Induced T-Cell Lymphomas. *Robertson E. (eds) Cancer Associated Viruses. Current Cancer Research.*

Parcells, M. S., Burnside, J., & Morgan, R. W. (2012). Marek's Disease Virus-Induced T-Cell Lymphomas. *Robertson E. (eds) Cancer Associated Viruses. Current Cancer Research.*

Parcells, M. S., Dienglewicz, R. L., Anderson, A. S., & Morgan, R. W. (1999). Recombinant Marek's disease virus (MDV)-derived lymphoblastoid cell lines: regulation of a marker gene within the context of the MDV genome. *J Virol, 73*(2), 1362-1373.

Pasini, D., Bracken, A. P., Jensen, M. R., Lazzerini Denchi, E., & Helin, K. (2004). Suz12 is essential for mouse development and for EZH2 histone methyltransferase activity. *Embo j, 23*(20), 4061-4071. doi:10.1038/sj.emboj.7600402

Peng, Q., & Shirazi, Y. (1996). Characterization of the protein product encoded by a splicing variant of the Marek's disease virus Eco-Q gene (Meq). *Virology, 226*(1), 77-82. doi:10.1006/viro.1996.0629

Prigge, J. T., Majerciak, V., Hunt, H. D., Dienglewicz, R. L., & Parcells, M. S. (2004). Construction and characterization of Marek's disease viruses having green fluorescent protein expression tied directly or indirectly to phosphoprotein 38 expression. *Avian Dis, 48*(3), 471-487. doi:10.1637/7110

Qian, Z., Brunovskis, P., Rauscher, F., 3rd, Lee, L., & Kung, H. J. (1995). Transactivation activity of Meq, a Marek's disease herpesvirus bZIP protein persistently expressed in latently infected transformed T cells. *J Virol, 69*(7), 4037-4044.

Raaphorst, F. M., van Kemenade, F. J., Blokzijl, T., Fieret, E., Hamer, K. M., Satijn, D. P., . . . Meijer, C. J. (2000). Coexpression of BMI-1 and EZH2 polycomb group genes in Reed-Sternberg cells of Hodgkin's disease. *Am J Pathol, 157*(3), 709-715. doi:10.1016/s0002-9440(10)64583-x

Raaphorst, F. M., van Kemenade, F. J., Blokzijl, T., Fieret, E., Hamer, K. M., Satijn, D. P. E., . . . Meijer, C. J. L. M. (2000). Coexpression of BMI-1 and EZH2 Polycomb Group Genes in Reed-Sternberg Cells of Hodgkin's Disease. *Am J Pathol, 157*(3), 709-715.

Rath, N. C., Parcells, M. S., Xie, H., & Santin, E. (2003). Characterization of a spontaneously transformed chicken mononuclear cell line. *Vet Immunol Immunopathol, 96*(1-2), 93-104.

Read, A. F., Baigent, S. J., Powers, C., Kgosana, L. B., Blackwell, L., Smith, L. P., . . . Nair, V. K. (2015). Imperfect Vaccination Can Enhance the Transmission of Highly Virulent Pathogens. *PLoS Biol, 13*(7), e1002198. doi:10.1371/journal.pbio.1002198

Reddy, S. M., Sui, D., Wu, P., & Lee, L. (1999). Identification and structural analysis of a MDV gene encoding a protein kinase. *Acta Virol, 43*(2-3), 174-180.

Ringrose, L., & Paro, R. (2004). Epigenetic regulation of cellular memory by the Polycomb and Trithorax group proteins. *Annu Rev Genet, 38*, 413-443. doi:10.1146/annurev.genet.38.072902.091907

Ross, N. L. (1999). T-cell transformation by Marek's disease virus. *Trends Microbiol, 7*(1), 22-29.

Schat, K. A., Chen, C. L., Calnek, B. W., & Char, D. (1991). Transformation of T-lymphocyte subsets by Marek's disease herpesvirus. *J Virol, 65*(3), 1408-1413.

Sewalt, R. G., Gunster, M. J., van der Vlag, J., Satijn, D. P., & Otte, A. P. (1999). C-Terminal binding protein is a transcriptional repressor that interacts with a specific class of vertebrate Polycomb proteins. *Mol Cell Biol, 19*(1), 777-787.

Shack, L. A., Buza, J. J., & Burgess, S. C. (2008). The neoplastically transformed (CD30hi) Marek's disease lymphoma cell phenotype most closely resembles T-regulatory cells. *Cancer Immunol Immunother, 57*(8), 1253-1262. doi:10.1007/s00262-008-0460-2

Shamblin, C. E., Greene, N., Arumugaswami, V., Dienglewicz, R. L., & Parcells, M. S. (2004). Comparative analysis of Marek's disease virus (MDV) glycoprotein-, lytic antigen pp38- and transformation antigen Meq-encoding genes: association of meq mutations with MDVs of high virulence. *Vet Microbiol, 102*(3-4), 147-167. doi:10.1016/j.vetmic.2004.06.007

Shek, W. R., Calnek, B. W., Schat, K. A., & Chen, C. H. (1983). Characterization of Marek's disease virus-infected lymphocytes: discrimination between cytolytically and latently infected cells. *J Natl Cancer Inst, 70*(3), 485-491.

Sherr, C. J. (2001). The INK4a/ARF network in tumour suppression. *Nat Rev Mol Cell Biol, 2*(10), 731-737. doi:10.1038/35096061

Simon, J. A., & Kingston, R. E. (2013). Occupying chromatin: Polycomb mechanisms for getting to genomic targets, stopping transcriptional traffic, and staying put. *Mol Cell, 49*(5), 808-824. doi:10.1016/j.molcel.2013.02.013

Sparmann, A., & van Lohuizen, M. (2006). Polycomb silencers control cell fate, development and cancer. *Nat Rev Cancer, 6*(11), 846-856. doi:10.1038/nrc1991

Stock, J. K., Giadrossi, S., Casanova, M., Brookes, E., Vidal, M., Koseki, H., . . . Pombo, A. (2007). Ring1-mediated ubiquitination of H2A restrains poised RNA polymerase II at bivalent genes in mouse ES cells. *Nat Cell Biol, 9*(12), 1428-1435. doi:10.1038/ncb1663

Takeshima, H., Wakabayashi, M., Hattori, N., Yamashita, S., & Ushijima, T. (2015). Identification of coexistence of DNA methylation and H3K27me3 specifically in cancer cells as a promising target for epigenetic therapy. *Carcinogenesis, 36*(2), 192-201. doi:10.1093/carcin/bgu238

Trimarchi, J. M., Fairchild, B., Wen, J., & Lees, J. A. (2001). The E2F6 transcription factor is a component of the mammalian Bmi1-containing polycomb complex. *Proc Natl Acad Sci U S A, 98*(4), 1519-1524. doi:10.1073/pnas.041597698

Tulman, E. R., Afonso, C. L., Lu, Z., Zsak, L., Rock, D. L., & Kutish, G. F. (2000). The genome of a very virulent Marek's disease virus. *J Virol, 74*(17), 7980-7988.

van Kemenade, F. J., Raaphorst, F. M., Blokzijl, T., Fieret, E., Hamer, K. M., Satijn, D. P., . . . Meijer, C. J. (2001). Coexpression of BMI-1 and EZH2 polycomb-group proteins is associated with cycling cells and degree of malignancy in B-cell non-Hodgkin lymphoma. *Blood, 97*(12), 3896-3901.

van Lohuizen, M., Frasch, M., Wientjens, E., & Berns, A. (1991). Sequence similarity between the mammalian bmi-1 proto-oncogene and the Drosophila regulatory genes Psc and Su(z)2. *Nature, 353*(6342), 353-355. doi:10.1038/353353a0

Varambally, S., Dhanasekaran, S. M., Zhou, M., Barrette, T. R., Kumar-Sinha, C., Sanda, M. G., . . . Chinnaiyan, A. M. (2002). The polycomb group protein EZH2 is involved in progression of prostate cancer. *Nature, 419*(6907), 624-629. doi:10.1038/nature01075

Weng, M. Y., Li, L., Feng, S. Y., & Hong, S. J. (2012). Expression of Bmi-1, P16, and CD44v6 in Uterine Cervical Carcinoma and Its Clinical Significance. *Cancer Biol Med, 9*(1), 48-53. doi:10.3969/j.issn.2095-3941.2012.01.009

Witter, R. L. (1983). Characteristics of Marek's disease viruses isolated from vaccinated commercial chicken flocks: association of viral pathotype with lymphoma frequency. *Avian Dis, 27*(1), 113-132.

Witter, R. L. (1997). Increased virulence of Marek's disease virus field isolates. *Avian Dis, 41*(1), 149-163.

Xia, R., Jin, F. Y., Lu, K., Wan, L., Xie, M., Xu, T. P., . . . Wang, Z. X. (2015). SUZ12 promotes gastric cancer cell proliferation and metastasis by regulating KLF2 and E-cadherin. *Tumour Biol, 36*(7), 5341-5351. doi:10.1007/s13277-015-3195-7

Yguerabide, J., Schmidt, J. A., & Yguerabide, E. E. (1982). Lateral mobility in membranes as detected by fluorescence recovery after photobleaching. *Biophys J, 40*(1), 69-75. doi:10.1016/s0006-3495(82)84459-7

Zapata, J. C., Campilongo, F., Barclay, R. A., DeMarino, C., Iglesias-Ussel, M. D., Kashanchi, F., & Romerio, F. (2017). The Human Immunodeficiency Virus 1 ASP RNA promotes viral latency by recruiting the Polycomb Repressor Complex 2 and promoting nucleosome assembly. *Virology, 506*, 34-44. doi:10.1016/j.virol.2017.03.002

Zhang, X., Tian, T., Sun, W., Liu, C., & Fang, X. (2017). Bmi-1 overexpression as an efficient prognostic marker in patients with nonsmall cell lung cancer. *Medicine (Baltimore), 96*(26), e7346. doi:10.1097/md.0000000000007346